Fakultät für
Mathematik und
Naturwissenschaften

RWTH AACHEN UNIVERSITY

Higgs Strahlung via contact interactions through next-to-next-to-leading order QCD

Von der Fakultät für Mathematik und Naturwissenschaften
der RWTH Aachen University zur Erlangung des akademischen Grades eines Doktors der Naturwissenschaften genehmigte Dissertation

vorgelegt von

Dmitrii Korneev, M.Sc.

aus

Moskau, Russland

Berichter:
Univ.-Prof. Dr. rer. nat. Robert Harlander
Univ.-Prof. Dr. rer. nat. Michael Krämer

Datum der mündlichen Prüfung: 30.04.2026

Diese Dissertation ist auf den Internetseiten der Universitätsbibliothek online verfügbar

Acknowledgments

This doctoral research was carried out at the Institute of Particle Theoretical Physics and Cosmology of RWTH Aachen University. The present manuscript is the result of numerous challenges and efforts that required the assistance and collaboration of several people. Each interaction has been very useful and I am grateful to have received unwavering technical and moral support from all of them.

I would like to express my deepest gratitude to the members of my doctoral committee for their time and effort in evaluating this thesis: Prof. Dr. **Stefan Schael** (Head of the Committee), Prof. Dr. **Johannes Erdmann**, Prof. Dr. **Robert Harlander**, and Prof. Dr. **Michael Krämer**.

This work would not have been possible without the support of my supervisor, Prof. Dr. **Robert Harlander**, who provided me with a unique opportunity to gain invaluable scientific experience and guided me throughout the entire project, despite much of it taking place during the challenging period of remote work. His discerning guidance and encouragement were pivotal to the successful completion of this work.

I am immensely grateful to Dr. **Marco Bonetti** for his indispensable contribution to the advancement of my project. Marco's comprehensive explanations were instrumental in elucidating numerous aspects that were initially opaque to me. He responded to a multitude of inquiries with remarkable patience and was always willing to provide guidance on both the technical and phenomenological aspects of the calculations. Moreover, by conducting parallel calculations, Marco enabled me to verify my results and gain a more profound understanding of the process.

I would like to thank Prof. **Raoul Röntsch** for taking on the challenging aspects of our collaborative work and employing my findings in a way that has brought us closer to reaching our ultimate objective.

I would also like to express my gratitude to Prof. Dr. **Kirill Melnikov** for his invaluable advice and insights during my work on this project, which significantly enhanced the overall quality of the research.

I am also deeply thankful to Dr. **Ming-Ming Long** and Dr. **Davide Maria Tagliabue** for their contribution to the project, particularly for performing calculations of key quantities that we were able to compare with my own results.

In addition, I would like to express my gratitude to the **Collaborative Research Center** (CRC) for sponsoring this work. The support provided by CRC TRR 257 "Particle Physics Phenomenology after the Higgs Discovery" (grant 369021762) has been fundamental in enabling me to carry out my research at RWTH Aachen University. The collaborative environment fostered by the CRC was invaluable, and I am grateful for the opportunity to be part of such an inspiring community of researchers.

I would like to express my sincere thanks to all my colleagues and friends who have provided invaluable support throughout this journey. Your encouragement, advice, and camaraderie have made this experience truly rewarding. Special thanks go to Dr. **Lukas Simon** for his assistance with many crucial details. Lukas and I frequently discussed various aspects of the project, and these discussions undoubtedly accelerated the progress and contributed to the improved quality of the work.

As this experience comes to an end, I know that I would never have been able to complete this stage without the unwavering support of my parents. I would like to express warm words of gratitude to my mother **Nataliia** and my father **Sergei**, thanks to their efforts, love and persistence this work became possible.

I am profoundly grateful to my wife **Anastasiia** for her unwavering love and support. Thank you for always believing in me and motivating me to pursue my goals, no matter the challenges.

Thank you to all my family, my friends, near and far. You have made this journey possible!

Zusammenfassung

Die vorliegende Dissertation präsentiert eine analytische Berechnung der quadrierten Amplituden für den Prozess $q\bar{q}' \to WH$, gefolgt vom Zerfall des W-Bosons in ein Lepton-Antilepton-Paar. Die genannten Berechnungen wurden im Rahmen der auf dem Standardmodell basierenden effektiven Feldtheorie (SMEFT) durchgeführt, wobei das Standardmodell selbst als ein spezifischer Grenzfall betrachtet wurde. Ein Vergleich der Ergebnisse zwischen SMEFT und dem Standardmodell ermöglichte die Quantifizierung potenzieller Abweichungen, die durch höherdimensionale Operatoren bedingt sind. Dies führte zu einem vertieften Verständnis der zugrunde liegenden Physik.

Das Hauptziel dieser Arbeit bestand darin, analytische Ausdrücke für die quadrierten Amplituden bis zur nächst-nächst-führenden Ordnung (NNLO) in der perturbativen Quantenchromodynamik zu entwickeln. Dabei war sicherzustellen, dass die Ergebnisse die erwarteten weichen und kollinearen Grenzwerte erfüllen. Das untersuchte SMEFT-Rahmenwerk ermöglicht eine systematische Einbeziehung potenzieller neuer Physik jenseits des Standardmodells, parametrisiert durch Wilson-Koeffizienten. Die Erweiterung der Berechnungen auf NNLO-Genauigkeit führte zu einer signifikanten Verbesserung der theoretischen Präzision für diesen wichtigen elektroschwachen Prozess, der insbesondere für Kollisionsexperimente wie diejenigen am Large Hadron Collider von großem Interesse ist. Die abgeleiteten Ausdrücke wurden einer rigorosen Konsistenz-prüfung unterzogen und mit bekannten Ergebnissen niedrigerer Ordnungen verglichen, wodurch ihre Robustheit und Verlässlichkeit sichergestellt wurde. Die vorliegende analytische Arbeit bildet eine Grundlage für präzise phänomenologische Studien zur Suche nach neuer Physik.

Des Weiteren wurden die Resultate innerhalb des Standardmodells einer numerischen Verifizierung unterzogen, welche mittels eines eigens dafür entwickelten Programms in Python erfolgte. Das Programm wurde entwickelt, um numerische Auswertungen der quadrierten Amplituden durchzuführen. Die Ergebnisse wurden mit etablierten Werkzeugen abgeglichen, welche die numerische Berechnung der quadrierten Amplituden ermöglichen. Der Validierungsschritt diente der Gewährleistung der Genauigkeit und Konsistenz der innerhalb des Standardmodells abgeleiteten analytischen Ausdrücke, wodurch die Zuverlässigkeit der in dieser Arbeit angewandten Methodik insgesamt gestärkt wurde.

Obschon sich diese Dissertation in erster Linie mit den theoretischen und analytischen Aspekten der Berechnungen befasst, wurde die Arbeit in enger Kooperation mit Kollegen durchgeführt, welche die Analyse auf numerische Vorhersagen der Wirkungsquerschnitte ausgedehnt haben. Die Berücksichtigung der bislang unbekannten Wilson-Koeffizienten sowie deren Einfluss auf die Streuwirkungsquerschnitte ermöglichte eine detaillierte Untersuchung, in welcher Form sich neue Physik in experimentellen Daten manifestieren könnte. Die vorliegende Arbeit stellt einen bedeutsamen Fortschritt im kontinuierlichen Bestreben dar, die Grenzen des Standardmodells zu erforschen und nach neuer Physik in Hochenergie-Kollisionsversuchen zu suchen.

Abstract

This thesis presents the analytical computation of squared amplitudes for the process $q\bar{q}' \to WH$, followed by the subsequent decay of the W boson into a lepton-antilepton pair. These calculations were performed within the framework of the Standard Model Effective Field Theory (SMEFT), with the Standard Model itself considered as a specific limiting case. A comparison of results between SMEFT and the Standard Model enabled us to quantify potential deviations due to higher-dimensional operators, thereby facilitating a more profound comprehension of the underlying physics.

The primary objective of this work was to derive precise analytical expressions for the squared amplitudes up to the next-to-next-to-leading order (NNLO) in perturbative quantum chromodynamics, ensuring that the results satisfy the expected soft and collinear limits. The studied framework of the Standard Model Effective Field Theory allows for a systematic inclusion of potential new physics effects beyond the Standard Model, parameterized by Wilson coefficients. By extending the calculations to NNLO accuracy, we were able to significantly improve the theoretical precision for this important electroweak process which is particularly relevant for collider experiments such as those conducted at the Large Hadron Collider (LHC). The derived expressions were subjected to rigorous testing for consistency and validated against known results at lower orders, thereby ensuring their robustness and reliability. This analytical work establishes a foundation for precise phenomenological studies of new physics in processes involving Higgs boson production.

In addition to the analytic calculations, the results within the Standard Model were verified numerically using a custom Python program developed for this purpose. This program was designed to perform numerical evaluations of the squared amplitudes, and the results were cross-checked against other established tools that are capable of computing squared amplitudes numerically. This validation step ensured the accuracy and consistency of the analytical expressions derived within the Standard Model framework, thereby further strengthening the overall reliability of the methodology employed in this work.

While this thesis is primarily concerned with the theoretical and analytical aspects of the computations, the work was conducted in close collaboration with colleagues who extended the analysis to obtain numerical cross-section predictions. The incorporation of the unknown Wilson coefficients and their impact on the scattering cross-sections enabled the detailed examination of how new physics might manifest in experimental data. This work represents a significant advancement in the ongoing effort to probe the limits of the Standard Model and to search for new physics in high-energy collider experiments.

Contents

1 Introduction **1**

2 Associated Electroweak and Higgs Boson Production **8**
2.1 Hadronic cross section . . . 8
2.2 Higgs Strahlung in the Standard Model . . . 9
2.3 Standard Model Effective Field Theory . . . 11
2.4 Relevant dimension-six operators . . . 14

3 Helicity Amplitude Formalism **17**
3.1 Overview of helicity formalism . . . 17
3.2 Quantum Chromodynamics in helicity formalism . . . 19
3.2.1 External fermions . . . 19
3.2.2 External massless bosons . . . 20
3.2.3 Color decomposition . . . 20
3.3 Soft and collinear factorization . . . 21

4 Next-to-Next-to-Leading Order Amplitudes **23**
4.1 Conventions and notations . . . 23
4.2 Leading Order . . . 25
4.3 Loop corrections . . . 26
4.3.1 General tensor structure of pure n-loop corrections . . . 26
4.3.2 Total helicity amplitudes for purely virtual n-loop case . . . 29
4.3.3 Two-loop form factors . . . 31
4.3.4 Two-loop renormalisation . . . 35
4.4 Single real corrections . . . 38
4.4.1 Tree-level . . . 39
4.4.2 NLO soft and collinear limits . . . 41
4.4.3 Virtual-real corrections . . . 43
4.4.4 Virtual-real form factor renormalization . . . 48
4.4.5 NNLO soft and collinear limits for a single gluon . . . 50
4.5 Double real corrections . . . 51
4.5.1 Soft limits . . . 52
4.5.2 Collinear limits . . . 54
4.5.3 Mixed soft-collinear limit . . . 56
4.6 Python implementation . . . 56
4.6.1 Overview of the modules . . . 57

5 Phase-Space Integration **59**
5.1 Partonic cross section . . . 59
5.2 Phase space integration . . . 60

6 Numerical Results and Discussion **64**

7 Conclusion **68**

A Explicit Results **69**
A.1 Pure loop corrections 69
A.2 Single gluon corrections 70

B Dirac Matrices in d-dimensional Spacetime **81**
B.1 Dirac matrices γ^μ 81
B.2 Matrix γ_5 82
B.2.1 HVBM's dimensional regularization scheme 83
B.2.2 Kreimer's dimensional regularization scheme 84
B.3 Levi-Civita symbol 85

C Spinor Helicity Formalism **87**
C.1 Spinor identities 87
C.2 Vector boson representation 90
C.3 Representation for numerical computation 91

References **93**

1 Introduction

The Standard Model of particle physics is one of the most successful and well-established theories in modern particle physics, providing a comprehensive framework that describes the fundamental particles and forces governing the universe. The development of the Standard Model represents the culmination of decades of theoretical progress and experimental verification, built upon the principles of quantum field theory, gauge symmetries, and spontaneous symmetry breaking.

The genesis of the Standard Model can be traced back to the early 20th century, when scientists first began to unravel the mysteries of atomic structure. The discovery of the electron by J.J. Thomson [1] in 1897 and the subsequent identification of the proton and neutron [2] laid the groundwork for understanding the fundamental building blocks of matter. However, it was not until the mid-20th century that significant advances in quantum theory permitted for the formulation of a more complete picture of particle interactions. The theory of quantum electrodynamics (QED), developed in the 1940s by Sin-Itiro Tomonaga [3], Julian Schwinger [4], and Richard Feynman [5], provided the first successful description of electromagnetic interactions at the quantum level, introducing the concept of force-carrying particles known as gauge bosons.

Building on the success of QED, the 1960s saw the emergence of a unified framework to describe the weak nuclear force and the electromagnetic force, known as the electroweak theory [6-9]. This was primarily developed by Sheldon Glashow, Abdus Salam, and Steven Weinberg, who were jointly awarded the Nobel Prize in Physics in 1979 for their work. The electroweak theory introduced the concept of spontaneous symmetry breaking [10-15], facilitated by the Higgs mechanism, which predicted the existence of the Higgs boson — a particle whose discovery would later become one of the crowning achievements of modern physics.

In parallel with these theoretical advancements, quantum chromodynamics (QCD) was developed to describe the strong nuclear force, which binds quarks together inside protons, neutrons, and other hadrons [16-19]. The strong force is transmitted by gluons, the gauge bosons of QCD, and operates under the principles of SU(3) gauge symmetry. Together with the electroweak theory, QCD constituted the foundation of the Standard Model which unifies three of the four fundamental forces of nature — the electromagnetic, weak, and strong interactions.

The experimental verification of the Standard Model has been equally remarkable. The discovery of the W [20] and Z [21] bosons at CERN in 1983 confirmed key predictions of the electroweak theory and provided strong support for the model's validity. Decades later, the long-sought Higgs boson was finally detected in 2012 by the ATLAS [22] and CMS [23] experiments at CERN's Large Hadron Collider, thereby confirming the Higgs mechanism as the source of mass for fundamental particles. These discoveries, along with the precise measurement of countless particle interactions, have established the Standard Model as the most accurate theory of subatomic particles to date.

Despite its success in describing the fundamental particles and their interactions, the Standard Model of particle physics is not considered a complete or final theory of nature. Several significant phenomena lie beyond its explanatory power, leading scientists to search for new theories that extend or supersede the Standard Model.

One of the primary limitations of the Standard Model is its inability to account for dark matter [24, 25]. Astrophysical observations, such as the rotation curves of galaxies and gravitational lensing, strongly suggest that about 85% of the matter in the universe

is dark matter — an invisible form of matter that does not interact with electromagnetic radiation. However, the Standard Model does not include any particle that could be identified as a dark matter candidate.

In addition to dark matter, the Standard Model is unable to explain even more mysterious dark energy, which is thought to constitute approximately 70% of the universe's energy density. Dark energy is associated with the accelerated expansion of the universe, as first observed through supernova data in the late 1990s [26]. While the Standard Model successfully describes the known particles and forces, it does not provide any mechanism for the cosmological constant or the energy driving this expansion.

A further significant limitation of the Standard Model is that it does not incorporate the gravitational interaction. The theory describes three of the four fundamental forces, but does not include a quantum description of gravitation. General relativity, the classical theory of gravitation, is an effective description of large-scale phenomena. However, it is in conflict with quantum mechanics at very small scales, such as near black holes or in the early universe [27, 28]. The absence of a unifying framework that includes both gravitation and the other forces remains a critical gap in our understanding of Nature.

Furthermore, the Standard Model itself is not without its own set of unresolved issues. To illustrate, the model does not explain the observed imbalance between matter and antimatter in the universe [29]. According to the Standard Model, matter and antimatter should have been created in equal amounts during the Big Bang. However, observations indicate that the universe is predominantly composed of matter. Additionally, the neutrino masses present a challenge to the theory. In its original formulation, the Standard Model assumes neutrinos are massless. However, experiments have shown that neutrinos do have tiny, but non-zero masses [30-33], indicating that the theory must be modified or extended to account for this.

Overall, although the Standard Model has been remarkably successful in explaining a number of fundamental physical phenomena, its inability to explain several fundamental questions suggests that it is an incomplete theory. Consequently, the last few decades have been marked by further attempts of scientists to create a fundamental theory, the so-called Theory of Everything, which makes correct predictions at any energy scale, explains all aspects of the universe, contains the Standard Model and the General Relativity as its limits. It was supposed that the strict consistency of quantum theory and gravitation would lead to a beautiful unique solution. Over the course of the past century, there have been numerous attempts to extend the boundaries of our knowledge and integrate the two limits.

Nevertheless, despite a series of attempts, beginning with the Kaluza–Klein theory and the Einstein–Maxwell–Dirac equations and continuing with the String Theory and M-Theory, decades later, without reaching or even significantly approaching the goal, now the focus has shifted to less ambitious, but practically useful theories that describe particular physical systems under particular conditions, known as *Effective Field Theories*. These theories are not valid across the entire energy spectrum and often describe fewer degrees of freedom than are required in the most general case, but they turned out to be a practical path to the fundamental goal of theoretical particle physics.

The Effective Field Theory approach was systematically expounded by Steven Weinberg in [34, 35]. The basic idea of Effective Field Theories [36-39] is that all things look simpler being observed from a distance. The most illustrative example is a system of electric charges situated together in a space region of characteristic size L. If we study physical effects of this distribution from a large distance $r \gg L$, we do not care about de-

tails. All we need is to approximate the system with a few terms of the multiple expansion with each subsequent term being multiplied by a higher power of L/r.

A similar phenomenon occurs in particle physics, with the only distinction that now the criterion for the difference between the two limits is the characteristic energy E. As in the case of electric charge distribution, where we do not need details at small distances, in particle physics study of a system at energy scale E does not require our knowledge at much higher scale $\Lambda \gg E$. When the energy scale $E \sim \Lambda$, all previously neglected interactions become significant (as well as in the case of electric charges at $r \sim L$) and perturbation theory is no longer applicable. In the context of effective field theory, Λ is called the cutoff parameter and is used to denote the scale at which the loops of slow modes are cut off (see, for example, [40, 41]) in Wilson's approach to the renormalization group[1].

The scale Λ may be characterized by a set of parameters. The values of these parameters can be extracted from experiments and their number depends on the desired level of precision in the prediction. In this manner, it is possible to theoretically differentiate energy scales on which physical systems can be described theoretically, without recourse to the fundamental theory. Details of the fundamental theory on the researched scale E are therefore encoded into the aforementioned parameters. It follows that a properly constructed effective field theory offers a more straightforward and equally precise account of physics at the energy scale of interest.

Additional structures in the effective Lagrangian can be built combining all possible terms containing all possible fields, their products and derivatives in order to preserve all symmetries. It is not difficult to guess that the number of terms that can be added to the considerations is infinite. The solution to treating a Lagrangian with an infinite number of terms lies in the feature of all effective field theories to contain one or more small expansion parameters that control possible influence of the physics we choose to neglect upon the degrees of freedom we choose to keep. In particle physics, such a small parameter is often the ratio $\delta = E/\Lambda$. This approach is based on the successful experience of creating models and describing phenomena without including effects that have not yet been discovered and cannot be verified experimentally. The small parameter δ controls how well we describe the full theory using the approximation by way of effective field theory.

Consequently, all supplementary terms are represented in the effective Lagrangian, which is multiplied by a priori arbitrary coupling constants, known as Wilson coefficients. The process of determining the precise values of these coefficients is known as matching and is typically conducted at the level of individual amplitudes and up to the desired order in the loop expansion.

One might be confused by the fact that effective field theories can contain an infinite number of parameters. Honestly speaking, such a theory seems to be unpredictable, and therefore useless, since an infinite number of Wilson coefficients have to be calculated. It can, however, become a valuable tool if any low-energy experiment with finite precision is described by a finite number of parameters. In such a case, a finite number of measurements are required to determine the values of these parameters.

It is therefore crucial to determine which degrees of freedom are relevant for describing

[1]Wilson developed an approach of describing field theories by the functional integral method, what makes distinction between renormalizable and non-renormalizable theories. The review of Wilson's ideas can be found in [42]. Furthermore, an example of this approach applied to the φ^4-theory can be found in Chapter 12 of [43].

the system under investigation at the specified energy scale, denoted by E, in order to construct an effective field theory. These variables will be used to construct the effective Lagrangian. The process of determining the relative importance of each term at a given energy scale, E, is known as *power counting*. It allows to organize the computations and single out the terms that make the most relevant contributions. It is possible to make a theory increasingly complex by adding less and less relevant structures, but then one will soon have to deal with extremely complex calculations that give small corrections that are imperceptible in experiments and which must therefore be neglected.

In the majority of cases, power counting can be performed based on the dimensions of the interaction terms alone. Only the terms up to a fixed dimension are retained, and interactions of higher dimensions are neglected due to their progressively diminished relevance as they are suppressed by higher and higher powers of the small parameter δ.

A contemporary strategy for probing the origins of Beyond Standard Model (BSM) physics entails the implementation of highly precise empirical investigations. The objective is to identify potential discrepancies between experimental results and the model's predictions. As experimental techniques continue to improve, yielding increasingly precise measurements at the percent level or better, it becomes imperative that theoretical predictions achieve comparable levels of accuracy. Nevertheless, leading-order (LO) and even next-to-leading order (NLO) calculations within perturbative quantum field theory (QFT) frequently fail to meet the requisite precision.

To address this gap, it is necessary to develop new methodologies and tools for achieving next-to-next-to-leading order (NNLO) accuracy in calculations. In recent years, there has been a notable increase in the drive towards achieving NNLO accuracy, with significant advances being made in this regard. This endeavor is driven by the recognition that higher-order calculations are indispensable for attaining precise theoretical predictions that can align with the rigorous standards set by experimental data, particularly in the context of high-energy particle collisions, such as those conducted at the LHC.

One of the primary motivations for pursuing NNLO precision is the potential it offers for uncovering subtle yet crucial discrepancies from the SM that could provide compelling evidence for BSM phenomena. Such deviations may be observed in processes involving the Higgs boson, vector boson scattering, or rare decay channels, where it is imperative to minimize theoretical uncertainties to detect new physics. Furthermore, NNLO calculations assist in reducing the dependence on unphysical parameters, such as renormalization and factorization scales, which is vital for enhancing the reliability of theoretical predictions.

Notwithstanding the considerable advancements that have been made, the complete automation of NNLO computations continues to represent a significant challenge. While automated tools have been developed to a considerable extent, certain complex processes – such as those involving multi-loop integrals [44-49] or intricate final states – still necessitate substantial computational resources and sophisticated algorithms. The conjunction of these theoretical challenges with the necessity for augmented computational power signifies that additional work is required before NNLO calculations can be fully automated and applied to all pertinent processes in particle physics.

Nevertheless, the continued development of NNLO techniques offers significant promise. As we advance the frontiers of precision in both theoretical and experimental pursuits, the prospect of uncovering new physics beyond the Standard Model becomes increasingly plausible. This makes this an exhilarating and pivotal domain of contemporary particle physics research.

At the present time, particle physics researchers are particularly interested in the Higgs boson. The study of processes involving this particle is of significant importance in modern particle physics, both within the framework of the SM and beyond it. The discovery of the Higgs boson at CERN's Large Hadron Collider (LHC) in 2012 confirmed the existence of the mechanism that gives mass to elementary particles, a key feature of the SM. This mechanism is responsible for imparting mass to particles, while leaving some of them massless. An understanding of the manner in which the Higgs boson interacts with other particles serves to validate this central tenet of the SM. It is therefore imperative that precision studies of the Higgs be conducted in order to confirm the theory's predictions and refine its parameters.

In the context of theoretical physics, the Higgs boson plays a pivotal role in probing potential new physics beyond the Standard Model. Theoretical extensions of the SM, such as supersymmetry or theories involving extra dimensions, predict modifications to the properties of the Higgs boson or its interactions with other particles. Any discrepancies between the SM predictions and the observed rates of Higgs production, decay modes, or couplings could serve as an indication of the presence of new physics. Furthermore, the Higgs boson may be linked to unresolved issues within the SM, such as the nature of dark matter or the stability of the universe at high energy scales. Consequently, following the discovery of the Higgs boson, the principal objective of high-energy colliders is to ascertain its properties.

Some Higgs observables were measured at the LHC during Run I [50-56] and Run II [57-59], however, still with relatively large uncertainties. One of the most important mechanisms for Higgs boson production at hadron colliders is the Higgs-strahlung process which refers to the associated production of a Higgs boson and a massive SM gauge boson in proton–proton fusion. This process plays a very important role in the determination of the Higgs boson properties. In accordance with the Standard Model predictions, the Higgs boson decays via the $H \to b\bar{b}$ channel. The most sensitive channel for detecting such a decay is the associated production of a Higgs and a massive electroweak boson, although its cross section is rather small in comparison with gluon-gluon fusion Higgs production. It can thus be surmised that forthcoming LHC measurements of VH production in proton–proton collisions will permit the postulation of the existence of non-standard Higgs interactions. The Standard Model Effective Field Theory (SMEFT) offers a systematically improvable theoretical framework for analyses of effects in processes beyond the Standard Model that can be used to probe the Higgs production and decay in colliders.

The study of perturbative corrections within the Standard Model for the process $PP \to VH$ is a highly developed field of research. The QCD corrections for WH production at NLO have been obtained in [60–62], while those for ZH production in [63, 64]. The NLO SUSY-QCD corrections have been calculated in [65]. NLO electroweak corrections have been calculated in [66, 67], and combined NLO QCD+EW corrections are also available [68–70].

Inclusive NNLO QCD corrections for $PP \to ZH$ have been available for quite some time [71] and are implemented in the program VH@NNLO [71–74]. The calculation of differential QCD corrections has been conducted up to NNLO in [75–77], including the $H \to b\bar{b}$ decay at NLO [77, 78] and at NNLO for WH [79] and ZH [80]. In [81], fully differential NNLO results for VH observables have been calculated, including the decays of the vector boson to leptons and the Higgs boson to b-quarks with off-shell propagators of the vector and Higgs bosons. In [82], the WH production in association with a hard gluon jet has been considered. The combination of fixed-order QCD computations with parton

showers has been studied at the next-to-leading order with parton showers (NLO+PS) in association with up to one jet [69, 83–85] and at NNLO+PS [86, 87].

A notable difference between the WH and ZH final states is that, beginning at the NNLO in QCD, the latter receives substantial contributions from the $gg \to ZH$ process. The loop-induced gluon-initiated contributions for this process, as outlined in [88, 89], enter at order $\mathcal{O}(\alpha_s^2)$ which is formally at NNLO considering the $PP \to VH$ process. However, they contribute approximately 6% of the total NNLO cross section, with the potential for this contribution to be twice as large in the boosted Higgs boson regime [90, 91]. Furthermore, the gluon-initiated subprocess is very sensitive to modified Yukawa couplings and the presence of non-standard particles running in the loop [90]. For these reasons, the NLO corrections to this process are of great significance. The aforementioned corrections contain two-loop integrals involving the masses of the Higgs boson, weak bosons and the top-quark, the analytical forms of which are currently unknown. Consequently, the QCD corrections have been calculated in various approximations so far [92, 93]. The two-loop virtual corrections to the process $gg \to ZH$, including massive top-quarks in the loops were calculated in [94]. Additionally, soft gluon resummation for the $gg \to ZH$ process has been calculated in [95].

With regard to the impact of higher-dimensional operators within the Standard Model Effective Field Theory, the NLO QCD corrections to the contributions to WH and ZH production have been the subject of investigation in [96–100]. In [101], all dimension-six operators that contribute to the $PP \to VH$ processes at leading order are considered and the next-to-leading order QCD corrections are interfaced with parton showering and hadronization in Pythia8 according to the POWHEG method. The accuracy of final state NNLO QCD plus parton shower with a subset of relevant dimension-six operators has been achieved in [102] for ZH production with subsequent decay of the Higgs to $b\bar{b}$-pair. The objective of the of calculations of the $PP \to VH \to l\bar{l}\ b\bar{b}$ process is to account for all relevant contributions of dimension-six operators to both $PP \to VH$ and $H \to b\bar{b}$ subprocesses, and to combine the production and the decay processes including higher-order QCD and EW corrections at fixed order, as well as parton shower effects.

This thesis examines the production of charged electroweak and Higgs bosons, followed by the subsequent decay of the electroweak boson into a lepton–antilepton pair. A comprehensive calculation of the NNLO QCD corrections to the differential cross section is presented, encompassing the complete set of pertinent dimension-six operators that give rise to non-standard interactions between quarks and anti-quarks, vector bosons, and the Higgs boson within the SMEFT framework. These precise theoretical predictions are of great importance for the investigation of potential deviations from the Standard Model and for the guidance of experimental searches for new physics.

Furthermore, a Python-based code has been developed for the numerical validation of analytic computations for any permissible value of the center-of-mass energy $\sqrt{s}$. This code is highly flexible and modular, allowing for straightforward modifications to accommodate different processes and extensions of the Standard Model. Moreover, it is structured in a way that facilitates easy expansion to incorporate new interactions or higher-order corrections, thus making it a valuable tool for future investigations in particle physics.

In this thesis, we discuss in detail the contribution of dimension-six operators to the differential cross section of the process $q\bar{q}' \to WH + X$ with the subsequent decay of the weak boson into a lepton-antilepton pair. We also provide an overview of the tools and theoretical background required for this analysis. The thesis is organized as follows:

In **Chapter 1**, we provide an overview of the significant milestones in the advancement of high-energy physics, with a particular focus on the findings derived from the associated electroweak and Higgs boson production following parton collisions. We examine the fundamental distinction between the two sub-processes that contribute to the overall scattering cross-section and review a substantial body of scientific literature devoted to this topic.

In **Chapter 2**, we present the principal properties of the Standard Model Effective Field Theory and introduce the notations that will be used throughout the remainder of this thesis. Furthermore, this chapter presents a discussion of a process in the Standard Model and its modification in the theory which is of critical importance for this study.

Chapter 3 provides an introduction to the method employed to calculate the differential scattering cross section in this work, namely the helicity amplitude method. This method is particularly advantageous for such calculations, as it not only eliminates the complexity associated with working with the γ_5 matrix in d-dimensional space, but also allows to automate the calculation process with reduced efforts.

Chapter 4, which constitutes the core of this thesis, provides a detailed account of the calculation of the partonic cross section by the helicity amplitude method within the Standard Model Effective Field Theory, as well as within the Standard Model itself. It also discusses the process of renormalization and the derivation of the relevant renormalization constants for the Wilson coefficients.

In **Chapter 5**, we present a detailed account of the integration over phase space, with a particular emphasis on a method that partitions the phase space into two distinct regions: the Born phase space and the radiation phase space. This approach permits a more efficacious management of divergences by distinguishing between regions with and without supplementary radiation, thereby facilitating the treatment of soft and collinear emissions.

In **Chapter 6**, we perform phenomenological studies discussing the interplay of higher-order QCD corrections and higher-dimensional SMEFT operators in WH production at the LHC.

Chapter 7 summarizes the key findings of this thesis and presents the conclusions.

The **Appendices** provide supplementary material to support the main study. Appendix A presents the explicit results of the helicity amplitudes. However, some of those results are too large to be fully included in the text. Instead, they are available in the auxiliary files accompanying this thesis. Appendix B offers an introduction to Dirac algebra in a fractional space-time dimension, with a detailed explanation of how to handle the γ_5 matrix and the Levi-Civita symbol. Appendix C introduces the helicity formalism, demonstrating its application to both massless and massive particles. It also explains how spinors can be represented for numerical computations.

2 Associated Electroweak and Higgs Boson Production

This chapter presents a discussion of the process of associated Higgs boson production with a charged gauge boson W. Section 1 is devoted to the description of this process in the framework of the Standard Model. Section 2 describes in detail the Standard Model Effective Field Theory which is the focus of our study. Section 3 discusses the relevant dimension-six operators and the Feynman rules they generate, which are discussed later in this thesis to calculate the total cross section.

2.1 Hadronic cross section

The cross section represents a fundamental quantity in particle physics, serving as a crucial element for comprehending and characterizing the interactions between particles. It represents the probability of occurrence of a specific interaction or scattering event when two particles collide. Cross sections provide a quantitative way to compare the probability of different processes. They serve as the bridge between theoretical predictions and experimental measurements, allowing physicists to test the validity of models and to search for signs of new physics beyond the Standard Model.

Mathematically, the differential cross section $d\sigma/d\Omega$ describes how the probability of a scattering event depends on the angle of scattering Ω and the energy of the incident particles. This quantity can be integrated over a range of angles or energies to yield the total cross section σ

$$\sigma = \int \frac{d\sigma}{d\Omega} d\Omega. \tag{2.1}$$

A comparison of theoretical calculations of cross sections with experimental data allows the extraction of valuable information about the fundamental forces and particles that govern the universe. For example, precise measurements of cross sections in high-energy particle collisions, such as those conducted at the LHC, have been instrumental in the discovery of the Higgs boson and the verification of the Standard Model's predictions. Moreover, cross sections are not only useful for confirming known physical phenomena but also for probing the unknown. A discrepancy between the predicted and measured values of cross sections could indicate the presence of new particles or interactions not accounted for by the Standard Model.

The calculation of scattering cross sections becomes more complex since protons are composite objects, composed of quarks and gluons, collectively referred to as partons. In the parton model, hadrons are conceived as extended objects comprising constituents held together by their fundamental interactions. At the level of the parton model, it is assumed that hadrons can be described in terms of virtual partonic states. However, the structure of these states cannot be calculated, which is why the so-called parton distribution functions (PDFs) become crucial.

The parton distribution function, denoted as $f_i(x, Q^2)$, describes the probability of finding a specific type of parton i (such as a quark, antiquark, or gluon) inside a proton, carrying a fraction x of the proton's total momentum, when probed at a certain energy scale Q^2. In the context of hadron colliders such as the LHC, the total cross section for a particular process is obtained by convoluting the PDFs with the partonic cross section, $\hat{\sigma}_{ij}(x_1, x_2, Q^2)$, which represents the cross section for the interaction between the partons

themselves. The partonic cross section is calculated using perturbative QCD and depends on the momentum fractions x_1 and x_2 of the two colliding partons. The total cross section for a process is then given by

$$\sigma = \sum_{i,j} \int_0^1 dx_1\, dx_2\, f_i(x_1, Q^2) f_j(x_2, Q^2)\, \hat{\sigma}_{ij}(x_1, x_2, Q^2), \tag{2.2}$$

where i, j label the types of partons (quarks, antiquarks, or gluons), x_1, x_2 are the momentum fractions of the two partons from the two colliding protons, $f_i(x_1, Q^2)$ and $f_j(x_2, Q^2)$ are the PDFs for partons i and j, respectively, and $\hat{\sigma}_{ij}(x_1, x_2, Q^2)$ is the partonic cross section which describes the fundamental interaction between the two partons.

The partonic cross section $\hat{\sigma}_{ij}$ represents the probability that two partons i and j will interact at a given center-of-mass energy determined by the momentum fractions x_1 and x_2 and the energy scale Q^2. In contrast to the total hadronic cross section, which includes contributions from all possible partons and their respective PDFs, the partonic cross section focuses on the fundamental interaction between the partons themselves. This makes it an essential component of the total cross section calculation.

The differential partonic cross section can be calculated in accordance with the following formula

$$d\hat{\sigma}_{ij\to f} = \frac{1}{2s} dPS_f \left|\mathcal{M}_{ij\to f}\big(p_i, p_j|\{p_f\}\big)\right|^2. \tag{2.3}$$

In Eq. (2.3), the parameter s represents the Lorentz-invariant Møller flux, which depends on the center-of-mass energy and satisfies the relation $Q = \sqrt{s}$. The quantity dPS_f denotes the final-state phase-space element which is also a Lorentz invariant. Finally, $\mathcal{M}_{ij\to f}$ is the scattering matrix element of the process under consideration which is also invariant under Lorentz transformations. All of these parameters are dependent upon the momenta of the particles participating in the process, which are p_i and p_j for the incoming partons and $\{p_f\}$ for all the final-state particles. In order to obtain the total unpolarized cross section σ, integration over the phase space must be carried out

$$\hat{\sigma}_{ij\to f} = \frac{1}{2s} \int dPS_f \overline{\left|\mathcal{M}_{ij\to f}\big(p_i, p_j|\{p_f\}\big)\right|^2}, \tag{2.4}$$

where, in order to obtain the squared matrix element, it is necessary to perform a summation over the colors of the final-state particles and an averaging over the spin and color of the initial-state particles.

The primary objective of this thesis is to calculate the squared matrix element for the process $q\bar{q}' \to WH + X$, where X denotes possible final-state gluons or quarks, with subsequent electroweak boson decay into a lepton-antilepton pair $W \to l\bar{l}$. This is achieved within the context of both the Standard Model Effective Field Theory and the Standard Model which represents its special case.

2.2 Higgs Strahlung in the Standard Model

At the LHC, which collides protons, the dominant contribution to the associated Higgs boson production cross section comes from partonic subprocesses involving quarks and gluons. Protons are composed of valence u and d quarks, as well as gluons and sea quarks $(\bar{u}, \bar{d}, s, \bar{s}, c, \bar{c})$. It should be noted, however, that this list is not exhaustive, as a Higgs

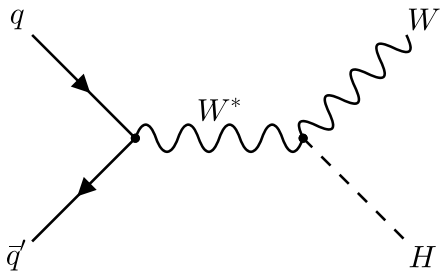

Figure 1: Drell-Yan-like associated electroweak and Higgs boson production $q\bar{q}' \to VH$.

boson can also be produced in association with an electroweak boson through processes involving heavier quarks such as top and bottom quarks [104]. These channels contribute only about 1% and 0.1% of the total cross section, respectively, and can safely be neglected in our study, which focuses on $pp \to WH$ production.

The process $q\bar{q}' \to WH + X$ initiated by two quarks and illustrated in Fig. 1, is of greater interest to us and requires more attention. In this case, a quark and an antiquark annihilate into a virtual weak boson which subsequently emits a Higgs boson and then decays into a lepton–antilepton pair. A comparison of the well-known Drell-Yan process $q\bar{q} \to \gamma^*/Z \to l\bar{l}$ [105] reveals that it is highly analogous to the process we consider. This allows us to refer Higgs boson production to the Drell-Yan process and factorize our cross section into two parts

$$\hat{\sigma}_{ij\to WH+X} = \int dq^2 \frac{d\Gamma_{W^*\to WH}(q^2)}{dq^2}\, \hat{\sigma}_{ij\to W+X}. \tag{2.5}$$

The first part of the cross section in Eq. (2.5) describes the emission of the Higgs boson by the weak boson, whereas the second part is responsible for the Drell-Yan-like process of quark-antiquark annihilation and the production of a weak boson with mass $\sqrt{q^2}$. Notable achievements in the calculation of the second part include higher order QCD corrections and were reviewed in Chapter 1. In our case, the Higgs boson emission by the weak boson necessitates only the leading-order contribution and can be described by the well-known differential decay function [106, 107]

$$\begin{aligned}\frac{d\Gamma_{W^*\to WH}(q^2)}{dq^2} = \frac{\sqrt{2}G_F}{4\pi^2}\frac{M_W^4}{\left(q^2 - M_W^2\right)^2}\times \\ \times \lambda^{1/2}\left(M_W^2, M_H^2; q^2\right)\left(1 + \frac{q^2}{12M_W^2}\lambda\left(M_W^2, M_H^2; q^2\right)\right),\end{aligned} \tag{2.6}$$

where $G_F \approx 1.167 \cdot 10^{-5}\,\mathrm{GeV}^{-2}$ is the Fermi constant introduced by Enrico Fermi to describe the weak interaction in his theory of beta decay [108] and the Källén function

$$\lambda(x, y; z) = \left(1 - \frac{x}{z} - \frac{y}{z}\right)^2 - \frac{4xy}{z}. \tag{2.7}$$

2.3 Standard Model Effective Field Theory

For the sake of brevity, we will not discuss famous and simpler examples of effective field theories, such as the Fermi Theory[2] and others. The Standard Model Effective Field Theory will now be introduced, as our computations of the Higgs Strahlung process will be carried out in the context of this theory. The Standard Model of Elementary Particles, which describes the interactions of quarks and leptons using electromagnetic, weak, and strong forces, is a well-established theory that has been tested extensively at colliders and has proven to be accurate up to very high energy scales. However, there is currently a consensus among the scientific community that the Standard Model does not fully account for all aspects of nature and that it should be extended to accommodate new phenomena.

It is not possible to state with certainty that no new, as yet undiscovered, particle exists in nature. In contrast, search for new particles is well motivated and, upon reflection, continues to engage the attention of physicists. However, given the absence of evidence for new physics in modern colliders, it can be assumed, as previously, that the still undiscovered particles have masses that are too large in comparison with the weak scale and can be integrated out from the more global theory. Therefore, the new effective field theory can contain only particles of the Standard Model from whose fields we should construct additional terms to the Standard Model Lagrangian and build the Standard Model Effective Field Theory. This theory has the same degrees of freedom and local symmetry $SU(3)_c \times SU(2)_L \times U(1)_Y$, where subscripts denote color, left-handed chirality and hypercharge, respectively.

Prior to the construction of an effective Lagrangian, it is prudent to briefly recall which fields are included in the Standard Model Lagrangian (for further details, see, for example, [110, 111]). The following types of fields are included

1. Vector fields G^a_μ, W^i_μ, B_μ (with $a = \overline{1,8}$, $i = \overline{1,3}$) which correspond to the gauge groups $SU(3)_c$, $SU(2)_L$ and $U(1)_Y$, respectively;

2. Three generations of fermions:

- left-handed quarks q_i (doublets under $SU(2)_L$),
- right-handed quarks u_i, d_i (singlets under $SU(2)_L$),
- left-handed leptons l_i (doublets under $SU(2)_L$),
- right-handed leptons e_i (singlets under $SU(2)_L$);

3. Scalar Higgs field φ (doublet under $SU(2)_L$).

In order to reduce the complexity of notations, it is common practice to introduce the gauge field strength tensors

[2]The original Fermi's framework [109] contains a description of neutron decay. As an effective field theory, it is understood in the sense of the low-energy limit of the Standard Model below the W-boson mass. At this energy scale, heavy particles such as W and Z bosons, the Higgs boson and the top quark, are integrated out and do not participate in interactions. This allows for the construction of an effective Lagrangian that contains only leptons, gluons, photon, and the other five generations of quarks. This aspect is explained in detail in section 3.1 of [43].

$$
\begin{aligned}
B_{\mu\nu} &= \partial_\mu B_\nu - \partial_\nu B_\mu, \\
W^i_{\mu\nu} &= \partial_\mu W^i_\nu - \partial_\nu W^i_\mu - g_W \varepsilon^{ijk} W_{\mu j} W_{\nu k}, \\
G^a_{\mu\nu} &= \partial_\mu G^a_\nu - \partial_\nu G^a_\mu - g_s f^{abc} G_{\mu b} G_{\nu c},
\end{aligned}
\tag{2.8}
$$

where g_W and g_s are the coupling constants which correspond to $SU(2)$ and $SU(3)$, respectively, ε^{ijk} is the Levi-Civita pseudotensor, f^{abc} are structure constants of the gauge group $SU(3)$. In addition, the complex conjugate of the Higgs field is designated as

$$
\widetilde{\varphi}^i = \varepsilon^{ij} \varphi^*_j. \tag{2.9}
$$

Covariant derivative of a field $\mathcal{F}$ is defined as

$$
D_\mu \mathcal{F}^{\alpha j} = \left[\delta^\alpha_\beta \delta^j_k \left(\partial_\mu + i g_B Y_{\mathcal{F}} B_\mu \right) + i g_W \delta^\alpha_\beta \left(\frac{\tau^i}{2} \right)^j_k W^i_\mu + i g_s \delta^j_k \left(\frac{\lambda^a}{2} \right)^\alpha_\beta G^a_\mu \right] \mathcal{F}^{\beta k}, \tag{2.10}
$$

where g_B is the coupling constant which corresponds to group $U(1)$, $Y_{\mathcal{F}}$ is the hypercharge of field $\mathcal{F}$, τ^i and λ^a are Pauli and Gell–Mann matrices, respectively.

The dimensions of field operators can be derived from the condition of zero dimension of the action. The canonical dimensions of operators are determined exclusively from the field contents, excluding any potential dimensional coupling constants. It can be readily deduced that the Standard Model Lagrangian comprises solely dimension-two and dimension-four operators constituted from the elements delineated in **Table 1**. The only dimension-two operator in the Standard Model Lagrangian is $\varphi^\dagger \varphi$. It is important to note that the derivatives, as well as the covariant derivatives and the d'Alembert operator, possess non-zero mass dimension, given that they contain gauge fields and ∂_μ is equivalent to the momentum operator.

	Field	**Dimension**
Gauge fields	$G^a_{\mu\nu}$	2
	$W^i_{\mu\nu}$	2
	$B_{\mu\nu}$	2
Fermions	Left-handed leptons (incl. neutrinos) l_s	3/2
	Right-handed leptons (incl. neutrinos) e_s	3/2
	Left-handed quarks q_s	3/2
	Right-handed quarks u_s, d_s	3/2
Higgs	φ	1
Derivatives	Usual derivative ∂^μ	1
	Covariant derivative D^μ	1
	d'Alembert operator $\Box = D^\mu D_\mu$	2

Table 1: Dimensions of the Standard Model fields.

The Standard Model Effective Field Theory is founded upon the dimensions of field operators and the decoupling of heavy particles with masses of order $\Lambda \gg v$ [112] (where $v = 246\,\text{GeV}$ is the vacuum expectation value) which are not yet discovered and have been integrated out. Such an approach leads to the appearance in the Standard Model Lagrangian of higher-dimensional operators suppressed by powers of Λ. Therefore, the Standard Model effective Lagrangian can be written schematically as

$$\mathcal{L}_{SMEFT} = \mathcal{L}_{SM} + \frac{1}{\Lambda}\sum_i C_i^{(5)} Q_i^{(5)} + \frac{1}{\Lambda^2}\sum_i C_i^{(6)} Q_i^{(6)} + \ ..., \tag{2.11}$$

where $Q_i^{(k)}$ are dimension-k operators and $C_i^{(k)}$ are corresponding Wilson coefficients.

The Lagrangian should contain only independent operators, that is, operators that cannot be expressed as a linear combination of other operators or their Hermitian conjugates and that do not satisfy the Standard Model equations of motion up to a total derivative. Furthermore, operators may be reduced through the application of integration by parts, field redefinition, or Fierz transformations. These methodologies ultimately yield relations between operators which permit the reduction of their number and, consequently, the streamlining of the effective theory description.

The only non-trivial dimension-five operator [113] is

$$Q_{fg}^{(5)} = \left(\widetilde{\varphi}^\dagger l_f\right)^T C \left(\widetilde{\varphi}^\dagger l_g\right) = \varepsilon_{jk}\varepsilon_{mn}\varphi^j\varphi^m \left(l_f^k\right)^T C\, l_g^n, \tag{2.12}$$

where f, g are flavor indices and $C = i\gamma^2\gamma^0$ is the charge conjugation matrix. Operator $Q^{(5)}$ provides masses of Majorana neutrinos after electroweak symmetry breaking

$$m_\nu \sim \frac{v^2}{2\Lambda} C^{(5)}. \tag{2.13}$$

A calculation based on the experimental data regarding the masses of neutrinos [114-117] leads to the conclusion that $C^{(5)}/\Lambda \lesssim 10^{-15}\text{GeV}^{-1}$. This result suggests that the leading contribution to the BSM predictions is provided by the next level operators, specifically the dimension-six ones. Additionally, the dimension-five operator violates lepton number L. However, integrating out new particles whose interactions conserve L cannot generate the dimension-five operator. In such a case, the effective expansion of the Standard Model Lagrangian begins with dimension six.

The role of dimension-six operators in describing the low-energy effects of heavy particles has long been recognized (see, for example, [118, 119]). The number of dimension-six operators is considerably greater than that of dimension-five operators. A minimal and non-redundant set of operators is referred to as a basis, and there are an infinite number of equivalent bases. A number of these have been described in the literature. The most renowned is the so-called Warsaw basis [120], typically employed for computations and comprising 59 dimension-six operators when lepton number conservation is enforced. A comprehensive list of these operators, along with four additional ones that violate lepton number, can be found in [121]. Additionally, the SILH basis (Strongly Interacting Light Higgs) is a suitable option, as outlined in [122-124]. In this thesis, however, we utilize operators constructed in the Warsaw basis.

The dimension-seven operators are presented in [125]. Such operators are known to violate lepton number as well as all odd-dimensional operators. The methodology for obtaining higher-dimensional operators is described in [120]. However, as the corrections provided by dimension-eight operators are already suppressed by the fourth power of Λ,

their effects should be insignificant in comparison with the effects given by dimension-six operators. For this reason, in Lagrangian (2.11), we will take only the group of operators suppressed by Λ^2 under our considerations.

Furthermore, it is important to note that additional terms in the effective Lagrangian have an impact on the Standard Model values [126]. For instance, the vacuum expectation value undergoes a shift as follows

$$\hat{v} = v\left(1 + \frac{3C_H}{8\lambda}v^2\right), \tag{2.14}$$

where $v = 246\,\text{GeV}$ is the Standard Model value, C_H is the Wilson coefficient which corresponds to the operator $Q_H^{(6)}$ (see [121]) and divided by Λ^2. Henceforth, parameter Λ will be absorbed by the Wilson coefficients, thus simplifying the notation. Consequently, the values C_i become small and have dimension

$$[C_i] = \text{mass}^{-2}. \tag{2.15}$$

The coupling constants of the gauge groups $U(1)$, $SU(2)$, and $SU(3)$ are presented in the following manner

$$\hat{g}_B = g_B\left(1 + C_{HB}\hat{v}^2\right), \quad \hat{g}_W = g_W\left(1 + C_{HW}\hat{v}^2\right), \quad \hat{g}_s = g_s\left(1 + C_{HG}\hat{v}^2\right), \tag{2.16}$$

where g_B, g_W and g_s are the corresponding Standard Model couplings.

The Higgs boson mass m_H is now given by

$$M_H^2 = m_H^2\left[1 + \left(2C_{H\Box} - \frac{1}{2}C_{HD} - \frac{3C_H}{2\lambda}\right)v^2\right], \tag{2.17}$$

and the charged electroweak bosons mass

$$\begin{aligned} M_W^2 = m_W^2\Bigg[1 + v^2\left(C_{HW} + \frac{3C_H}{4\lambda}\right) + v^4\,\frac{3C_H}{4\lambda}\left(2C_{HW} + \frac{9C_H}{16\lambda}\right) + \\ + v^6\,\frac{27C_H^2C_{HW}}{32\lambda^2} + v^8\,\frac{27C_H^3C_{HW}}{128\lambda^3} + v^{10}\,\frac{81C_H^4C_{HW}}{4096\lambda^4}\Bigg]. \end{aligned} \tag{2.18}$$

In Eqs. (2.14) and (2.16)–(2.18), the Wilson coefficients C_i correspond to dimension-six operators $Q_i^{(6)}$. The parameter λ is the self-interaction constant of the Higgs field, which plays a key role in the mechanism of spontaneous symmetry breaking.

The neutral electroweak boson mass requires even more extensive corrections which are, however, irrelevant for the purposes of this thesis.

2.4 Relevant dimension-six operators

This thesis considers the process $q\bar{q}' \to WH + X$, with subsequent decay of the weak boson into a lepton-antilepton pair, described by dimension-six operators within the Standard Model Effective Field Theory. Accordingly, the amplitude of the aforementioned process contains Wilson coefficients divided by the squared scale of new physics, which we denote as Λ. Our objective is to calculate the squared matrix element for the process at order $O(C_i)$. The Feynman rules for all possible processes in the Standard Model Effective Field Theory provided by the dimension-six operators have already been reached automatically in reference [127]. In our research, we consider four dimension-six operators that make

it possible to produce the WH directly after a quark-antiquark collision without any intermediate state. These dimension-six operators are given by reference [121]

$$\begin{aligned} Q_{uW} &= \big(\bar{q}_f \sigma^{\mu\nu} u_g\big)\tau^i \widetilde{\varphi}\, W^i_{\mu\nu}, & Q^{(3)}_{\varphi q} &= \Big(i\varphi^\dagger \overset{\leftrightarrow}{D}{}^j_\mu\, \varphi\Big)\big(\bar{q}_f \tau^j \gamma^\mu q_g\big), \\ Q_{dW} &= \big(\bar{q}_f \sigma^{\mu\nu} d_g\big)\tau^i \varphi W^i_{\mu\nu}, & Q_{\varphi ud} &= \big(i\widetilde{\varphi}^\dagger D_\mu \varphi\big)\big(\bar{u}_f \gamma^\mu d_g\big), \end{aligned} \tag{2.19}$$

where f and g denote fermion flavor, $W^i_{\mu\nu}$ is the gauge field strength tensor defined in Eq. (2.8), τ^i and γ^μ are the Pauli and Dirac matrices, respectively,

$$\sigma^{\mu\nu} = \frac{i}{2}\left[\gamma^\mu, \gamma^\nu\right] \tag{2.20}$$

and the Hermitian derivatives

$$\begin{aligned} \varphi^\dagger \overset{\leftarrow}{D}_\mu \varphi &= (D_\mu \varphi)^\dagger \varphi, \\ \varphi^\dagger i \overset{\leftrightarrow}{D}_\mu \varphi &= i\varphi^\dagger \Big(D_\mu - \overset{\leftarrow}{D}_\mu\Big)\varphi, \\ \varphi^\dagger i \overset{\leftrightarrow}{D}{}^j_\mu \varphi &= i\varphi^\dagger \Big(\tau^j D_\mu - \overset{\leftarrow}{D}_\mu \tau^j\Big)\varphi \end{aligned} \tag{2.21}$$

with the covariant derivative D_μ defined in Eq. (2.10).

Operators (2.19) define the addition to the SM Lagrangian relevant for this thesis as follows

$$\delta\mathcal{L} = C_{uW}Q_{uW} + C_{dW}Q_{dW} + C^{(3)}_{\phi q}Q^{(3)}_{\phi q} + C_{\phi ud}Q_{\phi ud} \tag{2.22}$$

and generate the following Feynman rules

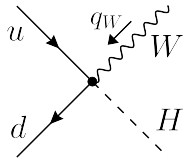

$$= iC_1[\gamma^\mu, \not{p}_W]P_L + iC_2[\gamma^\mu, \not{p}_W]P_R + iC_3\gamma^\mu P_L + iC_4\gamma^\mu P_R \equiv iA^\mu, \tag{2.23}$$

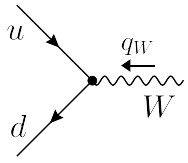

$$\begin{aligned} &= ivC_1[\gamma^\mu, \not{p}_W]P_L + ivC_2[\gamma^\mu, \not{p}_W]P_R \\ &\quad + i\left(S_3 + \frac{v}{2}C_3\right)\gamma^\mu P_L + \frac{iv}{2}C_4\gamma^\mu P_R \equiv iB^\mu. \end{aligned} \tag{2.24}$$

In Eqs. (2.23) and (2.24), the slashed weak boson momentum is defined classically as $\not{p}_W = \gamma^\mu p_{W\mu}$, P_L and P_R are left- and right-handed projectors, respectively, defined through the fifth Dirac matrix γ_5 as follows

$$P_L = \frac{1-\gamma_5}{2}, \qquad P_R = \frac{1+\gamma_5}{2}. \tag{2.25}$$

The coefficient S_3 represents the Standard Model term, which is dependent upon the specific type of weak boson and is equal to $S_3^{(W)} = g_W/\sqrt{2}$ in the context of W-production. The numbers C_i in Eqs. (2.23) and (2.24) are the result of dimension-six operators and are expressed in terms of Wilson coefficients. Furthermore, they are contingent upon the boson that is present in the final state. In the case of W boson production,

$$\begin{aligned} C_1 &= C_{uW}^{\dagger} V, & C_3 &= \sqrt{2} g_W v \big(V C_{\varphi q 3}\big), \\ C_2 &= V C_{dW}, & C_4 &= \frac{g_W v}{\sqrt{2}} \big(V C_{\varphi u d}\big), \end{aligned} \tag{2.26}$$

where all matrices C_i on the right-hand side are matrices of the Wilson coefficients, which correspond to the dimension-six operators by subscript indices. The matrix V represents the Calibbo–Kobayashi–Maskawa matrix (CKM-matrix) [128–130]

$$V_{fg} = \begin{pmatrix} V_{ud} & V_{us} & V_{ub} \\ V_{cd} & V_{cs} & V_{cb} \\ V_{td} & V_{ts} & V_{tb} \end{pmatrix} \approx \begin{pmatrix} 0.9737 & 0.2243 & 0.0038 \\ 0.2210 & 0.9750 & 0.0408 \\ 0.0086 & 0.0415 & 1.0140 \end{pmatrix}. \tag{2.27}$$

While the structure of Eqs. (2.23) and (2.24) appears to be highly similar, these two Feynman rules yield distinct results for two fundamental reasons. The first reason is that in the case of a four-point vertex, the momentum conservation law is given by the equations $p_1 + p_2 = p_W + p_H$ and $p_W = p_3 + p_4$. In contrast, in the case of a three-point vertex, the momentum conservation law is given by the equations $p_1 + p_2 = p_{W^*}$ and $p_{W^*} = p_W + p_H = p_3 + p_4 + p_H$. Therefore, we may conclude that $p_{W^*} \neq p_W$. This discrepancy in momentum leads to a different helicity structure.

The second reason is that in order to obtain the total amplitude, the four-point amplitude $\mathcal{M}_4^{\mu}$ must be contracted with the W boson propagator and the lepton current. In contrast, the three-point amplitude $\mathcal{M}_3^{\mu}$ must be contracted with the virtual W^* boson propagator, the WH-vertex, the W-propagator, and the lepton current. These aspects are discussed in detail in Chapter 4.

3 Helicity Amplitude Formalism

The spinor helicity method [131, 132] represents a highly effective computational technique in quantum field theory, particularly in the context of calculating scattering amplitudes in gauge theories such as quantum chromodynamics and quantum electrodynamics. The method offers an elegant and efficient alternative to traditional Feynman diagrammatic approaches, allowing for the calculation of scattering amplitudes with greater simplicity and clarity. This short chapter provides an introduction to the spinor helicity formalism, explains its advantages over classical methods, and outlines its relevance in modern particle physics calculations.

3.1 Overview of helicity formalism

In essence, the spinor helicity method represents scattering amplitudes in terms of spinor variables, rather than utilising four-vector representations. In conventional quantum field theory, external particles are described in terms of their momenta and polarization vectors. However, the complexity of Feynman diagrams increases rapidly with the number of external particles, leading to unwieldy expressions for scattering amplitudes. The spinor helicity formalism addresses this by exploiting the fact that massless particles can be more naturally described in terms of two-component spinors.

In standard relativistic theory, the vector p^μ is used to describe the state of the particle. However, in the spinor helicity form, an alternative notation for this four-momentum can be adopted. In Minkowski space, the four-momentum of a massless particle can be expressed in terms of spinor variables. This is achieved by employing the relation between four-vectors and spinor indices in a space with a Lorentz structure

$$p^\mu \big(\sigma_\mu\big)^{\alpha\dot{\alpha}} = \lambda^\alpha \tilde{\lambda}^{\dot{\alpha}}, \tag{3.1}$$

where σ_μ are the Pauli matrices, which establish a correspondence between the four-vector and the spinor components; λ^α and $\tilde{\lambda}^{\dot{\alpha}}$ are two-component Weyl spinors, known as helicity spinors. The use of spinors enables the description of the polarization states of massless particles in a way that simplifies calculations of scattering amplitudes. The helicity of a particle corresponds to the projection of its spin along the direction of its momentum, and the spinor helicity method naturally encodes this information into the formalism.

One of the principal motivations for employing the spinor helicity approach is the significant reduction in complexity compared to traditional Feynman diagram calculations. The classical approach involves the summation over many intermediate states each of which contributes to the overall amplitude. For processes with many external particles, this can lead to an explosion in the number of diagrams and the complexity of the resulting expressions, making traditional calculations highly impractical.

In contrast, the spinor helicity formalism markedly simplifies the calculations. To illustrate, in the case of gluon scattering, amplitudes that traditionally would require the summation of numerous Feynman diagrams can often be expressed as a single compact formula using spinor helicity variables. This is achieved by directly computing the on-shell scattering amplitudes, bypassing the need to calculate off-shell intermediate states, which are a central feature of the Feynman approach.

The spinor helicity method has found widespread use in gauge theories, particularly in QCD, where gluon scattering processes play a central role. This has proven particularly advantageous in the context of high-energy collider experiments, such as those

conducted at the LHC, where accurate predictions of scattering amplitudes are essential for comparing theory with experimental data.

Furthermore, the method offers a natural framework for the organisation and simplification of the color structure of scattering amplitudes in QCD. Since gluons carry color charge, traditional Feynman diagram calculations involve the summation of color indices which can become onerous for multi-gluon processes. The spinor helicity formalism, frequently used in conjunction with color-decomposition techniques, streamlines these calculations by separating the color structure from the kinematic part of the amplitude.

The famous Parke-Taylor formula [133] for tree-level gluon scattering amplitudes is a classic example of the power of this approach. In the case of n-gluon scattering, the amplitude can be compactly expressed in terms of helicity spinors, effectively simplifying a complex expression into a concise and elegant form.

$$\mathcal{M}\big(p_1^+, p_2^+, ..., p_i^-, ..., p_j^-, ..., p_n^+\big) = g_s^{n-2} \frac{\langle p_i p_j \rangle^4}{\langle p_1 p_2 \rangle \langle p_2 p_3 \rangle ... \langle p_n p_1 \rangle}, \tag{3.2}$$

where p_i^- and p_j^- are the only negative-helicity (left-handed) gluons, while all other gluons have positive helicity; $\langle pq \rangle$ represents the spinor helicity brackets (see Appendix C for more details) which are antisymmetric and encode the spinor inner product for massless particles.

In practical terms, the Parke-Taylor formula and similar results have been pivotal in enhancing the efficacy of calculations for processes at high-energy colliders, such as those conducted at the LHC. The capacity to compute scattering amplitudes with greater efficiency is of paramount importance for the comparison of theoretical predictions with experimental data, which in turn facilitates the refinement of our understanding of both QCD and the Standard Model.

Moreover, the spinor helicity method has been instrumental in the development of on-shell recursion relations, such as the Britto-Cachazo-Feng-Witten (BCFW) recursion relations [134, 135], which allow for the efficient computation of tree-level scattering amplitudes in gauge theories. These relations further exploit the simplicity of on-shell amplitudes and the spinor helicity formalism to recursively construct amplitudes from simpler building blocks, thereby avoiding the need to explicitly calculate all Feynman diagrams.

The fundamental concept underlying the BCFW recursion relations is the decomposition of a complex scattering amplitude into simpler "building blocks", which can then be recursively calculated. This is achieved by shifting the momenta of two external particles in the amplitude by introducing a complex parameter z, while maintaining momentum conservation and keeping all particles on-shell. By analyzing the behavior of the amplitude as a function of z, it can be reconstructed from its poles which correspond to physical factorization channels where internal particles go on-shell. The final amplitude is obtained by summing the contributions from these residues. This method avoids the necessity to compute each Feynman diagram individually, significantly reducing the computational complexity. In the spinor helicity formalism, the BCFW shifts can be applied directly to the helicity spinors, taking advantage of the compact and simplified representation of scattering amplitudes. The recursion relations permit the construction of amplitudes with an arbitrary number of external particles to be constructed iteratively from those with fewer particles, significantly simplifying the process.

In addition to its applications within the Standard Model, the spinor helicity method has also been employed in the study of Beyond the Standard Model physics. A significant number of these scenarios result in the introduction of new particles, including supersym-

metric partners, which can be effectively analysed using spinor helicity techniques. The spinor helicity formalism is particularly well-suited to calculations in supersymmetric theories, which often introduce massless fermions and gauge bosons. Moreover, the method has demonstrated its utility in the context of string theory and the analysis of scattering amplitudes in supergravity and super Yang-Mills theories.

3.2 Quantum Chromodynamics in helicity formalism

In the context of our study, the helicity amplitude method also proves to be very useful. In high-energy collider processes, such as those at the LHC, most fermions are ultra-relativistic, behaving effectively as massless particles. In the case of massless fermions interacting via gauge interactions, helicity becomes a conserved quantity. This fact makes the helicity basis especially convenient for computations, as we can exploit this helicity conservation. Although vector particles, such as photons and gluons, do not possess conserved helicity in the same way, there is a notable feature: tree-level amplitudes for processes that maximally violate helicity tend to vanish, due to an underlying symmetry, often referred to as a hidden supersymmetry, that links bosonic and fermionic amplitudes.

A related and crucial question is that of the kinematic variables that should be employed when computing scattering amplitudes for particles with spin. As previously stated, the traditional approach to these calculations employs the four-momenta p^μ and the Lorentz-invariant quantities, such as the Mandelstam variables $s_{ij} = (p_i + p_j)^2$. However, since most of the Standard Model particles (excluding the Higgs boson) have spin, there exists a more efficient selection of variables. It is possible to reduce the dimensionality of the kinematic variables by representing the four-momenta not as Lorentz vectors but in terms of spinors.

In the case of massless particles, the most compact and efficient description is provided by Weyl spinors, which are two-dimensional representations of the Lorentz group. Consequently, the four-momentum p^μ is replaced with a pair of spinor variables as it mentioned in Eq. (3.1). This transformation from vector to spinor representation not only simplifies the structure of the amplitude but also aligns naturally with the spinor helicity formalism, where spinor products, such as $\langle p_i p_j \rangle$ and $[p_i p_j]$, encode the scattering kinematics more effectively than traditional momentum products.

3.2.1 External fermions

In order to describe the specific helicities of external particles, it is proposed that the method be based on the use of two-component spinors. In this work, however, we will adhere to the usual four-dimensional formalism [131] which is also widely used and in which, for particles with left- and right-handed helicities, the corresponding left- and right-handed four-component spinors are introduced:

$$\begin{aligned} |p] = U_L(p) &= N_p \begin{pmatrix} u_L(p) \\ 0 \end{pmatrix}, & |p\rangle = U_R(p) &= N_p \begin{pmatrix} 0 \\ u_R(p) \end{pmatrix}, \\ \langle p| = \overline{U}_L(p) &= N_p \begin{pmatrix} 0 & u_L^\dagger(p) \end{pmatrix}, & [p| = \overline{U}_R(p) &= N_p \begin{pmatrix} u_R^\dagger(p) & 0 \end{pmatrix}, \end{aligned} \tag{3.3}$$

where N_p is a normalization constant. Two-component spinors u_R and u_L are identical to the spinors mentioned in Eq. (3.1) as λ^α and $\lambda^{\dot{\alpha}}$, respectively, as another popular designation.

This notation allows the calculation of the scattering amplitude for a process involving particles with specified helicities, such as $q_L\bar{q}'_L \to W(\to l_L\bar{l}_L)H + g_R$. Of course, to obtain the total scattering amplitude, one has to sum over all possible combinations of particle helicities:

$$\mathcal{M}\big(q\bar{q}' \to l\bar{l}H + g\big) = \mathcal{M}\big(q_L\bar{q}'_L \to l_L\bar{l}_L H + g_L\big) + \mathcal{M}\big(q_L\bar{q}'_R \to l_L\bar{l}_L H + g_L\big) + ... \quad (3.4)$$

However, the advantage of the helicity amplitude method lies in the fact that one is not required to calculate all the helicity amplitudes, as they are related to each other by very simple relations (discussed in detail in Appendix C) due to the spinor properties.

3.2.2 External massless bosons

In light of the fact that in our study we also consider the emission of external gluons, it is necessary to employ their representation in helicity formalism as well. In essence, spinor helicity techniques started with the recognition [136–140] that polarization vectors for massless bosons with specific helicity can be constructed from a pair of massless spinors. For the **outgoing** (marked by a star) massless bosons in four-component notation, these vectors are given by

$$\varepsilon^*_{\mu,L}(p) = \frac{[r|\gamma_\mu|p\rangle}{\sqrt{2}[pr]}, \qquad \varepsilon^*_{\mu,R}(p) = -\frac{\langle r|\gamma_\mu|p]}{\sqrt{2}\langle pr\rangle}, \quad (3.5)$$

where r is an additional massless vector called the reference momentum. It is possible to select different reference vectors r_i for each of the external states i. This freedom is what is known as the residual on-shell gauge invariance. This implies that the amplitudes must remain unchanged when the polarization vector is shifted by an amount proportional to the momentum. A judicious choice of reference vectors can greatly simplify the computation of the Feynman diagram, making many diagrams disappear.

One important consequence follows from relations (3.5). By multiplying the polarization vectors scalarly by a vector p^μ, one can see that polarization vectors satisfy the required transversality with respect to the gluon momentum, also called the Ward identity[3]

$$p^\mu \varepsilon^*_{\mu,L/R}(p) = 0. \quad (3.6)$$

The given relations are also applicable to photons as massless bosons which, however, are not within the scope of our interests of the present work.

3.2.3 Color decomposition

The next question which should be discussed here is how to organize the color degrees of freedom in QCD amplitudes, in order to separate out pieces that have simpler analytic properties. In the context of QCD, color decomposition is a powerful method that is employed to simplify the computation of scattering amplitudes by systematically organizing the color structure of the interaction. This approach is particularly beneficial in handling the non-Abelian nature of QCD, where gluons carry color charge and self-interact. The fundamental idea behind color decomposition is to separate the color factors from the

[3]For further details, please refer to Appendix C

kinematic factors, allowing for the independent treatment of the more complicated color structure. This leads to a reduction in the complexity of the calculation and provides insights into how color flows in the scattering process.

The conventional approach to perform color decomposition is to express the color structure in terms of the generators of the Lie algebra associated with the gauge group $SU(N_c)$ of QCD. To illustrate, in the context of gluon scattering amplitudes, each gluon is associated with a color index, and the amplitude can be expressed in terms of the structure constants f^{abc} of the $SU(N_c)$ group. By employing color decomposition, the structure constants can be replaced by the generators[4] t^a of the fundamental representation of $SU(N_c)$

$$[t^a, t^b] = i f^{abc} t_c. \tag{3.7}$$

Similarly, in cases involving both quarks and gluons, the color decomposition can be applied to factor out the color matrices for quarks from the kinematic amplitudes. For instance, in processes involving quark-gluon interactions, the color structure typically involves a product of the form $t^{a_1} t^{a_2} \dots t^{a_n}$. This decomposition drastically simplifies the task of summing over color indices and evaluating Feynman diagrams, especially in complex multi-leg QCD processes. By organizing the color factors in this way, color decomposition enables efficient computations and makes the connection between gauge symmetry and scattering amplitudes more transparent.

3.3 Soft and collinear factorization

Soft and collinear factorization plays a crucial role in simplifying scattering amplitudes, particularly in the context of massless gauge theories, such as QCD. These factorization properties describe how the scattering amplitudes behave in certain kinematic limits, namely when an external particle becomes soft (its energy tends to zero) or when two particles become collinear (their momenta become parallel). These limits are of great importance for understanding the infrared structure of amplitudes, leading to a better grasp of divergences in loop calculations and the behavior of real radiation processes.

In the soft limit [141], when the momentum p_g of an emitted gluon becomes soft ($p_g \to 0$), the amplitude factorizes into a simpler form. The scattering amplitude involving a soft gluon can be expressed as the original amplitude (without the soft gluon) multiplied by a universal soft factor, which encodes the interaction of the soft gluon with the other particles in the process. For an amplitude $\mathcal{M}_{n+1}$ with an additional soft gluon, the factorization relation is as follows

$$\mathcal{M}_{n+1}(\dots, p_i, p_g, p_j, \dots) \xrightarrow{p_g \to 0} g_s S(p_i, p_j, p_g) \mathcal{M}_n(\dots, p_i, p_j, \dots), \tag{3.8}$$

where $S(p_i, p_j, p_g)$ is the soft factor which depends on the momenta of the adjacent particles p_i and p_j in the amplitude, and g_s is the strong coupling constant. The soft factor is a simple expression that involves the momenta of the hard particles. In most cases, it can be expressed as a singular function as $p_g \to 0$.

In the soft limit for the process we are considering, the gluon is emitted with a very low energy, and the scattering amplitude exhibits a universal behavior described by the soft factor. The latter is expressed as a function of the emission of a low-energy gluon from a quark or antiquark, and takes the following form

[4]Here we refer to generators that satisfy the normalization relation $\mathrm{Tr}(t^a t^b) = \delta^{ab}/2$

$$\mathcal{M}\big(q\bar{q}' \to WH + g\big) \xrightarrow{p_g \to 0} \mathcal{M}\big(q\bar{q}' \to WH\big) \left(\frac{(p_q \cdot \varepsilon_g)}{(p_q \cdot p_g)} - \frac{(p_{\bar{q}'} \cdot \varepsilon_g)}{(p_{\bar{q}'} \cdot p_g)} \right), \tag{3.9}$$

where p_g is the gluon momentum and ε_g is its polarization vector. The first component of the soft factor describes the emission of a soft gluon from a quark, whereas the second term describes the emission from an antiquark.

In the collinear limit [142, 143], when the momenta of two massless particles become nearly parallel, the combined amplitude factorizes as well. If two particles with momenta p_i and p_j become collinear, such that $p_i \parallel p_j$, the amplitude factorizes into a simpler amplitude with one fewer particle, multiplied by a splitting function that describes how the two collinear particles behave like a single effective particle. The collinear factorization can be written as

$$\mathcal{M}_{n+1}(\dots, p_i, p_j, \dots) \xrightarrow{p_i \| p_j} \frac{1}{s_{ij}} Sp_{h\to ij}(\lambda_i, \lambda_j) \mathcal{M}_n(\dots, p_h, \dots), \tag{3.10}$$

where $s_{ij} = (p_i + p_j)^2$ is the invariant mass of the collinear pair, $Sp_{h\to ij}$ is the splitting function that depends on the helicities λ_i and λ_j of the collinear particles, and p_h represents the momentum of the effective particle replacing p_i and p_j. The splitting function $Sp_{h\to ij}$ encodes the probability for the two particles to emerge from a single particle, and it takes a universal form that depends only on the type of particles involved and their helicities.

The soft-collinear limit describes the case when the emitted particle simultaneously has low energy and its direction is nearly identical to that of the direction of the emitting particle. Soft-collinear divergences are a defining feature of quantum field theory, and must be accounted for and compensated for in the context of finite physical observables, such as cross sections. Such divergences do not give rise to physical issues, as the final result is obtained by taking into account virtual corrections that compensate for the divergences from the real gluon emission. In addition, divergences due to collinear emission can be taken into account by factorizing parton distribution functions that already contain such divergences.

It is evident that these two limits must also be satisfied within the helicity amplitude method, a fact that has been directly verified in the course of this work for both NLO and NNLO real corrections.

4 Next-to-Next-to-Leading Order Amplitudes

The ultimate goal of this work is to calculate NNLO QCD corrections for the squared matrix element for the process $q\bar{q}' \to W(\to l\bar{l})H + X$ within the Standard Model Effective Field Theory. The symbol X can represent either nothing or some real particles (gluons or quarks). The squared matrix element should be computed up to and including NNLO in the strong coupling constant α_s. Moreover, since we consider the process within the Standard Model Effective Field Theory, which includes small Wilson coefficients C_i, we employ the Standard Model expressions which are given, for example, in Appendix D of reference [144] for all the remaining vertices and propagators.

4.1 Conventions and notations

It is convenient to work with an open index μ and consider amplitudes $\mathcal{M}_4$ and $\mathcal{M}_3$ for four- and three-point vertices, respectively (see Fig. 2), since the remaining parts of the diagrams do not change for all processes under consideration.

We introduce the incoming quark q with polarization λ_1 and momentum p_1 and the incoming antiquark $\bar{q}'$ with polarization λ_2 and momentum p_2. Similarly, we introduce the outgoing lepton l which has polarization λ_3 and momentum p_3 and the outgoing antilepton with polarization λ_4 and momentum p_4. The intermediate state of a charged electroweak boson with mass m_W is described by momentum p_W and the Higgs boson with mass m_H is described by momentum p_H. In the case of a two-loop process, loop momenta are denoted by k_1 and k_2. In the case of a one-loop process, loop momentum is denoted by k. The outgoing gluon (or quark-antiquark pair) momenta are denoted through p_5 and p_6. The same subscript notation is used for their helicities, which are denoted by λ_5 and λ_6.

In accordance with Eqs. (2.23) and (2.24), the four- and three-point amplitudes can be written as follows

$$\mathcal{M}_4 = \mathcal{M}_4^{\mu} \cdot \frac{g_W/\sqrt{2}}{p_W^2 - m_W^2 + i\varepsilon} \mathcal{L}_{\mu}, \tag{4.1}$$

$$\mathcal{M}_3 = \mathcal{M}_3^{\mu} \cdot \frac{m_W g_W^2/\sqrt{2}}{\left(p_{W^*}^2 - m_W^2 + i\varepsilon\right)\left(p_W^2 - m_W^2 + i\varepsilon\right)} \mathcal{L}_{\mu}, \tag{4.2}$$

with $p_W = p_3 + p_4$, $p_{W^*} = p_1 + p_2$ and the lepton current

$$\mathcal{L}_{\mu} = \overline{U}_{\lambda_3}(p_3)\gamma_{\mu}P_L U_{\lambda_4}(p_4). \tag{4.3}$$

The introduction of the $i\varepsilon$-term in the propagator in Eqs. (4.1) and (4.2) serves the purpose of correctly defining the integration contours in the complex plane. This approach allows one to circumvent the poles in the propagator, thereby allowing the attainment of physically meaningful outcomes pertaining to particle scattering and decay.

Based on Eq. (4.3) and spinor algebra relations (see Appendix C), such as $P_L U(p) = U_L(p) = |p]$ and $[q|\gamma^{\mu}|p] = 0$, one can simplify the expression for the lepton current by noting that

$$\begin{aligned} \mathcal{L}_{\mu} &= \overline{U}_{\lambda_3}(p_3)\gamma_{\mu}U_L(p_4) = \overline{U}_R(p_3)\gamma_{\mu}U_L(p_4) + \overline{U}_L(p_3)\gamma_{\mu}U_L(p_4) \\ &= \langle p_3|\gamma_{\mu}|p_4] + [p_3|\gamma_{\mu}|p_4]. \end{aligned} \tag{4.4}$$

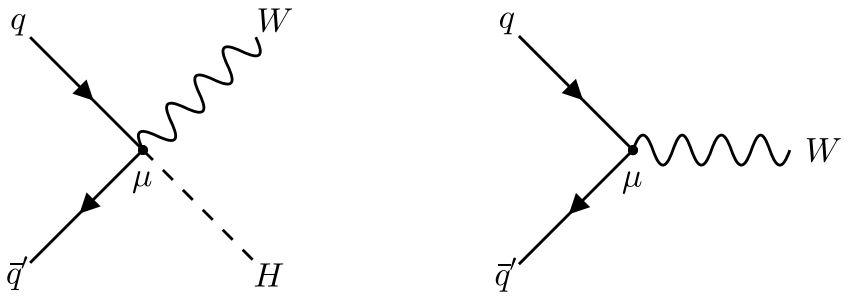

Figure 2: Four-point (a) and three-point (3) Feynman diagrams for the process $q\bar{q}' \to WH$ at leading order within the Standard Model Effective Field Theory.

Therefore, the lepton current finally reads

$$\mathcal{L}_\mu = \langle p_3 | \gamma_\mu | p_4]. \tag{4.5}$$

This implies that, when considering solely the W boson, then both leptons can only have left-handed helicity, since the decay vertex of the W boson is still within the Standard Model. This reduces the number of helicity amplitudes by four times.

Another point is that intermediate results for the 4-point amplitude can be used to simplify the calculations of the 3-point amplitude, at the level of the amplitudes with open index μ which contains only QCD corrections, and the following behavior can be expected

$$\lim_{p_H \to 0} \mathcal{M}_4^\mu = \mathcal{M}_3^\mu. \tag{4.6}$$

However, this property has been verified in this thesis directly.

Physical processes take place in four-dimensional space-time. In the four-dimensional evaluation of loop amplitudes one encounters ultraviolet and infrared divergences that have to be properly regularized. The most efficient method to simultaneously regularize both kind of divergences in gauge theories is dimensional regularization in d space-time dimensions. In this work, we use the 't Hooft–Veltman dimensional regularization [145, 146] to leave out ultraviolet and infrared divergences by taking them into account in the form of $1/\varepsilon^n$-poles with an integer number n and a small parameter ε. The key ingredient of dimensional regularization is the analytic continuation of loop momenta. To this end, we make all our calculations in d-dimensional spacetime, where $d = 4 - 2\varepsilon$. After all divergences will have been canceled, we go to the 4-dimensional spacetime by turning ε to 0 and obtain finite result.

In accordance with the introduced momenta, the following invariants are employed in this thesis:

$$
\begin{aligned}
s_{12} &= (p_1 + p_2)^2 = 2\,(p_1 \cdot p_2)\,, \\
s_{1W} &= (p_1 + p_W)^2 = m_W^2 + 2\,(p_1 \cdot p_W)\,, \\
s_{2W} &= (p_2 + p_W)^2 = m_W^2 + 2\,(p_2 \cdot p_W)\,, \\
s_{15} &= (p_1 + p_5)^2 = 2\,(p_1 \cdot p_5)\,, \\
s_{25} &= (p_2 + p_5)^2 = 2\,(p_2 \cdot p_5)\,, \\
s_{16} &= (p_1 + p_6)^2 = 2\,(p_1 \cdot p_6)\,, \\
s_{26} &= (p_2 + p_6)^2 = 2\,(p_2 \cdot p_6)\,, \\
s_{56} &= (p_5 + p_6)^2 = 2\,(p_5 \cdot p_6)\,, \\
s_{5W} &= (p_W + p_5)^2 = m_W^2 + 2\,(p_5 \cdot p_W)\,, \\
s_{6W} &= (p_W + p_6)^2 = m_W^2 + 2\,(p_6 \cdot p_W)\,.
\end{aligned}
\tag{4.7}
$$

The Greek alphabet (α, β, μ, ν, λ, ect.) is used to indicate Lorentz indices and the Latin alphabet (a, b, c, ect.) is used to denote QCD color.

Crossed symbols denote contraction of γ-matrix with a momentum

$$
\not{p} = \gamma^\mu p_\mu. \tag{4.8}
$$

Wilson coefficients C_i are implied to be divided by the high energy scale Λ^2, i.e. their dimension is $[C_i] = \text{mass}^{-2}$.

4.2 Leading Order

As mentioned above, two diagrams, showed in the Fig. 2, contribute to the amplitude at the leading order. We shall initially focus on the 4-point diagram. As usual, the arrows in the figure indicate the direction of the charge, but not the momentum. The incoming quark q has momentum p_1, whereas the incoming antiquark $\bar{q}'$ has momentum p_2. Subsequent to the collision, they annihilate into a Higgs boson H with momentum p_H and a weak boson W with momentum p_W. The momentum conservation law in this case can be written as follows

$$
p_1 + p_2 - p_H = p_W = p_3 + p_4, \tag{4.9}
$$

where p_3 and p_4 are the momenta of the outgoing lepton and antilepton, respectively.

As previously stated, we will work with an open index μ and calculate the amplitude $\mathcal{M}^\mu_{\lambda_1\lambda_2}$, where initial particle helicities $\lambda_{1,2} = \{L, R\}$. The leading order calculation is straightforward and simple, but they will help as to understand the helicity structure of the total leading order amplitude. According to Fig. 2(a), the four-point amplitude with the open index μ can be expressed as

$$
\mathcal{M}^{(0)\mu}_{4\;\lambda_1\lambda_2} = \overline{U}_{\lambda_2}(p_2)\Big(C_1[\gamma^\mu, \not{p}_W]P_L + C_2[\gamma^\mu, \not{p}_W]P_R + C_3\gamma^\mu P_L + C_4\gamma^\mu P_R\Big)U_{\lambda_1}(p_1). \tag{4.10}
$$

In general, we have four variants of helicity amplitudes, because each of the two incoming quarks can be either left-handed or right-handed. Consider the case with $\lambda_1 = L$ and $\lambda_2 = R$, then Eq. (4.10) becomes the following expression in spinor notation

$$
\mathcal{M}^{(0)\mu}_{4\;LR} = [p_2|\Big(C_1[\gamma^\mu, \not{p}_W]P_L + C_2[\gamma^\mu, \not{p}_W]P_R + C_3\gamma^\mu P_L + C_4\gamma^\mu P_R\Big)|p_1]. \tag{4.11}
$$

However, since $P_R|p_1] = 0$ and, moreover, for any momenta p and q the relation $[p|\gamma^\mu|q] = 0$ holds, only the first term in Eq. (4.11) survives and the amplitude becomes

$$\mathcal{M}^{(0)\mu}_{4\ LR} = C_1[p_2|[\gamma^\mu, \not{p}_W]|p_1]. \tag{4.12}$$

Now one can notice that

$$\begin{aligned}[\gamma^\mu, \not{p}_W] &= p_{W\nu}[\gamma^\mu, \gamma^\nu] = p_{W\nu}\big(\gamma^\mu\gamma^\nu - \gamma^\nu\gamma^\mu\big) = p_{W\nu}\big(\gamma^\mu\gamma^\nu - (2g^{\mu\nu} - \gamma^\mu\gamma^\nu)\big) \\ &= p_{W\nu}\big(2\gamma^\mu\gamma^\nu - 2g^{\mu\nu}\big) = 2\gamma^\mu\not{p}_W - 2p^\mu_W.\end{aligned} \tag{4.13}$$

Substitution of this result into Eq. (4.12) yields the final expression for the amplitude $\mathcal{M}^{(0)\mu}_{LR}$. In an absolutely similar way, one can calculate the remaining three leading order helicity amplitudes. Then, for the leading order, we can write

$$\begin{aligned}\mathcal{M}^{(0)\mu}_{4\ LR} &= 2C_1[p_2|(\gamma^\mu\not{p}_W - p^\mu_W)|p_1], \qquad \mathcal{M}^{(0)\mu}_{4\ LL} = C_3\langle p_2|\gamma^\mu|p_1], \\ \mathcal{M}^{(0)\mu}_{4\ RL} &= 2C_2\langle p_2|(\gamma^\mu\not{p}_W - p^\mu_W)|p_1\rangle, \qquad \mathcal{M}^{(0)\mu}_{4\ RR} = C_4[p_2|\gamma^\mu|p_1\rangle.\end{aligned} \tag{4.14}$$

In order to obtain the helicity amplitudes for the 3-point diagram, it is sufficient to exchange the pre-factors and replace the momentum of the weak boson p_W with p_{W^*}:

$$\begin{aligned}\mathcal{M}^{(0)\mu}_{3\ LR} &= 2vC_1[p_2|(\gamma^\mu\not{p}_{W^*} - p^\mu_{W^*})|p_1], \qquad \mathcal{M}^{(0)\mu}_{3\ LL} = \left(S_3 + \frac{v}{2}C_3\right)\langle p_2|\gamma^\mu|p_1], \\ \mathcal{M}^{(0)\mu}_{3\ RL} &= 2vC_2\langle p_2|(\gamma^\mu\not{p}_{W^*} - p^\mu_{W^*})|p_1\rangle, \qquad \mathcal{M}^{(0)\mu}_{3\ RR} = \frac{v}{2}C_4[p_2|\gamma^\mu|p_1\rangle.\end{aligned} \tag{4.15}$$

It is important to note that the Standard Model is included in this result and contributes solely by the amplitude $\mathcal{M}^{(0)\mu}_{3\ LL}$.

4.3 Loop corrections

Prior to undertaking the calculation of the squared amplitude at NNLO, it is first necessary to examine the one-loop case in order to derive the general structure of the purely virtual corrections in all orders of perturbation theory. The result may then be employed in the calculation of two-loop corrections, and in higher orders, should the necessity arise.

We will begin with the general expansion of loop corrections within the context of perturbation theory. The matrix element can be evaluated in QCD perturbation theory as a power series expansion in the QCD coupling g_s or, equivalently, in the strong coupling constant $\alpha_s = g_s^2/4\pi$:

$$\mathcal{M}^\mu_{\lambda_1\lambda_2} = \mathcal{M}^{(0)\mu}_{\lambda_1\lambda_2} + \frac{\alpha_s}{2\pi}\mathcal{M}^{(1)\mu}_{\lambda_1\lambda_2} + \left(\frac{\alpha_s}{2\pi}\right)^2\mathcal{M}^{(2)\mu}_{\lambda_1\lambda_2} + \mathcal{O}\left(\alpha_s^3\right). \tag{4.16}$$

4.3.1 General tensor structure of pure n-loop corrections

In this section, we derive a general tensor structure for the vertex function in the general case of n loops, where only pure loop corrections are taken into account. This greatly simplifies higher order computations which we will demonstrate by computing the two-loop amplitude. The one-loop diagram for the four-point vertex is illustrated in Fig. 3. As in the case of the leading order, only one diagram contributes in this instance to each of the two processes.

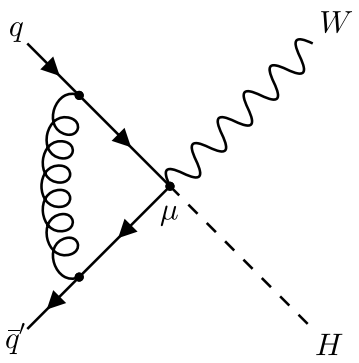

Figure 3: Four-point Feynman diagram within the Standard Model Effective Field Theory at one loop.

Employing Feynman rules enables the expression of the amplitude describing the one-loop process in the following form:

$$\frac{\alpha_s}{2\pi}\mathcal{M}^{(1)\mu}_{4\,\lambda_1\lambda_2} = g_s^2 C_F \mu_0^{2\varepsilon} \int \frac{d^dk}{(2\pi)^d} \frac{\overline{U}_{\lambda_2}(p_2)\gamma^\nu(\not{p}_2 - \not{k})A^\mu(\not{p}_1 + \not{k})\gamma_\nu U_{\lambda_1}(p_1)}{k^2(p_1+k)^2(p_2-k)^2}. \tag{4.17}$$

In Eq. (4.17), k represents the loop momentum, the vertex function A^μ is defined in Eq. (2.23), and the dimension regularisation mass parameter μ_0 is introduced to ensure that the integral over the loop momentum is four-dimensional.

By substituting A^μ by its explicit expression, using Dirac algebra and making the momentum shift $k \to l = k + xp_1 - yp_2$ in accordance with the Feynman parametrization method [147], the numerator N^μ of (4.17) can be rewritten as

$$\begin{aligned} N^\mu = \overline{U}_{\lambda_2}(p_2)\Bigg[\Bigg(4s(1-x-y) + 2(d-4)xys - \frac{2(d-4)^2l^2}{d}\Bigg)T_1^\mu + \\ + 8(d-4)xyT_2^\mu\Bigg](C_1P_L + C_2P_R)U_{\lambda_1}(p_1) + \\ + \overline{U}_{\lambda_2}(p_2)\Bigg[2s(1-x-y) + (d-2)xys - \frac{(d-2)^2l^2}{d}\Bigg]\times \\ \times T_3^\mu(C_3P_L + C_4P_R)U_{\lambda_1}(p_1), \end{aligned} \tag{4.18}$$

where the following tensor structures appeared

$$T_1^\mu = \gamma^\mu \not{p}_W - p_W^\mu, \qquad T_2^\mu = (p_2 \cdot p_W)p_1^\mu - (p_1 \cdot p_W)p_2^\mu, \qquad T_3^\mu = \gamma^\mu. \tag{4.19}$$

As can be seen from Eq. (4.18), the one-loop amplitude can be expressed in terms of tensor structures (4.19) as follows

$$\sum_{\lambda_1,\lambda_2} \mathcal{M}^{(1)\mu}_{4\,\lambda_1\lambda_2} = \mathcal{M}^{(1)\mu}_{4\,LR} + \mathcal{M}^{(1)\mu}_{4\,RL} + \mathcal{M}^{(1)\mu}_{4\,LL} + \mathcal{M}^{(1)\mu}_{4\,RR}, \tag{4.20}$$

where helicity amplitudes

$$
\begin{aligned}
\mathcal{M}^{(1)\mu}_{4\,LR} &= C_1\,\overline{U}_R(p_2)\left(A^{(1)}_1 T^\mu_1 + A^{(1)}_2 T^\mu_2\right) U_L(p_1),\\
\mathcal{M}^{(1)\mu}_{4\,RL} &= C_2\,\overline{U}_L(p_2)\left(A^{(1)}_1 T^\mu_1 + A^{(1)}_2 T^\mu_2\right) U_R(p_1),\\
\mathcal{M}^{(1)\mu}_{4\,LL} &= C_3\,\overline{U}_L(p_2) A^{(1)}_3 T^\mu_3 U_L(p_1),\\
\mathcal{M}^{(1)\mu}_{4\,RR} &= C_4\,\overline{U}_R(p_2) A^{(1)}_3 T^\mu_3 U_R(p_1)
\end{aligned}
\tag{4.21}
$$

and the complex numbers $A^{(1)}_i$, called one-loop form factors, can be expressed explicitly in terms of one-loop Feynman integrals. The REDUZE software[5] [148] facilitates the reduction of one-loop calculations by reducing one-loop Feynman integrals to a single master integral

$$
I^{(1)} = \mu_0^\varepsilon \int \frac{d^d k}{(2\pi)^d} \frac{1}{(p_1+k)^2 (p_2-k)^2}. \tag{4.22}
$$

The one-loop integral (4.22) belongs to the class of standard two-point functions in quantum field theory and has been the subject of extensive study in the scientific literature. For a detailed solution, the reader is directed to classical works on the calculation of loop integrals, such as [146, 149, 150]. The explicit solution is thus transformed into a formal expression through the gamma function

$$
I^{(1)} = \frac{i}{16\pi^2} \left(\frac{4\pi\mu_0^2}{-s_{12}}\right)^\varepsilon \frac{\Gamma(\varepsilon)\Gamma(1-\varepsilon)}{\Gamma(2-2\varepsilon)}. \tag{4.23}
$$

A comparison of Eqs. (4.14) and (4.21) allows us to extract the expressions for the leading order form factors

$$
A^{(0)}_1 = 2, \qquad A^{(0)}_2 = 0, \qquad A^{(0)}_3 = 1. \tag{4.24}
$$

The set of tensor structures (4.19) may be employed for computations at higher orders for diagrams containing only internal loops. It can be demonstrated that every tensor structure is provided by the initial tensors in the vertex, that is to say, by the tensors γ^μ and $[\gamma^\mu, \not{p}_W]$. In the case of a loop diagram comprising an arbitrary number of gluon loops, it is inevitable that an odd number of gamma matrices will be generated when the γ^μ-term is taken into account. Similarly, if the commutator is employed in place of the vertex function A^μ, an even number of γ-matrices will be always generated.

It is irrelevant how many times the anticommutative relation is applied to permute γ-matrices, their number will always remain odd, if it was odd, and even, if it was even. This implies that a single γ^μ can provide only tensor structures of an odd number of γ-matrices. However, this can only be the case for the γ^μ itself, because slashed momenta $\not{p}_1$ and $\not{p}_2$ vanish upon application of the Dirac equation. Consequently, $\not{p}_W$ cannot appear at all, since there is no weak boson momentum in the amplitude, and there is also no other momentum. Similarly, the commutator $[\gamma^\mu, \not{p}_W]$ can only provide tensor structures with an even number of γ-matrices. Moreover, as a consequence of the fact that the commutator $[\gamma^\mu, \not{p}_W]$ yields zero upon contraction with $p_{W\mu}$, all tensor structures provided by this commutator must also satisfy this condition. In this context, it is possible to construct

[5]The official website of the REDUZE project, which contains the relevant documentation, can be accessed via the following link: reduze.hepforge.org

the tensor structures T_1^μ and T_2^μ given in (4.19). Since $\not{p}_1$ and $\not{p}_2$ vanish when the Dirac equation is applied, no other tensor structures are possible.

In light of these considerations, we may formulate the general purely n-loop corrections for the 4-point helicity amplitudes

$$\begin{aligned}
\mathcal{M}^{(n)\mu}_{4\ LR} &= C_1\ [p_2|\left(A_1^{(n)}T_1^\mu + A_2^{(n)}T_2^\mu\right)|p_1], \\
\mathcal{M}^{(n)\mu}_{4\ RL} &= C_2\ \langle p_2|\left(A_1^{(n)}T_1^\mu + A_2^{(n)}T_2^\mu\right)|p_1\rangle, \\
\mathcal{M}^{(n)\mu}_{4\ LL} &= C_3\ \langle p_2|A_3^{(n)}T_3^\mu|p_1], \\
\mathcal{M}^{(n)\mu}_{4\ RR} &= C_4\ [p_2|A_3^{(n)}T_3^\mu|p_1\rangle
\end{aligned} \tag{4.25}$$

As previously stated, the 3-point helicity amplitudes can be obtained from Eq. (4.25) by exchanging coefficients and replacing the weak boson momentum as it has been done at the leading order:

$$\begin{aligned}
\mathcal{M}^{(n)\mu}_{3\ LR} &= vC_1\big(p_2^\mu - p_1^\mu\big)\ [p_2|\left(A_1^{(n)} + \frac{s_{12}}{2}A_2^{(n)}\right)|p_1], \\
\mathcal{M}^{(n)\mu}_{3\ RL} &= vC_2\big(p_2^\mu - p_1^\mu\big)\ \langle p_2|\left(A_1^{(n)} + \frac{s_{12}}{2}A_2^{(n)}\right)|p_1\rangle, \\
\mathcal{M}^{(n)\mu}_{3\ LL} &= \left(S_3 + \frac{v}{2}C_3\right)\ \langle p_2|A_3^{(n)}T_3^\mu|p_1], \\
\mathcal{M}^{(n)\mu}_{3\ RR} &= \frac{v}{2}C_4\ [p_2|A_3^{(n)}T_3^\mu|p_1\rangle
\end{aligned} \tag{4.26}$$

4.3.2 Total helicity amplitudes for purely virtual n-loop case

In order to calculate total helicity amplitudes for the purely virtual case, it is necessary to consider $\mathcal{M}_4^\mu$ and $\mathcal{M}_3^\mu$ separately. In the case of the 4-point vertex, the amplitude with an open index μ should be contracted with the weak boson propagator and the lepton current using Eq. (4.1). In a particular case, this is expressed explicitly as follows

$$\begin{aligned}
\mathcal{M}^{(n)}_{4\ LR;LL} = C_1\ [p_2|\left(A_1^{(n)}\big(\gamma^\mu \not{p}_W - p^\mu\big) + A_2^{(n)}\big((p_2\cdot p_W)p_1^\mu - (p_1\cdot p_W)p_2^\mu\big)\right)|p_1]\times \\
\times\ \frac{g_W/\sqrt{2}}{p_W^2 - m_W^2 + i\Gamma_W m_W}\ \langle p_3|\gamma_\mu|p_4],
\end{aligned} \tag{4.27}$$

where $\Gamma_W \approx 2.085 \pm 0.042$ GeV is the decay width of W boson. In the description of unstable particles, the particle mass is replaced by a complex value $m_W \to m_W - i\Gamma_W/2$ in order to account for the finite lifetime of the particle in question. This is due to the fact that such particles undergo a process of decay and possess a finite decay width which corresponds to the inverse of the particle lifetime.

The next step is to contract the free indices and apply the rules of spinor algebra to Eq. (4.27). Using certain relations from Appendix C and replacing the weak boson momentum p_W with $p_3 + p_4$, the following result can be obtained

$$\begin{aligned}\mathcal{M}^{(n)}_{4\,LR;LL} = \frac{C_1 g_W \sqrt{2}}{p_W^2 - m_W^2 + i\Gamma_W m_W} \times \\ \times \Big(2A_1^{(n)}[p_4 p_1][p_2 p_4]\langle p_3 p_4\rangle \\ + A_2^{(n)}(p_2 \cdot p_W)[p_1 p_2]\langle p_1 p_3\rangle[p_1 p_4] \\ - A_2^{(n)}(p_1 \cdot p_W)[p_1 p_2]\langle p_2 p_3\rangle[p_2 p_4]\Big).\end{aligned} \tag{4.28}$$

The amplitude $\mathcal{M}^{(n)}_{4\,RL;LL}$ can be obtained in an absolutely similar way, and the two remaining 4-point helicity amplitudes are even more straightforward to calculate. Finally, using Eq. (4.25) one can obtain

$$\begin{aligned}\mathcal{M}^{(n)}_{4\,LR;LL} &= \frac{C_1 g_W \sqrt{2}}{\Pi_W} \Big(2A_1^{(n)}[p_4 p_1][p_2 p_4]\langle p_3 p_4\rangle \\ &\quad + A_2^{(n)} \frac{s_{2W} - m_W^2}{2} [p_1 p_2]\langle p_1 p_3\rangle[p_1 p_4] \\ &\quad + A_2^{(n)} \frac{m_W^2 - s_{1W}}{2} [p_1 p_2]\langle p_2 p_3\rangle[p_2 p_4]\Big), \\ \mathcal{M}^{(n)}_{4\,RL;LL} &= \frac{C_2 g_W \sqrt{2}}{\Pi_W} \Big(2A_1^{(n)}\langle p_1 p_3\rangle\langle p_2 p_3\rangle[p_3 p_4] \\ &\quad + A_2^{(n)} \frac{s_{2W} - m_W^2}{2} \langle p_1 p_2\rangle\langle p_1 p_3\rangle[p_1 p_4] \\ &\quad + A_2^{(n)} \frac{m_W^2 - s_{1W}}{2} \langle p_1 p_2\rangle\langle p_2 p_3\rangle[p_2 p_4]\Big), \\ \mathcal{M}^{(n)}_{4\,LL;LL} &= \frac{C_3 g_W \sqrt{2}}{\Pi_W} A_3^{(n)}\langle p_2 p_3\rangle[p_4 p_1], \\ \mathcal{M}^{(n)}_{4\,RR;LL} &= \frac{C_4 g_W \sqrt{2}}{\Pi_W} A_3^{(n)}[p_2 p_4]\langle p_3 p_1\rangle,\end{aligned} \tag{4.29}$$

where

$$\Pi_W = p_W^2 - m_W^2 + i\Gamma_W m_W. \tag{4.30}$$

In Eqs. (4.29), the helicities of the amplitudes are given in the following sequence: quark, antiquark, lepton, antilepton.

In order to calculate helicity amplitudes for the 3-point vertex we can use Eq. (4.26). By replacing the weak boson momentum p_{W^*} with $p_1 + p_2$ and using Eq. (4.2) one can obtain

$$
\begin{aligned}
\mathcal{M}^{(n)}_{3\,LR;LL} &= \frac{vC_1 m_W g_W^2}{\sqrt{2}\,\Pi_W \Pi_{W^*}} \left(B_1^{(n)} - \frac{s_{12}}{2} B_2^{(n)}\right) \times \\
&\qquad \times [p_1 p_2]\Big(\langle p_3 p_1\rangle [p_1 p_4] - \langle p_3 p_2\rangle [p_2 p_4]\Big), \\
\mathcal{M}^{(n)}_{3\,RL;LL} &= \frac{vC_2 m_W g_W^2}{\sqrt{2}\,\Pi_W \Pi_{W^*}} \left(B_1^{(n)} - \frac{s_{12}}{2} B_2^{(n)}\right) \times \\
&\qquad \times \langle p_1 p_2\rangle\Big(\langle p_3 p_1\rangle [p_1 p_4] - \langle p_3 p_2\rangle [p_2 p_4]\Big), \\
\mathcal{M}^{(n)}_{3\,LL;LL} &= \left(S_3 + \frac{v}{2} C_3\right) \frac{m_W g_W^2 \sqrt{2}}{\Pi_W \Pi_{W^*}}\, B_3^{(n)} \langle p_2 p_3\rangle [p_4 p_1], \\
\mathcal{M}^{(n)}_{3\,RR;LL} &= \frac{vC_4 m_W g_W^2}{\sqrt{2}\,\Pi_W \Pi_{W^*}}\, B_3^{(n)} [p_2 p_4] \langle p_3 p_1\rangle,
\end{aligned}
\tag{4.31}
$$

where

$$
\Pi_{W^*} = s_{12} - m_W^2 + i\Gamma_W m_W. \tag{4.32}
$$

The explicit expressions for the form factors $A_i^{(n)}$ and $B_i^{(n)}$ up to two loops are provided in Appendix A.

4.3.3 Two-loop form factors

This section will present a general technique for computing form factors for the case of higher-order corrections, which has been employed in this thesis to compute the two-loop form factors[6].

In the two-loop case, we consider the contribution of the diagrams with two virtual particles, as illustrated in Fig. 4 for the four-point vertex. As is customary, the three-point amplitude is comprised of the same set of diagrams. The interferences between this type of diagrams and the amplitudes of the LO process lead, together with squared one-loop amplitudes, to the double-virtual corrections.

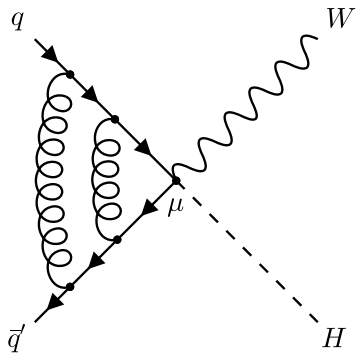

Figure 4: Representative four-point Feynman diagram within the Standard Model Effective Field Theory at two loops.

[6]There are a number of alternative techniques that may be employed for such computations. One such technique, the Passarino–Veltman approach [151, 152], was utilised by my collaborators in the parallel computation of two-loop corrections. For an introduction to this technique, please refer to paper [153].

As previously outlined in Section 4.3.1, the tensor structure of the amplitudes is maintained in the purely virtual scenario for all orders of perturbation theory. For this reason, in this section, we will undertake the calculations in the general case, which can then be readily applied to the two-loop scenario.

We start with the 4-point amplitude with an open index μ again. As it has been discussed in the previous subsection, we can use set of tensor structures (4.19) also in the two-loop case. Then using Eq. (4.25) we can write that

$$\begin{aligned}\mathcal{M}_{4\,\lambda_1\lambda_2}^{(n)\mu} = \overline{U}_{\lambda_2}(p_2)\Big[&\Big(A_1^{(n)}T_1^\mu + A_2^{(n)}T_2^\mu\Big)\Big(C_1P_L + C_2P_R\Big) \\ &+ A_3^{(n)}T_3^\mu\Big(C_3P_L + C_4P_R\Big)\Big]U_{\lambda_1}(p_1).\end{aligned} \tag{4.33}$$

As previously demonstrated, each helicity amplitude is defined by a unique value of the coefficient C_i. In order to work with the total amplitude, it is therefore possible to set aside the projectors P_L and P_R from Eq. (4.33)[7].

In order to compute the n-loop form factors, one can multiply Eq. (4.33) by a function of the form $\overline{U}(p_1)f_\mu U(p_2)$, where the specific tensor structure for f_μ can be selected. If we select $f_\mu = \gamma_\mu$, then after trace computations, two of the three tensor structures vanish, since there will be an odd number of γ-matrices on the right-hand side, therefore, by multiplying Eq. (4.33) by $\overline{U}(p_1)\gamma_\mu U(p_2)$, the amplitude is projected directly onto γ^μ and an expression for $A_3^{(2)}$ can be immediately obtained. Indeed,

$$\begin{aligned}\mathcal{M}_4^{(n)\mu}\,\overline{U}(p_1)\gamma_\mu U(p_2) &= \mathrm{tr}\Big[\not{p}_2\big(A_1^{(n)}T_1^\mu + A_2^{(n)}T_2^\mu + A_3^{(n)}T_3^\mu\big)\not{p}_1\gamma_\mu\Big] \\ &= A_3^{(n)}\mathrm{tr}\left(\not{p}_2\gamma^\mu\not{p}_1\gamma_\mu\right).\end{aligned} \tag{4.34}$$

By employing the standard rules of γ-matrix algebra discussed in Appendix B, one can compute the trace in Eq. (4.34), thereby deriving the following relation

$$A_3^{(n)} = \frac{\mathcal{M}_4^{(n)\mu}\,U(p_2)\gamma_\mu\overline{U}(p_1)}{2(2-d)s_{12}}. \tag{4.35}$$

The right-handed side of Eq. (4.35) contains the trace of a certain number of γ-matrices which can be readily calculated using modern computational tools, such as, for instance, FORM[8].

In regard to the remaining two form factors, it is necessary to select a tensor f_μ comprising an even number of γ-matrices for the purpose of extracting them from Eq. (4.33). The most straightforward option is to select $f_\mu = p_{1\mu}$. Subsequently,

$$\begin{aligned}\mathcal{M}_4^{(n)\mu}\,\overline{U}(p_1)p_{1\mu}U(p_2) &= \mathrm{tr}\Big[\not{p}_2\Big(A_1^{(n)}T_1^\mu + A_2^{(n)}T_2^\mu + A_3^{(n)}T_3^\mu\Big)\not{p}_1\not{p}_{1\mu}\Big] \\ &= \Big[A_1^{(n)}\mathrm{tr}\Big(\not{p}_2\not{p}_1\not{p}_W\not{p}_1 - (p_1\cdot p_W)\not{p}_2\not{p}_1\Big) \\ &\quad - A_2^{(n)}(p_1\cdot p_W)(p_1\cdot p_2)\mathrm{tr}\left(\not{p}_2\not{p}_1\right)\Big] \\ &= (p_1\cdot p_W)s_{12}\left(s_{12}A_2^{(n)} - 2A_1^{(n)}\right).\end{aligned} \tag{4.36}$$

[7]Naturally, this assertion can be verified through direct examination.

[8]A detailed description and comprehensive documentation of this invaluable tool can be accessed at https://www.nikhef.nl/~form/

If we now select $f_\mu = p_{2\mu}$, we find that the result is once again Eq. (4.36). Furthermore, the option of selecting the momentum p_W as f_μ is also unsuitable, as the helicity amplitudes proportional to C_1 and C_2 are zeroed out when contracted with this momentum. Consequently, the next variant is $f_\mu = \gamma_\mu \not{p}_W$. In a similar manner, the following equation can be derived

$$\begin{aligned}\mathcal{M}_4^{(n)\mu}\, \overline{U}(p_1)\gamma_\mu \not{p}_W U(p_2) \\ &= A_1^{(n)}\Big(8(d-2)(p_1\cdot p_W)(p_2\cdot p_W) + 2(3-d)s_{12}m_W^2\Big) \\ &\quad - 8A_2^{(n)} s_{12}(p_1\cdot p_W)(p_2\cdot p_W).\end{aligned} \tag{4.37}$$

By solving Eqs. (4.36) and (4.37) together, one can express the form factors $A_1^{(n)}$ and $A_2^{(n)}$ in terms of the n-loop amplitude as follows

$$\begin{aligned}A_1^{(n)} &= \frac{(d-2)(d-3)s_{12}m_W^2 - (s_{1W}-m_W^2)(s_{2W}-m_W^2)}{(d-3)s_{12}(s_{1W}-m_W^2)\big((s_{1W}-m_W^2)(s_{2W}-m_W^2) - (d-3)s_{12}m_W^2\big)}\,\mathcal{Y}^{(n)} \\ &\quad + \frac{\widetilde{\mathcal{Y}}^{(n)}}{2(d-3)\big((s_{1W}-m_W^2)(s_{2W}-m_W^2) - s_{12}m_W^2\big)},\end{aligned} \tag{4.38}$$

$$\begin{aligned}A_2^{(n)} &= \frac{1}{(d-3)s_{12}\big((s_{1W}-m_W^2)(s_{2W}-m_W^2) - s_{12}m_W^2\big)}\times \\ &\quad \times\left(\widetilde{\mathcal{Y}}^{(n)} - \frac{2\big((d-2)(s_{1W}-m_W^2)(s_{2W}-m_W^2) + (3-d)s_{12}m_W^2\big)}{s_{12}(s_{1W}-m_W^2)}\,\mathcal{Y}^{(n)}\right),\end{aligned} \tag{4.39}$$

where $\mathcal{Y}^{(n)} = \mathcal{M}_4^{(n)\mu}\,\overline{U}(p_1)p_{1\mu}U(p_2)$, $\widetilde{\mathcal{Y}}^{(n)} = \mathcal{M}_4^{(n)\mu}\,\overline{U}(p_1)\gamma_\mu \not{p}_W U(p_2)$ and definitions of the invariants (4.7) have been applied.

The results obtained in Eqs. (4.35), (4.38), and (4.39) can now be applied to the two-loop case. Once the total expressions for each two-loop diagram have been obtained from QGRAF[9], one can use FORM to obtain the total expression for the two-loop four-point amplitude $\mathcal{M}_4^{(2)\mu}$ and evaluate the right-handed sides of the mentioned equations. After computing these, a multitude of two-loop tensor integrals are produced. To reduce them to two-loop scalar integrals, all possible scalar products can be exchanged by propagators of the integrals.

The propagators are classified according to the so-called topologies, which comprise the minimum possible set of propagators in total amplitude. In the present case, the propagators can be divided into two groups, since one of the diagrams is non-planar:

Topology 1:

$$\begin{aligned}&D_1 = k_1^2, && D_2 = (k_1-p_1)^2, && D_3 = (k_1-p_1-p_2)^2, \\ &D_4 = (k_1-k_2)^2, && D_5 = k_2^2, && D_6 = (k_2+p_W)^2, \\ &D_7 = (k_2-p_1-p_2)^2, && D_8 = (k_2-p_1)^2, && D_9 = (k_1+p_W)^2,\end{aligned} \tag{4.40}$$

[9]QGRAF is a computer program that generates Feynman diagrams for a variety of QFT models. Further details and an introduction to this tool can be found at http://cfif.ist.utl.pt/~paulo/qgraf.html

Topology 2:

$$\begin{aligned}
&\widetilde{D}_1 = (k_1 - k_2 - p_1)^2, \qquad \widetilde{D}_2 = (k_2 - p_1)^2, \qquad \widetilde{D}_3 = (k_1 - p_1 - p_2)^2, \\
&\widetilde{D}_4 = (k_1 - k_2)^2, \qquad \widetilde{D}_5 = k_2^2, \qquad \widetilde{D}_6 = (k_2 + p_W)^2, \\
&\widetilde{D}_7 = (k_2 - p_1 - p_2)^2, \qquad \widetilde{D}_8 = k_1^2, \qquad \widetilde{D}_9 = (k_1 + p_W)^2.
\end{aligned} \tag{4.41}$$

It is evident that propagators containing momentum p_W cannot appear in the denominator, given that only QCD corrections are being considered. However, these propagators were introduced artificially into the topologies to facilitate the evaluation of the corresponding scalar products in the numerator and the calculation of the tensor loop integrals.

After a sufficient number of computations have been performed, it is possible to express two-loop form factors in terms of a large number of two-loop scalar integrals. The subsequent application of the REDUZE software facilitates the interchange of each of these quantities with a combination of master integrals. In the present case, there are four of them:

$$\begin{aligned}
I_1^{(2)} &= \mu_0^{4\varepsilon} \int \frac{d^dk_1}{(2\pi)^d} \frac{d^dk_2}{(2\pi)^d} \frac{1}{D_1 D_4 D_7}, \\
I_2^{(2)} &= \mu_0^{4\varepsilon} \int \frac{d^dk_1}{(2\pi)^d} \frac{d^dk_2}{(2\pi)^d} \frac{1}{D_1 D_3 D_4 D_8}, \\
I_3^{(2)} &= \mu_0^{4\varepsilon} \int \frac{d^dk_1}{(2\pi)^d} \frac{d^dk_2}{(2\pi)^d} \frac{1}{D_1 D_3 D_5 D_7}, \\
I_4^{(2)} &= \mu_0^{4\varepsilon} \int \frac{d^dk_1}{(2\pi)^d} \frac{d^dk_2}{(2\pi)^d} \frac{1}{\widetilde{D}_1 \widetilde{D}_2 \widetilde{D}_3 \widetilde{D}_4 \widetilde{D}_7 \widetilde{D}_8}.
\end{aligned} \tag{4.42}$$

The graphical interpretation of these two-loop scalar massless integrals is presented in Fig. 5.

The solutions for the first three master integrals can be found in section 5 of reference [154], whereas the solution for the integral $I_4^{(2)}$ is presented in equation (A.6) of reference [155]:

$$\begin{aligned}
I_1^{(2)} &= \frac{s_{12}}{64\pi^4} \left(\frac{4\pi\mu_0^2}{-s_{12}}\right)^{2\varepsilon} \frac{S_d^2}{(d-3)(d-4)} \frac{\Gamma(5-d)\,\Gamma^2(d-3)}{\Gamma\left(\frac{6-d}{2}\right)\Gamma\left(\frac{d-2}{2}\right)\Gamma\left(\frac{3d-6}{2}\right)}, \\
I_2^{(2)} &= -\frac{1}{32\pi^4} \left(\frac{4\pi\mu_0^2}{-s_{12}}\right)^{2\varepsilon} \frac{S_d^2}{(d-3)(d-4)^2} \frac{\Gamma^3(d-3)\,\Gamma(5-d)}{\Gamma\left(\frac{6-d}{2}\right)\Gamma^2\left(\frac{d-2}{2}\right)\Gamma\left(\frac{3d-8}{2}\right)}, \\
I_3^{(2)} &= -\frac{1}{16\pi^4} \left(\frac{4\pi\mu_0^2}{-s_{12}}\right)^{2\varepsilon} \frac{S_d^2}{(d-3)^2(d-4)^2}, \\
I_4^{(2)} &= \frac{1}{64\pi^4 s_{12}^2} \left(\frac{4\pi\mu_0^2}{-s_{12}}\right)^{2\varepsilon} \left(\frac{1}{\varepsilon^4} - \frac{5\pi^2}{6}\frac{1}{\varepsilon^2} - \frac{27\zeta(3)}{\varepsilon} - \frac{23\pi^4}{36} + \right. \\
&\qquad \left. + \left(8\pi^2\zeta(3) - 117\zeta(5)\right)\varepsilon - \left(\frac{19\pi^6}{315} - 267\zeta^2(3)\right)\varepsilon^2 + \mathcal{O}(\varepsilon^3)\right),
\end{aligned} \tag{4.43}$$

where

$$S_d = \frac{\Gamma\left(\frac{6-d}{2}\right)\Gamma^2\left(\frac{d-2}{2}\right)}{\Gamma(d-3)}, \tag{4.44}$$

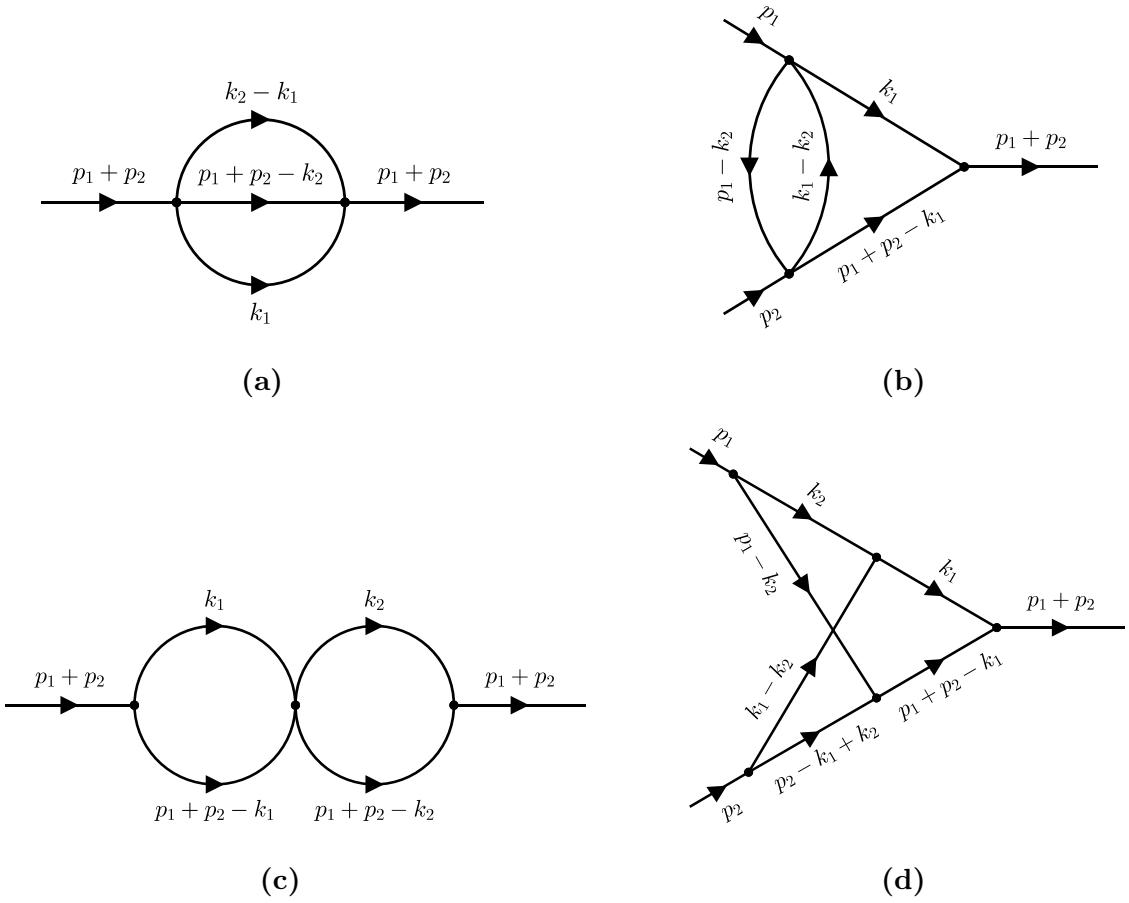

Figure 5: Two-loop master integrals: "sunrise" $I_1^{(2)}$ (a), "triangle" $I_2^{(2)}$ (b), "double bubble" $I_3^{(2)}$ (c), "non-planar" $I_4^{(2)}$ (d) (see Eqs. (4.41)).

$\gamma_E \approx 0.5772$ is the Euler–Mascheroni constant [156] and $\zeta(x)$ is the Euler–Riemann zeta function.

4.3.4 Two-loop renormalisation

The one-loop and the two-loop form factors appeared to be divergent, but as we are studying a physical process, it is evident that the final amplitude must be finite. The divergences contained by the form factors may be classified as either ultraviolet or infrared; however, distinguishing between these two categories represents a significant challenge. Fortunately, Stefano Catani published a paper in 1998, which demonstrated the infrared behavior of QCD amplitudes in one- and two-loop cases [157]. This allows the infrared divergences to be subtracted from the form factors. Ultraviolet divergences require renormalization, and there are generally three different things to be renarmalized: external legs, the coupling constant and the Wilson coefficients.

In the present case, external legs do not require renormalization, since we consider massless incoming quarks and, therefore, renormalization is trivial. Renormalization of the bare coupling constant α_s^B can be conducted in accordance with the standard methodology (see, e.g. [157])

$$\alpha_s^B \mu_0^{2\varepsilon} S_\varepsilon = \alpha_s(\mu^2)\mu^{2\varepsilon}\left(1 - \alpha_s(\mu^2)\frac{\beta_0}{\varepsilon} + \mathcal{O}\left(\alpha_s^2(\mu^2)\right)\right), \tag{4.45}$$

where μ is the renormalization scale, $S_\varepsilon = e^{\varepsilon[\log(4\pi)+\psi(1)]}$ and $\psi(1) = -\gamma_E$ is the polygamma function, so that

$$S_\varepsilon = (4\pi)^\varepsilon e^{-\gamma_E \varepsilon} \tag{4.46}$$

and the first coefficient of the QCD β-function

$$\beta_0 = \frac{11C_A - 4T_R N_f}{12} = \frac{33 - 2N_f}{12}, \tag{4.47}$$

where N_f is the number of active flavors, C_A is the quadratic Casimir operator of the adjoint representation of the group $SU(N)$, T_R is the standard normalization of the trace of the fundamental representation generators: $\mathrm{tr}\left(t^a t^b\right) = T_R \delta^{ab}$.

Following the application of the Catani subtraction procedure, the infrared divergences are no longer present in the form factors. Subsequently, ultraviolet divergences must be canceled by multiplying the form factors by quantities known as renormalisation constants, which serve to perform the necessary renormalisation of the Wilson coefficients. These constants can be extracted from the relevant literature, which will be referenced below.

It should be noted that the subtraction of infrared poles by the Catani operator and the renormalization of the Wilson coefficients are two operations that commute with one another. Consequently, the order in which they are carried out is unimportant. In this thesis, the following order is employed for the implementation of the requisite renormalization steps: firstly, the renormalization of the strong coupling constant α_s; secondly, the Catani subtraction; and finally, the renormalization of the Wilson coefficients.

The total two-loop non-renormalized form factors corresponding to the four-point amplitude can be expressed in perturbation theory as follows

$$A_i = A_i^{(0)} + \frac{\alpha_s^B}{2\pi} A_i^{(1)} + \left(\frac{\alpha_s^B}{2\pi}\right)^2 A_i^{(2)} + \mathcal{O}\left(\left(\alpha_s^B\right)^3\right), \tag{4.48}$$

This equation demonstrates that the renormalization of α_s^B at the one-loop level contributes to the two-loop divergences. Indeed, by applying Eq. (4.45) to Eq. (4.48), the following expression can be obtained

$$\begin{aligned} A_i = A_i^{(0)} + \frac{\alpha_s(\mu^2)}{2\pi}\left(\frac{\mu^2}{\mu_0^2}\right)^\varepsilon S_\varepsilon^{-1} A_i^{(1)} + \\ + \left(\frac{\alpha_s(\mu^2)}{2\pi}\right)^2 \left[-\left(\frac{\mu^2}{\mu_0^2}\right)^\varepsilon S_\varepsilon^{-1} \frac{2\beta_0}{\varepsilon} A_i^{(1)} + \left(\frac{\mu^2}{\mu_0^2}\right)^{2\varepsilon} S_\varepsilon^{-2} A_i^{(2)}\right] + \mathcal{O}\left(\alpha_s^3\right). \end{aligned} \tag{4.49}$$

Henceforth in this section, the renormalized coupling constant will be denoted by α_s.

The second step of the renormalization process is to subtract infrared divergences using the Catani operator. In the two-loop case, the form factor that contains only ultraviolet divergences and finite terms can be expressed as follows [157]

$$A_i^{\mathrm{UV+fin}} = A_i^{(2)} - \mathcal{I}^{(1)}(\varepsilon) A_i^{(1)} - \mathcal{I}^{(2)}(\varepsilon) A_i^{(0)}, \tag{4.50}$$

where $\mathcal{I}^{(1)}(\varepsilon)$ and $\mathcal{I}^{(2)}(\varepsilon)$ are the one-loop and two-loop Catani operators, respectively, which are given by

$$\mathcal{I}^{(1)}(\varepsilon) = \frac{e^{\varepsilon\gamma_E}}{\Gamma(1-\varepsilon)}\left(\frac{C_F}{\varepsilon^2}+\frac{3C_F}{2\varepsilon}\right)\left(\frac{\mu^2 e^{-i\pi}}{2(p_1\cdot p_2)}\right)^{\varepsilon}, \tag{4.51}$$

$$\begin{aligned}\mathcal{I}^{(2)}(\varepsilon) = &-\frac{1}{2}\mathcal{I}^{(1)}(\varepsilon)\left(\mathcal{I}^{(1)}(\varepsilon)+4\pi\beta_0\frac{1}{\varepsilon}\right)\\ &+\frac{e^{-\varepsilon\gamma_E}\Gamma(1-2\varepsilon)}{\Gamma(1-\varepsilon)}\left(2\pi\beta_0\frac{1}{\varepsilon}+K\right)\mathcal{I}^{(1)}(2\varepsilon)+H_2(\varepsilon).\end{aligned} \tag{4.52}$$

The two-loop Catani operator is dependent on the operator $H_2(\varepsilon)$ for which a general expression is provided in [158, 159]. However, for our process, this operator can be extracted from [157]

$$\begin{aligned}H_2(\varepsilon) = \frac{1}{4\varepsilon}\frac{e^{\varepsilon\gamma_E}}{\Gamma(1-\varepsilon)}\left(\frac{\mu^2 e^{-i\pi}}{2(p_1\cdot p_2)}\right)^{2\varepsilon}&\left(\frac{1}{4}\gamma_{(1)}+3C_F K\right.\\ &\left.+5\pi\xi(2)\beta_0 C_F-\frac{56}{9}\pi\beta_0 C_F-\left(\frac{16}{9}-7\xi(3)\right)C_F C_A\right),\end{aligned} \tag{4.53}$$

where

$$\begin{aligned}\gamma_{(1)} = &\big(-3+24\xi(2)-48\xi(3)\big)C_F^2\\ &+\left(-\frac{17}{3}-\frac{88}{3}\xi(2)+24\xi(3)\right)C_F C_A+\left(\frac{4}{3}+\frac{32}{3}\xi(2)\right)C_F T_R N_f\end{aligned} \tag{4.54}$$

and, finally,

$$K = \left(\frac{67}{18}-\frac{\pi^2}{6}\right)C_A-\frac{10}{9}T_R N_f. \tag{4.55}$$

The ultraviolet poles in $A_i^{\text{UV+fin}}$ in Eq. (4.50) can be canceled by renormalization of the Wilson coefficients. This is achieved by writing down the total finite form factor as

$$\begin{aligned}A_i^{\text{fin}} &= A_i^{(0)}+\frac{\alpha_s}{2\pi}A_i^{(1)\text{fin}}+\left(\frac{\alpha_s}{2\pi}\right)^2 A_i^{(2)\text{fin}}+\mathcal{O}\left(\alpha_s^3\right)=\\ &= Z\left(A_i^{(0)}+\frac{\alpha_s}{2\pi}A_i^{(1)\text{UV+fin}}+\left(\frac{\alpha_s}{2\pi}\right)^2 A_i^{(2)\text{UV+fin}}+\mathcal{O}\left(\alpha_s^3\right)\right),\end{aligned} \tag{4.56}$$

where the one-loop form factor $A_i^{(1)\text{UV+fin}}$ can be calculated as follows

$$A_i^{(1)\text{UV+fin}} = A_i^{(1)}-\mathcal{I}^{(1)}(\varepsilon)A_i^{(0)} \tag{4.57}$$

and the two-loop renormalization function is defined as

$$Z = 1+\frac{\alpha_s}{2\pi}\frac{z^{(1,1)}}{\varepsilon}+\left(\frac{\alpha_s}{2\pi}\right)^2\left(\frac{z^{(2,2)}}{\varepsilon^2}+\frac{z^{(2,1)}}{\varepsilon}\right)+\mathcal{O}(\alpha_s^3). \tag{4.58}$$

In light of the fact that value (4.56) should not contain any divergences, it is possible to adjust the renormalization constants $z^{(1,1)}$, $z^{(2,1)}$ and $z^{(2,2)}$ in such a way, so that all divergences are canceled. This leads to the following expressions

$$
\begin{aligned}
z^{(1,1)} &= -\frac{C_F}{2}, \\
z^{(2,1)} &= \frac{C_F}{16}\left(19C_F + \frac{26}{9}N_f - \frac{257}{9}N_c\right), \\
z^{(2,2)} &= \frac{C_F}{2}\left(\beta_0 - \frac{C_F}{2}\right),
\end{aligned}
\tag{4.59}
$$

which agrees with results in reference [101].

This procedure allows us to renormalize all three two-loop form factors. As form factor A_2 does not appear at the leading order, its renormalization is trivial and terminates upon the exchanging of the bare coupling constant α_s^B by the renormalized one. The finite remainder is found to be zero. With regard to the form factor A_3, its renormalization function appears to be equal to 1, indicating that A_3 contains infrared divergences only and is non-renormalizable at the one- and two-loop levels. Thus, if we introduce the 4×4 renormalization matrix

$$
Z_{ij} = \delta_{ij} + \frac{\alpha_s}{2\pi}\frac{z_{ij}^{(1,1)}}{\varepsilon} + \left(\frac{\alpha_s}{2\pi}\right)^2\left(\frac{z_{ij}^{(2,2)}}{\varepsilon^2} + \frac{z_{ij}^{(2,1)}}{\varepsilon}\right) + \mathcal{O}(\alpha_s^3),
\tag{4.60}
$$

where rows and columns correspond to the Wilson coefficients related to C_1, C_2, C_3, C_4, respectively, the following expressions can be formulated

$$
\begin{aligned}
z_{ij}^{(1,1)} &= -\frac{C_F}{2}\begin{pmatrix} 1 & 0 & 0 & 0 \\ 0 & 1 & 0 & 0 \\ 0 & 0 & 0 & 0 \\ 0 & 0 & 0 & 0 \end{pmatrix}, \\
z_{ij}^{(2,1)} &= \frac{C_F}{16}\left(19C_F + \frac{26}{9}N_f - \frac{257}{9}N_c\right)\begin{pmatrix} 1 & 0 & 0 & 0 \\ 0 & 1 & 0 & 0 \\ 0 & 0 & 0 & 0 \\ 0 & 0 & 0 & 0 \end{pmatrix}, \\
z_{ij}^{(2,2)} &= \frac{C_F}{2}\left(\beta_0 - \frac{C_F}{2}\right)\begin{pmatrix} 1 & 0 & 0 & 0 \\ 0 & 1 & 0 & 0 \\ 0 & 0 & 0 & 0 \\ 0 & 0 & 0 & 0 \end{pmatrix},
\end{aligned}
\tag{4.61}
$$

where, as previously stated, C_F is the quadratic Casimir operator of $SU(3)$; N_f and N_c denote the numbers of active flavors and colors, respectively.

Non-renormalized and renormalized LO, NLO and NNLO form factors A_i and B_i for pure loop corrections are presented in Appendix A.

4.4 Single real corrections

In addition to purely virtual corrections, there are also corrections that result from the emission of real particles. Furthermore, such corrections also contain divergences which must be precisely cancelled by the divergences from the loop corrections at the level of cross sections, that is to say, after integration over the phase space. Additionally, the soft-collinear limits should be satisfied, as has been verified in this thesis.

4.4.1 Tree-level

Two diagrams, shown in Fig. 6, contribute to the four-point amplitude at order $\mathcal{O}\left(\alpha_s^{1/2}\right)$ and describe tree-level single real gluon emission for the four-point vertex.

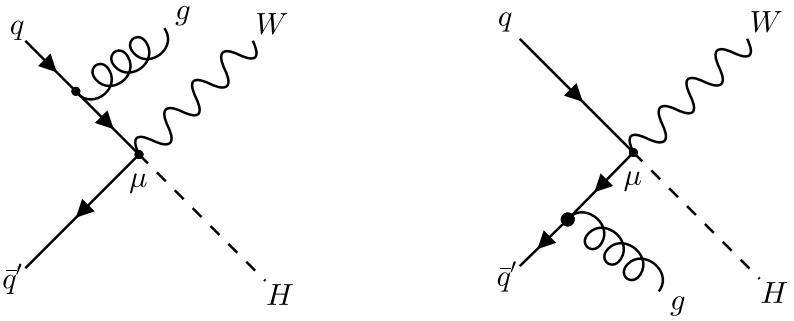

Figure 6: Four-point Feynman diagrams for single real gluon corrections at tree level.

The introduction of the real gluon momentum p_5 and helicity λ_5 allows us to derive a simple expression for the four-point amplitude with open index μ as follows

$$\begin{aligned}\left(\frac{\alpha_s}{2\pi}\right)^{1/2}\mathcal{M}^{(g)\mu a}_{4\;\lambda_1\lambda_2;\lambda_5} = &\frac{g_s t^a}{s_{25}}\,\overline{U}_{\lambda_2}(p_2)\not{\varepsilon}^{\,*}_{5\lambda_5}(p_5)(\not{p}_2-\not{p}_5)A^\mu U_{\lambda_1}(p_1)- \\ &-\frac{g_s t^a}{s_{15}}\,\overline{U}_{\lambda_2}(p_2)A^\mu(\not{p}_1-\not{p}_5)\not{\varepsilon}^{\,*}_{5\lambda_5}(p_5)U_{\lambda_1}(p_1),\end{aligned} \tag{4.62}$$

where A^μ is given in (2.23), ε_5 is the real gluon polarization vector, and the definitions (4.7) have been used.

The total expression (4.62) assumes different forms for left- and right-handed gluons (i.e. for $\lambda_5 = \{L, R\}$). By employing the spinor algebra relations outlined in Appendix C, one can rewrite Eq. (4.62) in terms of helicity amplitudes as a sum of all possible helicity combinations, such as $\mathcal{M}^{(g)\mu a}_{4\;LR;L}$, $\mathcal{M}^{(g)\mu a}_{4\;LR;R}$, etc. As an example,

$$\mathcal{M}^{(g)\mu a}_{4\;LR;L} = 4\pi\sqrt{2}\;t^a C_1\,\frac{[p_2|[\gamma^\mu,\not{p}_W]|p_1]}{[p_5 r_5]}\left(\frac{[p_2 r_5]\langle p_5 p_2\rangle}{s_{25}}-\frac{\langle p_1 p_5\rangle[r_5 p_1]}{s_{15}}\right), \tag{4.63}$$

where an arbitrary massless reference vector r_5 has been introduced. It is possible to select this vector to be equal to any incoming vector, p_1 or p_2, thereby fixing the gauge. Nevertheless, we will maintain this vector explicitly in order to demonstrate the gauge invariance of helicity amplitudes and, consequently, the total amplitude in a more explicit manner.

Expression (4.63) can be evaluated using some relations of spinor algebra, such as Schouten identities and others (see Appendix C), and also Eq. (4.7). In an absolutely similar way, other seven four-point helicity amplitudes can be obtained and we can write

$$
\begin{aligned}
\mathcal{M}^{(g)\mu a}_{4\;LR;L} &= 4\pi\sqrt{2}\; t^a C_1\; \frac{[p_2p_1][p_2|\big(\gamma^\mu \not{p}_W - p_W^\mu\big)|p_1]}{[p_1p_5][p_2p_5]},\\
\mathcal{M}^{(g)\mu a}_{4\;LR;R} &= 4\pi\sqrt{2}\; t^a C_1\; \frac{\langle p_1p_2\rangle[p_2|\big(\gamma^\mu \not{p}_W - p_W^\mu\big)|p_1]}{\langle p_1p_5\rangle\langle p_2p_5\rangle} +\\
&\quad + 4\pi\sqrt{2}\; t^a C_1 \bigg(\frac{[p_2\big(\gamma^\mu \not{p}_W - p_W^\mu\big)|p_5]}{\langle p_1p_5\rangle} - \frac{[p_5|\big(\gamma^\mu \not{p}_W - p_W^\mu\big)|p_1]}{\langle p_2p_5\rangle}\bigg),\\
\mathcal{M}^{(g)\mu a}_{4\;RL;L} &= 4\pi\sqrt{2}\; t^a C_2\; \frac{[p_2p_1]\langle p_2|\big(\gamma^\mu \not{p}_W - p_W^\mu\big)p_1\rangle}{[p_1p_5][p_2p_5]} +\\
&\quad + 4\pi\sqrt{2}\; t^a C_2 \bigg(\frac{\langle p_5|\big(\gamma^\mu \not{p}_W - p_W^\mu\big)|p_1\rangle}{[p_2p_5]} - \frac{\langle p_2|\big(\gamma^\mu \not{p}_W - p_W^\mu\big)|p_5\rangle}{[p_1p_5]}\bigg),\\
\mathcal{M}^{(g)\mu a}_{4\;RL;R} &= 4\pi\sqrt{2}\; t^a C_2\; \frac{\langle p_1p_2\rangle\langle p_2|\big(\gamma^\mu \not{p}_W - p_W^\mu\big)|p_1\rangle}{\langle p_1p_5\rangle\langle p_2p_5\rangle},\\
\mathcal{M}^{(g)\mu}_{4\;LL;L} &= 2\pi\sqrt{2}\; t^a C_3 \bigg(\frac{[p_2p_1]\langle p_2|\gamma^\mu|p_1]}{[p_1p_5][p_2p_5]} + \frac{\langle p_5|\gamma^\mu|p_1]}{[p_2p_5]}\bigg),\\
\mathcal{M}^{(g)\mu a}_{4\;LL;R} &= 2\pi\sqrt{2}\; t^a C_3 \bigg(\frac{\langle p_1p_2\rangle\langle p_2|\gamma^\mu|p_1]}{\langle p_1p_5\rangle\langle p_2p_5\rangle} + \frac{\langle p_2|\gamma^\mu|p_5]}{\langle p_1p_5\rangle}\bigg),\\
\mathcal{M}^{(g)\mu a}_{4\;RR;L} &= 2\pi\sqrt{2}\; t^a C_4 \bigg(\frac{[p_2p_1][p_2|\gamma^\mu|p_1\rangle}{[p_1p_5][p_2p_5]} + \frac{[p_2|\gamma^\mu|p_5\rangle}{[p_5p_1]}\bigg),\\
\mathcal{M}^{(g)\mu a}_{4\;RR;R} &= 2\pi\sqrt{2}\; t^a C_4 \bigg(\frac{\langle p_1p_2\rangle[p_2|\gamma^\mu|p_1\rangle}{\langle p_1p_5\rangle\langle p_2p_5\rangle} + \frac{[p_5|\gamma^\mu|p_1\rangle}{\langle p_5p_2\rangle}\bigg).
\end{aligned}
\tag{4.64}
$$

As evidenced by the results (4.64), the arbitrary reference vector r_5 vanishes, thereby guaranteeing gauge independence of the amplitudes. Upon exchanging p_W with $p_{W^*} = p_1 + p_2$, the expressions for the 3-point helicity amplitudes can be readily obtained

$$
\begin{aligned}
\mathcal{M}^{(g)\mu a}_{3\;LR;L} &= 4\pi\sqrt{2}\; t^a v C_1\; \frac{[p_1p_2]^2}{[p_1p_5][p_2p_5]}\big(p_2^\mu - p_1^\mu\big),\\
\mathcal{M}^{(g)\mu a}_{3\;LR;R} &= 4\pi\sqrt{2}\; t^a v C_1 \frac{\big(-s_{12}-s_{15}-s_{25}\big)p_1^\mu + \big(s_{12}-s_{15}+s_{25}\big)p_2^\mu}{\langle p_1p_5\rangle\langle p_2p_5\rangle}\\
&\quad + 4\pi\sqrt{2}\; t^a v C_1 \bigg(\frac{[p_2|\gamma^\mu|p_1\rangle[p_1p_5]}{\langle p_1p_5\rangle} + \frac{[p_5|\gamma^\mu|p_2\rangle[p_1p_2]}{\langle p_2p_5\rangle}\bigg),\\
\mathcal{M}^{(g)\mu a}_{3\;RL;L} &= 4\pi\sqrt{2}\; t^a v C_2 \frac{\big(s_{12}+s_{15}+s_{25}\big)p_1^\mu + \big(-s_{12}+s_{15}-s_{25}\big)p_2^\mu}{[p_1p_5][p_2p_5]}\\
&\quad + 4\pi\sqrt{2}\; t^a v C_2 \bigg(\frac{\langle p_5|\gamma^\mu|p_2]\langle p_2p_1\rangle}{[p_2p_5]} + \frac{\langle p_2|\gamma^\mu|p_1]\langle p_5p_1\rangle}{[p_1p_5]}\bigg),\\
\mathcal{M}^{(g)\mu a}_{3\;RL;R} &= 4\pi\sqrt{2}\; t^a v C_2\; \frac{\langle p_1p_2\rangle^2}{\langle p_1p_5\rangle\langle p_2p_5\rangle}\big(p_1^\mu - p_2^\mu\big),\\
\mathcal{M}^{(g)\mu}_{3\;LL;L} &= 2\pi\sqrt{2}\; t^a \Big(S_3 + \frac{v}{2}C_3\Big) \bigg(\frac{[p_2p_1]\langle p_2|\gamma^\mu|p_1]}{[p_1p_5][p_2p_5]} + \frac{\langle p_5|\gamma^\mu|p_1]}{[p_2p_5]}\bigg),\\
\mathcal{M}^{(g)\mu a}_{3\;LL;R} &= 2\pi\sqrt{2}\; t^a \Big(S_3 + \frac{v}{2}C_3\Big) \bigg(\frac{\langle p_1p_2\rangle\langle p_2|\gamma^\mu|p_1]}{\langle p_1p_5\rangle\langle p_2p_5\rangle} + \frac{\langle p_2|\gamma^\mu|p_5]}{\langle p_1p_5\rangle}\bigg),
\end{aligned}
\tag{4.65}
$$

$$\mathcal{M}^{(g)\mu a}_{3\ RR;L} = \pi\sqrt{2}\ t^a v C_4 \bigg(\frac{[p_2 p_1][p_2|\gamma^\mu|p_1\rangle}{[p_1 p_5][p_2 p_5]} + \frac{[p_2|\gamma^\mu|p_5\rangle}{[p_5 p_1]} \bigg),$$
$$\mathcal{M}^{(g)\mu a}_{3\ RR;R} = \pi\sqrt{2}\ t^a v C_4 \bigg(\frac{\langle p_1 p_2\rangle[p_2|\gamma^\mu|p_1\rangle}{\langle p_1 p_5\rangle\langle p_2 p_5\rangle} + \frac{[p_5|\gamma^\mu|p_1\rangle}{\langle p_5 p_2\rangle} \bigg).$$

4.4.2 NLO soft and collinear limits

This section presents an explicit verification of the soft-collinear limit of the scattering amplitude for the Higgs-Strahlung process at NLO. The objective is to confirm the accuracy of the calculated amplitudes by ensuring that they exhibit the anticipated behavior in these singular limits. By examining the soft and collinear limits, it is possible to identify and validate any potential singularities, which is an essential step before extending the computation to higher orders. This approach focuses on the direct inspection of the soft and collinear regions in the amplitude, ensuring the consistency of the calculations and providing a foundation for future extensions to NNLO corrections.

Soft limit

The lepton current, which arises from the decay of the weak boson, does not affect the soft limit of the amplitude under consideration. Nevertheless, the established formulae are derived with precision at the level of total amplitudes. Furthermore, working with an open index in this case becomes inconvenient. Therefore, we should contract the amplitudes we obtained in Eq. (4.64) with the lepton current (4.5). On the other hand, we can use relations (4.29) to calculate the total tree-level amplitude.

By substituting tree-level form factors (4.24) into Eq. (4.29) and making summation over all helicity configurations one can obtain

$$\begin{aligned}\mathcal{M}^{(0)}_4 &= \mathcal{M}^{(0)}_{4\ LR;LL} + \mathcal{M}^{(0)}_{4\ RL;LL} + \mathcal{M}^{(0)}_{4\ LL;LL} + \mathcal{M}^{(0)}_{4\ RR;LL} \\ &= \frac{g_W\sqrt{2}}{p_W^2 - m_W^2 + i\Gamma_W m_W} \Big(4C_1[p_4 p_1][p_2 p_4]\langle p_3 p_4\rangle + 4C_2\langle p_1 p_3\rangle\langle p_2 p_3\rangle[p_3 p_4] \\ &\qquad + C_3\langle p_2 p_3\rangle[p_4 p_1] + C_4[p_2 p_4]\langle p_3 p_1\rangle \Big).\end{aligned} \tag{4.66}$$

A direct calculation of the total four-point amplitude with a real left-handed gluon reveals that[10]

$$\begin{aligned}\mathcal{M}^{(g)a}_{4,L} &= \mathcal{M}^{(g)a}_{4\ LR;LL;L} + \mathcal{M}^{(g)a}_{4\ RL;LL;L} + \mathcal{M}^{(g)a}_{4\ LL;LL;L} + \mathcal{M}^{(g)a}_{4\ RR;LL;L} \\ &\approx \frac{2 g_s g_W t^a}{p_W^2 - m_W^2 + i\Gamma_W m_W} \frac{[p_2 p_1]}{[p_1 p_5][p_2 p_5]} \Big(4C_1[p_4 p_1][p_2 p_4]\langle p_3 p_4\rangle \\ &\qquad + 4C_2\langle p_1 p_3\rangle\langle p_2 p_3\rangle[p_3 p_4] + C_3\langle p_2 p_3\rangle[p_4 p_1] + C_4[p_2 p_4]\langle p_3 p_1\rangle \Big),\end{aligned} \tag{4.67}$$

where all singularities of order less than $1/p_5$ are neglected, as we consider the soft limit $p_5 \to 0$.

Expression (4.67) can be transformed in a cunning way. By employing the Schouten identity (C.21), one can derive

[10] The external particle helicities are ordered as follows: quark (p_1), antiquark (p_2), lepton (p_3), antilepton (p_4), gluon (p_5).

$$\begin{aligned}\mathcal{M}_{4,L}^{(g)a} &= \mathcal{M}_4^{(0)} g_s t^a \sqrt{2}\, \frac{[p_2 p_1]}{[p_1 p_5][p_2 p_5]} = \mathcal{M}_4^{(0)} g_s t^a\, \frac{\sqrt{2}}{[p_5 r_5]}\, \frac{[r_5 p_1][p_5 p_2] - [r_5 p_2][p_5 p_1]}{[p_1 p_5][p_2 p_5]} \\ &= \mathcal{M}_4^{(0)} g_s t^a \left(\frac{1}{(p_1 \cdot p_5)} \frac{p_1^\mu [r_5|\gamma_\mu|p_5\rangle}{\sqrt{2}[p_5 r_5]} - \frac{1}{(p_2 \cdot p_5)} \frac{p_2^\mu [r_5|\gamma_\mu|p_5\rangle}{\sqrt{2}[p_5 r_5]} \right) \\ &= \mathcal{M}_4^{(0)} g_s \left(t^a \frac{(p_1 \cdot \varepsilon_{5L}^*)}{(p_1 \cdot p_5)} - t^a \frac{(p_2 \cdot \varepsilon_{5L}^*)}{(p_2 \cdot p_5)} \right),\end{aligned} \tag{4.68}$$

where $\varepsilon_{5L}^*(p_5)$ is the polarization vector of the left-handed real gluon. The same result is also applicable to the right-handed gluon.

Relation (4.68) is in exact correspondence with the soft limit formula [160, 161] which, in the specific case under consideration, assumes the following form

$$\mathcal{M}_4^{(g)a} \xrightarrow{p_5 \to 0} g_s \varepsilon_5^{\mu *}(p_5) J_\mu^{(0)a}(p_5) \mathcal{M}_4^{(0)}, \tag{4.69}$$

where

$$J_\mu^{a(0)}(q) = \sum_{i=1}^{m} T_i^a \frac{p_i^\mu}{(p_i \cdot q)} \tag{4.70}$$

is the tree-level soft-gluon current and m represents the number of external partons in the process without the real gluon. In Eq. (4.70), $T_i^a = t^a$ for a quark and $T_i^a = -t^a$ for an antiquark. The same result is also applicable to the three-point amplitude.

The emission of a soft gluon does not affect the momenta and spins of the radiating hard partons. However, it does affect their color because the gluon always carries away some color charge, no matter how soft it is. Unlike the case of soft-photon emission in QED, soft-gluon emission thus does not factorize exactly and leads to color correlations.

Collinear limit

The objective of this study is to examine the behavior of the amplitude in a kinematical configuration where one of the incoming partons and the outgoing gluon become almost collinear. To illustrate, we consider the case where the gluon is collinear with the quark. In this case, the momenta p_1 and $-p_5$ are approximately equal, resulting in a small invariant $s_{15} = (p_1 + p_5)^2$, which leads to a singular amplitude.

The collinear momenta can be parametrized as

$$p_i^\mu = x_i p^\mu + k_{\perp i}^\mu - \frac{k_{\perp i}^2}{x_i} \cdot \frac{n^\mu}{2(p \cdot n)}, \tag{4.71}$$

where, in our case, $i = 1$ or 5, x_i are longitudinal components, p^μ denotes collinear direction, n^μ is an auxiliary vector which is necessary to specify the transverse components $k_{\perp i}^\mu$. Vectors p^μ and n^μ are light-like ($p^2 = 0$ and $n^2 = 0$) and also the relations $(k_{\perp i} \cdot p) = 0$ and $(k_{\perp i} \cdot n) = 0$ should be satisfied, while $k_{\perp i}^2 < 0$. We also define another light-like momentum

$$\widetilde{P}_{ij}^\mu = (p_i + p_j)^\mu - \frac{s_{ij} n^\mu}{2(p_i \cdot n) + 2(p_j \cdot n)}. \tag{4.72}$$

The collinear limit is dependent upon the helicity of the particles, and thus it becomes especially important to consider each combination of helicities separately when working

in the helicity amplitude method. To illustrate, consider the amplitudes $\mathcal{M}^{(0)}_{4\,LR;LL}$ and $\mathcal{M}^{(g)a}_{4\,LR;LL;L}$. The exact expression for the former is already known from Eq. (4.66), and the expression for the latter can be easily obtained using Eqs. (4.64) and (4.1).

By carrying out parameterization (4.71) in the exact amplitude $\mathcal{M}^{(g)a}_{4\,LR;LL;L}$ to make the collinear limit $p_1 || p_5$, one can come to the following relation [162, 163]

$$\mathcal{M}^{(g)a}_{4\,\lambda_1\lambda_2;LL;\lambda_5}(p_1,p_2,p_5) \xrightarrow{p_5 || p_1} Sp^{(0)a}_{q\to qg}(p_1,p_5,\widetilde{P}_{15})\mathcal{M}^{(0)}_{4\,\lambda_1\lambda_2;LL}(p_2,\widetilde{P}_{15}), \tag{4.73}$$

where $Sp^{(0)a}_{q\to qg}(p_1,p_5,\widetilde{P}_{15})$ is the leading order splitting matrix which is, technically speaking, a matrix in color + spin space. It acts between the color space of the 2 partons of $\mathcal{M}^{(0)}_4(p_2,\widetilde{P}_{15})$ and the color space of the 3 partons of the original amplitude $\mathcal{M}^{(g)a}_4(p_1,p_2,p_5)$. It should be noted that in Eq. (4.73), the terms that are less singular than $1/s_{15}$ have been neglected. To precisely define the collinear limit, one can rescale the transverse momenta $k_{\perp i}$ by an overall factor λ, namely, $k_{\perp i} \to \lambda k_{\perp i}$. In this limit, the behavior of the matrix element is proportional to $1/\lambda$. In this case, the terms that are less singular than $1/\lambda$ can be neglected.

The precise expression for the leading order splitting matrix for the process under consideration is as follows:

$$Sp^{(0)a}_{q\to qg}(p_1,p_5,\widetilde{P}_{15}) = g_s T^a \frac{1}{s_{15}} \overline{U}(p_1)\not{\varepsilon}^*(p_5)U(\widetilde{P}_{15}), \tag{4.74}$$

where $T^a = t^a$, if the gluon with momentum p_5 is collinear to the quark with momentum p_1. If the gluon with momentum p_5 is collinear to the antiquark with momentum p_2, then $T^a = -t^a$.

As is clearly seen from Eq. (4.74), the splitting matrix depends on the helicities of the collinear particles. Consequently, the collinear limit must be considered for each of the eight amplitudes individually. The same procedure must be followed when considering the collinear limit for three-point amplitudes.

It can thus be concluded that the soft-collinear limit is satisfied with precision for both the four-point amplitude and the three-point amplitude at the NLO level. As a consequence, this outcome is also applicable to the total amplitude $\mathcal{M} = \mathcal{M}_3 + \mathcal{M}_4$.

4.4.3 Virtual-real corrections

In this section, we will examine the most intricate aspect of the calculations, namely the virtual-real corrections. A parallel calculation of the virtual-real amplitude in another method has been carried out by my collaborators. This allowed us to verify the correctness of my own calculations by comparing the analytical results. The diagrams shown in Fig. 7 contribute to the total amplitude at order $\mathcal{O}\left(\alpha_s^{3/2}\right)$.

In this section, the amplitude $\mathcal{M}^{(VR)\mu a}_{\lambda_1\lambda_2;\lambda_5}$ is computed. As previously, the open index μ will be used, which can be contracted with the lepton current of a lepton-antilepton pair at a later stage.

In order to facilitate the calculations and circumvent the direct evaluation of complicated tensor one-loop integrals, it is essential to gain a comprehensive understanding of what the amplitude $\mathcal{M}^{(VR)\mu a}_{\lambda_1\lambda_2;\lambda_5}$ can contain after the formal integration over the loop momentum k. It is established that the expression always comprises the spinor $\overline{U}_{\lambda_2}(p_2)$

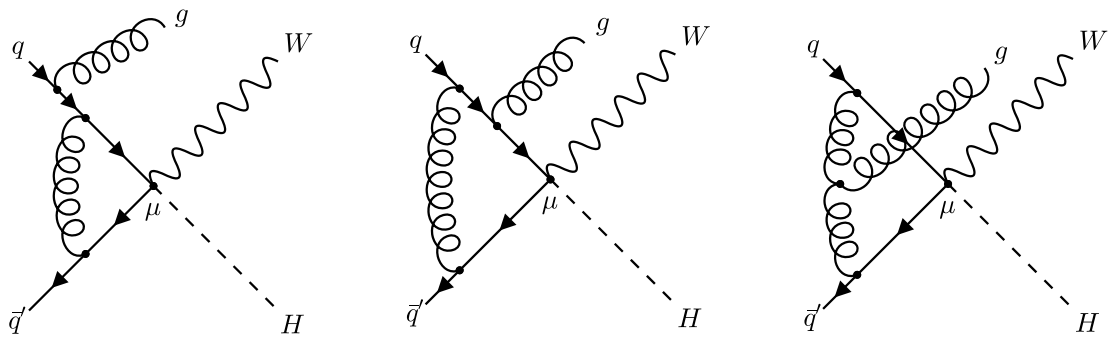

Figure 7: Representative Feynman diagrams for single real gluon emission at one loop.

on the left, the spinor $U_{\lambda_1}(p_1)$ on the right, the polarization vector $\varepsilon^*_{5\nu}(p_5)$ and some combination of γ-matrices between the spinors. Therefore, the amplitude $\mathcal{M}^{(VR)\mu a}_{\lambda_1\lambda_2;\lambda_5}$ describing virtual-real corrections can be represented as $\overline{U}_{\lambda_2}(p_2)\mathcal{A}^{\mu a}U_{\lambda_1}(p_1)$, where $\mathcal{A}^{\mu a}$ contains all the information pertaining to the vertex, including the real gluon.

In essence, the vertex function A^μ in (2.23) comprises both a single γ-matrix and the commutator $[\gamma^\mu, \not{p}_W]$. If we initially consider γ^μ, then in the amplitude $\mathcal{M}^{(VR)\mu a}_{\lambda_1\lambda_2;\lambda_5}$, the number of γ-matrices between the spinors $\overline{U}_{\lambda_2}(p_2)$ and $U_{\lambda_1}(p_1)$ is always odd. Theoretically, this combination can include up to six distinct γ-matrices: γ^μ, $\not{\varepsilon}^*_5$, $\not{p}_1$, $\not{p}_2$, $\not{p}_5$, $\not{p}_W$ and their possible combinations. However, matrix $\not{p}_W$ cannot appear, if we consider only γ^μ in the vertex, as this would result in the amplitude lacking any reference to momentum p_W. Furthermore, matrices $\not{p}_1$ and $\not{p}_2$ vanish when the anticommutative relation and the Dirac equation are employed. Consequently, a set of three γ-matrices is obtained: γ^μ, $\not{\varepsilon}^*_5$, and $\not{p}_5$.

It is necessary that any combination constructed contains free index μ which can be derived from either γ^μ or from any of the external momenta p_1^μ, p_2^μ and p_5^μ. The index ν contracted with the gluon polarization vector is provided by either γ^ν or by the momenta p_1^ν and p_2^ν. However, it cannot be provided by vector p_5^ν, as the polarization vector satisfies the Ward identity $(\varepsilon^*_5 \cdot p_5) = 0$.

In light of the aforementioned arguments, one can posit the following set of tensor structures between spinors $\overline{U}_{\lambda_2}(p_2)$ and $U_{\lambda_1}(p_1)$

$$
\begin{array}{llll}
\not{\varepsilon}^*_5 p_1^\mu, & \not{\varepsilon}^*_5 \not{p}_5 \gamma^\mu, & (\varepsilon^*_5 \cdot p_1)\not{p}_5 p_1^\mu, & (\varepsilon^*_5 \cdot p_2)\not{p}_5 p_1^\mu, \\
\not{\varepsilon}^*_5 p_2^\mu, & (\varepsilon^*_5 \cdot p_1)\gamma^\mu, & (\varepsilon^*_5 \cdot p_1)\not{p}_5 p_2^\mu, & (\varepsilon^*_5 \cdot p_2)\not{p}_5 p_2^\mu, \\
\not{\varepsilon}^*_5 p_5^\mu, & (\varepsilon^*_5 \cdot p_2)\gamma^\mu, & (\varepsilon^*_5 \cdot p_1)\not{p}_5 p_5^\mu, & (\varepsilon^*_5 \cdot p_2)\not{p}_5 p_5^\mu. \\
\not{p}_5 \varepsilon^{*\mu}_5, & & &
\end{array}
\tag{4.75}
$$

The use of tensor structures (4.75) enables the amplitude to be decomposed into independent components, thereby greatly simplifying its calculation. Nevertheless, the calculation process can be further streamlined by employing the Gram matrix to discern any linearly dependent structures among these tensor structures and subsequently reduce their number [153]. This method is frequently employed in the calculation of amplitudes in QCD, QED, and field theory at high perturbation orders. The method's fundamental principle is the construction of the Gram matrix based on scalar products of tensor structures. This approach enables the identification of linearly dependent structures, thereby greatly simplifying the subsequent calculation of amplitudes.

Therefore, as discussed in reference [164], there exist a total of seven independent Lorentz structures, constructed from these thirteen:

$$
\begin{aligned}
T_1^\mu &= \not{p}_5(\varepsilon_5^*\cdot p_1)p_1^\mu - \frac{s_{15}}{2}\not{\varepsilon}_5^* p_1^\mu + \frac{s_{12}}{4}\not{\varepsilon}_5^*\not{p}_5\gamma^\mu,\\
T_2^\mu &= \not{p}_5(\varepsilon_5^*\cdot p_1)p_2^\mu - \frac{s_{15}}{2}\not{\varepsilon}_5^* p_2^\mu + \frac{s_{12}}{4}\not{\varepsilon}_5^*\not{p}_5\gamma^\mu,\\
T_3^\mu &= \not{p}_5(\varepsilon_5^*\cdot p_1)p_5^\mu - \frac{s_{15}}{2}\not{\varepsilon}_5^* p_5^\mu + \frac{s_{125}}{4}\not{\varepsilon}_5^*\not{p}_5\gamma^\mu,\\
T_4^\mu &= \not{p}_5(\varepsilon_5^*\cdot p_2)p_1^\mu - \frac{s_{25}}{2}\not{\varepsilon}_5^* p_1^\mu + \frac{s_{12}}{4}\gamma^\mu\not{p}_5\not{\varepsilon}_5^*,\\
T_5^\mu &= \not{p}_5(\varepsilon_5^*\cdot p_2)p_2^\mu - \frac{s_{25}}{2}\not{\varepsilon}_5^* p_2^\mu + \frac{s_{12}}{4}\gamma^\mu\not{p}_5\not{\varepsilon}_5^*,\\
T_6^\mu &= \not{p}_5(\varepsilon_5^*\cdot p_2)p_5^\mu - \frac{s_{25}}{2}\not{\varepsilon}_5^* p_5^\mu + \frac{s_{125}}{4}\gamma^\mu\not{p}_5\not{\varepsilon}_5^*,\\
T_7^\mu &= s_{25}\left(\gamma^\mu(\varepsilon_5^*\cdot p_1) + \frac{1}{2}\not{\varepsilon}_5^*\not{p}_5\gamma^\mu\right) - s_{15}\left(\gamma^\mu(\varepsilon_5^*\cdot p_2) + \frac{1}{2}\gamma^\mu\not{p}_5\not{\varepsilon}_5^*\right),
\end{aligned}
\tag{4.76}
$$

where

$$
s_{125} = (p_1+p_2+p_5)^2 = s_{12}+s_{15}+s_{25}. \tag{4.77}
$$

The Lorentz structures corresponding to the commutator $[\gamma^\mu, \not{p}_W]$ can be obtained in the same manner. There are sixteen of them and the computation of the corresponding form factors is performed in similar steps, although this case is considerably more intricate and requires a substantially greater amount of computational time. The tensor structures are

$$
\begin{aligned}
T_8^\mu &= [\gamma^\mu, \not{p}_W]\not{p}_5\not{\varepsilon}_5^*,\\
T_9^\mu &= \not{\varepsilon}_5^*\not{p}_5[\gamma^\mu, \not{p}_W],\\
T_{10}^\mu &= \big(s_{1W}p_5^\mu - s_{5W}p_1^\mu\big)\not{p}_5\not{\varepsilon}_5^*,\\
T_{11}^\mu &= \big(s_{2W}p_5^\mu - s_{5W}p_2^\mu\big)\not{p}_5\not{\varepsilon}_5^*,\\
T_{12}^\mu &= [\gamma^\mu, \not{p}_W]\big(s_{25}(\varepsilon_5^*\cdot p_1) - s_{15}(\varepsilon_5^*\cdot p_2)\big),\\
T_{13}^\mu &= \Big(p_1^\mu\not{p}_W\not{p}_5 - \frac{1}{2}s_{1W}\gamma^\mu\not{p}_5\Big)\big(s_{25}(\varepsilon_5^*\cdot p_1) - s_{15}(\varepsilon_5^*\cdot p_2)\big),\\
T_{14}^\mu &= \Big(p_2^\mu\not{p}_W\not{p}_5 - \frac{1}{2}s_{2W}\gamma^\mu\not{p}_5\Big)\big(s_{25}(\varepsilon_5^*\cdot p_1) - s_{15}(\varepsilon_5^*\cdot p_2)\big),\\
T_{15}^\mu &= \Big(p_5^\mu\not{p}_W\not{p}_5 - \frac{1}{2}s_{5W}\gamma^\mu\not{p}_5\Big)\big(s_{25}(\varepsilon_5^*\cdot p_1) - s_{15}(\varepsilon_5^*\cdot p_2)\big),\\
T_{16}^\mu &= \frac{1}{2}s_{25}p_1^\mu\not{p}_W\not{\varepsilon}_5^* + \frac{1}{2}s_{1W}(\varepsilon_5^*\cdot p_2)\gamma^\mu\not{p}_5 - p_1^\mu(\varepsilon_5^*\cdot p_2)\not{p}_W\not{p}_5 - \frac{1}{4}s_{25}s_{1W}\gamma^\mu\not{\varepsilon}_5^*,\\
T_{17}^\mu &= \frac{1}{2}s_{25}p_2^\mu\not{p}_W\not{\varepsilon}_5^* + \frac{1}{2}s_{2W}(\varepsilon_5^*\cdot p_2)\gamma^\mu\not{p}_5 - p_2^\mu(\varepsilon_5^*\cdot p_2)\not{p}_W\not{p}_5 - \frac{1}{4}s_{25}s_{2W}\gamma^\mu\not{\varepsilon}_5^*,\\
T_{18}^\mu &= \frac{1}{2}s_{25}p_5^\mu\not{p}_W\not{\varepsilon}_5^* + \frac{1}{2}s_{5W}(\varepsilon_5^*\cdot p_2)\gamma^\mu\not{p}_5 - p_5^\mu(\varepsilon_5^*\cdot p_2)\not{p}_W\not{p}_5 - \frac{1}{4}s_{25}s_{5W}\gamma^\mu\not{\varepsilon}_5^*,\\
T_{19}^\mu &= p_5^\mu\,(\varepsilon_5^*\cdot p_W) - \frac{1}{4}s_{5W}\gamma^\mu\not{\varepsilon}_5^* - \frac{1}{4}s_{5W}\not{\varepsilon}_5^*\gamma^\mu,
\end{aligned}
\tag{4.78}
$$

$$
\begin{aligned}
T^{\mu}_{20} =& \Big(p_1^{\mu}\big(s_{15}(\varepsilon_5^*\cdot p_W) - s_{5W}(\varepsilon_5^*\cdot p_1)\big) + s_{1W}p_5^{\mu}(\varepsilon_5^*\cdot p_1)\Big) - \frac{1}{4}s_{15}s_{1W}\{\gamma^{\mu},\not{\varepsilon}_5^*\},\\
T^{\mu}_{21} =& \Big(p_2^{\mu}\big(s_{15}(\varepsilon_5^*\cdot p_W) - s_{5W}(\varepsilon_5^*\cdot p_1)\big) + s_{2W}p_5^{\mu}(\varepsilon_5^*\cdot p_1)\Big) - \frac{1}{4}s_{15}s_{2W}\{\gamma^{\mu},\not{\varepsilon}_5^*\},\\
T^{\mu}_{22} =& \Big(p_1^{\mu}\big(s_{25}(\varepsilon_5^*\cdot p_W) - s_{5W}(\varepsilon_5^*\cdot p_2)\big) + s_{1W}p_5^{\mu}(\varepsilon_5^*\cdot p_2)\Big) - \frac{1}{4}s_{25}s_{1W}\{\gamma^{\mu},\not{\varepsilon}_5^*\},\\
T^{\mu}_{23} =& \Big(p_2^{\mu}\big(s_{25}(\varepsilon_5^*\cdot p_W) - s_{5W}(\varepsilon_5^*\cdot p_2)\big) + s_{2W}p_5^{\mu}(\varepsilon_5^*\cdot p_2)\Big) - \frac{1}{4}s_{25}s_{2W}\{\gamma^{\mu},\not{\varepsilon}_5^*\}.
\end{aligned}
$$

Analogous to the purely virtual case, the amplitude with a single real gluon emission with open index μ can be written as

$$
\mathcal{M}^{\mu a}_{\lambda_1\lambda_2;\lambda_5} = \mathcal{M}^{\mu a}_{LR;\lambda_5} + \mathcal{M}^{\mu a}_{RL;\lambda_5} + \mathcal{M}^{\mu a}_{LL;\lambda_5} + \mathcal{M}^{\mu a}_{RR;\lambda_5}, \tag{4.79}
$$

where summation over the gluon helicity λ_5 is implied and the helicity amplitudes are

$$
\begin{aligned}
\mathcal{M}^{\mu a}_{LR;\lambda_5} &= C_1 t^a\ [p_2|\mathcal{A}_2^{\mu}|p_1], & \mathcal{M}^{\mu a}_{LL;\lambda_5} &= C_3 t^a\ \langle p_2|\mathcal{A}_1^{\mu}|p_1], \\
\mathcal{M}^{\mu a}_{RL;\lambda_5} &= C_2 t^a\ \langle p_2|\mathcal{A}_2^{\mu}|p_1\rangle, & \mathcal{M}^{\mu a}_{RR;\lambda_5} &= C_4 t^a\ [p_2|\mathcal{A}_1^{\mu}|p_1\rangle
\end{aligned} \tag{4.80}
$$

with

$$
\begin{aligned}
\mathcal{A}_1^{\mu} &= \sum_{i=1}^{7} A_i^{(VR)} T_i^{\mu}, \\
\mathcal{A}_2^{\mu} &= \sum_{i=8}^{23} A_i^{(VR)} T_i^{\mu}.
\end{aligned} \tag{4.81}
$$

From Eq. (4.62), the tensor structures (4.76) and (4.78) can be readily extracted, thereby enabling the determination of the tree-level form factors. Indeed, for the single γ-matrix, we can express it as follows

$$
\begin{aligned}
\mathcal{M}^{(g)\mu a}_{\lambda_1\lambda_2;\lambda_5} &= g_s t^a \overline{U}_{\lambda_2}(p_2)\Big[s_{25}\left(\gamma^{\mu}(\varepsilon_5^*\cdot p_1) + \frac{1}{2}\not{\varepsilon}_5^*\not{p}_5\gamma^{\mu}\right) \\
&\qquad - s_{15}\left(\gamma^{\mu}(\varepsilon_5^*\cdot p_2) + \frac{1}{2}\gamma^{\mu}\not{p}_5\not{\varepsilon}_5^*\right)\Big] U_{\lambda_1}(p_1) \times \left(-\frac{2}{s_{15}s_{25}}\right) \\
&= g_s t^a \overline{U}_{\lambda_2}(p_2) A_7^{(g)} T_7^{\mu} U_{\lambda_1}(p_1),
\end{aligned} \tag{4.82}
$$

where

$$
A_7^{(g)} = -\frac{2}{s_{15}s_{25}}, \tag{4.83}
$$

what agrees with [164]. In the case of the commutator $[\gamma^{\mu},\not{p}_W]$, the following structure of the tree-level amplitude can be observed

$$
\begin{aligned}
\mathcal{M}^{(g)\mu a}_{\lambda_1\lambda_2;\lambda_5} &= g_s t^a \overline{U}_{\lambda_2}(p_2)\Bigg[\frac{1}{s_{15}}[\gamma^{\mu},\not{p}_W]\not{p}_5\not{\varepsilon}_5^* - \frac{1}{s_{25}}\not{\varepsilon}_5^*\not{p}_5[\gamma^{\mu},\not{p}_W] \\
&\qquad + [\gamma^{\mu},\not{p}_W]\left[s_{25}(\varepsilon_5^*\cdot p_1) - s_{15}(\varepsilon_5^*\cdot p_2)\right] \times \left(-\frac{2}{s_{15}s_{25}}\right)\Bigg] U_{\lambda_1}(p_1) \\
&= g_s t^a \overline{U}_{\lambda_2}(p_2)\left(A_8^{(g)} T_8^{\mu} + A_9^{(g)} T_9^{\mu} + A_{12}^{(g)} T_{12}^{\mu}\right) U_{\lambda_1}(p_1),
\end{aligned} \tag{4.84}
$$

where

$$A_8^{(g)} = \frac{1}{s_{15}}, \qquad A_9^{(g)} = -\frac{1}{s_{25}}, \qquad A_{12}^{(g)} = -\frac{2}{s_{15}s_{25}}. \tag{4.85}$$

The computation of the form factors for the virtual-real case is based on the same steps as those employed in the purely virtual two-loop case. However, due to the increased complexity, it requires a greater degree of patience. In order to compute the form factors, we contract Eq. (4.79) with each of the 23 tensor structures (4.76) and (4.78) and utilise summation over the gluon polarizations

$$\sum_{\lambda_5\lambda_5'} \varepsilon_{\nu\lambda_5}(p_5)\varepsilon^*_{\sigma\lambda_5'}(p_5) = -g_{\nu\sigma}, \tag{4.86}$$

as the gluon is massless. This process yields a system of 23 equations for 23 variables. Each equation comprises a linear combination of form factors on the right-hand side and a linear combination of one-loop Feynman integrals on the left-hand side. The form factors $A_i^{(VR)}$ are the solution to the aforementioned system. However, as the first seven equations are independent of the remaining 16, we may consider two distinct systems: one for the seven variables and another for the 16 ones. This approach facilitates the simplification of the calculations.

Subsequently, all 23 form factors are obtained through the evaluation of one-loop tensor integrals over the loop momentum k. The tensor structure is derived from scalar products such as $(p_1 \cdot k)$ and so forth. As was done in the two-loop case, the scalar products in the numerator can be expressed through propagators. This results in a set of one-loop scalar integrals, which can be expressed in terms of master integrals in REDUZE. The final analytical expression for the form factors $A_i^{(VR)}$ can then be derived through the following master integrals

$$\begin{aligned}
I_1^{(1)} &= \mu_0^{2\varepsilon}\int\frac{d^dk}{(2\pi)^d}\frac{1}{D_2D_6}, & I_5^{(1)} &= \mu_0^{2\varepsilon}\int\frac{d^dk}{(2\pi)^d}\frac{1}{D_1D_2D_4D_6},\\
I_2^{(1)} &= \mu_0^{2\varepsilon}\int\frac{d^dk}{(2\pi)^d}\frac{1}{D_1D_6}, & I_6^{(1)} &= \mu_0^{2\varepsilon}\int\frac{d^dk}{(2\pi)^d}\frac{1}{D_1D_3D_4D_6},\\
I_3^{(1)} &= \mu_0^{2\varepsilon}\int\frac{d^dk}{(2\pi)^d}\frac{1}{D_1D_4}, & I_7^{(1)} &= \mu_0^{2\varepsilon}\int\frac{d^dk}{(2\pi)^d}\frac{1}{D_1D_3D_5D_6}.\\
I_4^{(1)} &= \mu_0^{2\varepsilon}\int\frac{d^dk}{(2\pi)^d}\frac{1}{D_3D_6},
\end{aligned} \tag{4.87}$$

where the only topology is

$$\begin{aligned}
D_1 &= k^2, & D_4 &= (p_1+p_2+k)^2,\\
D_2 &= (p_1+k)^2, & D_5 &= (p_2-p_5+k)^2,\\
D_3 &= (p_2+k)^2, & D_6 &= (p_1+p_2-p_5+k)^2.
\end{aligned} \tag{4.88}$$

Solutions to these integrals can be found, for example, in reference [165]

$$
\begin{aligned}
I_1^{(1)} &= \frac{i}{16\pi^2}\left(\frac{4\pi\mu_0^2}{-s_{25}}\right)^{\varepsilon}\frac{\Gamma^2(1-\varepsilon)\Gamma(\varepsilon)}{\Gamma(2-2\varepsilon)},\\
I_2^{(1)} &= \frac{i}{16\pi^2}\left(\frac{4\pi\mu_0^2}{-s_{125}}\right)^{\varepsilon}\frac{\Gamma^2(1-\varepsilon)\Gamma(\varepsilon)}{\Gamma(2-2\varepsilon)},\\
I_3^{(1)} &= \frac{i}{16\pi^2}\left(\frac{4\pi\mu_0^2}{-s_{12}}\right)^{\varepsilon}\frac{\Gamma^2(1-\varepsilon)\Gamma(\varepsilon)}{\Gamma(2-2\varepsilon)},\\
I_4^{(1)} &= \frac{i}{16\pi^2}\left(\frac{4\pi\mu_0^2}{-s_{15}}\right)^{\varepsilon}\frac{\Gamma^2(1-\varepsilon)\Gamma(\varepsilon)}{\Gamma(2-2\varepsilon)},\\
I_5^{(1)} &= -\frac{i}{16\pi^2}\frac{1}{s_{12}s_{25}}\frac{\Gamma^2(1-\varepsilon)\Gamma(1+\varepsilon)}{\Gamma(1-2\varepsilon)}\times\\
&\quad\times\left[\frac{2}{\varepsilon^2}\left(\left(\frac{4\pi\mu_0^2}{-s_{12}}\right)^{\varepsilon}+\left(\frac{4\pi\mu_0^2}{-s_{25}}\right)^{\varepsilon}-\left(\frac{4\pi\mu_0^2}{-s_{125}}\right)^{\varepsilon}\right)-\frac{\pi^2}{3}-\right.\\
&\quad\left.-\log\left(\frac{s_{12}}{-s_{25}}\right)-2\mathrm{Li}_2\left(\frac{s_{15}+s_{25}}{-s_{12}}\right)-2\mathrm{Li}_2\left(\frac{s_{12}-s_{15}}{-s_{25}}\right)\right]+\mathcal{O}(\varepsilon),\qquad (4.89)\\
I_6^{(1)} &= -\frac{i}{16\pi^2}\frac{1}{s_{12}s_{15}}\frac{\Gamma^2(1-\varepsilon)\Gamma(1+\varepsilon)}{\Gamma(1-2\varepsilon)}\times\\
&\quad\times\left[\frac{2}{\varepsilon^2}\left(\left(\frac{4\pi\mu_0^2}{-s_{12}}\right)^{\varepsilon}+\left(\frac{4\pi\mu_0^2}{-s_{25}}\right)^{\varepsilon}-\left(\frac{4\pi\mu_0^2}{-s_{125}}\right)^{\varepsilon}\right)-\frac{\pi^2}{3}-\right.\\
&\quad\left.-\log\left(\frac{s_{12}}{-s_{15}}\right)-2\mathrm{Li}_2\left(\frac{s_{15}+s_{25}}{-s_{12}}\right)-2\mathrm{Li}_2\left(\frac{s_{12}-s_{25}}{-s_{15}}\right)\right]+\mathcal{O}(\varepsilon),\\
I_7^{(1)} &= \frac{i}{16\pi^2}\frac{1}{s_{15}s_{25}}\frac{\Gamma^2(1-\varepsilon)\Gamma(1+\varepsilon)}{\Gamma(1-2\varepsilon)}\times\\
&\quad\times\left[\frac{2}{\varepsilon^2}\left(\left(\frac{4\pi\mu_0^2}{-s_{15}}\right)^{\varepsilon}+\left(\frac{4\pi\mu_0^2}{-s_{25}}\right)^{\varepsilon}-\left(\frac{4\pi\mu_0^2}{-s_{125}}\right)^{\varepsilon}\right)-\frac{\pi^2}{3}-\right.\\
&\quad\left.-\log\left(\frac{s_{25}}{s_{15}}\right)-2\mathrm{Li}_2\left(\frac{s_{12}-s_{15}}{-s_{25}}\right)-2\mathrm{Li}_2\left(\frac{s_{12}-s_{25}}{-s_{15}}\right)\right]+\mathcal{O}(\varepsilon).
\end{aligned}
$$

4.4.4 Virtual-real form factor renormalization

In the case of a real gluon, the process of renarmalization can be carried out in a manner analogous to that employed for the one-loop case. This entails three distinct steps: renormalization of the strong coupling constant α_s using Eq. (4.45), the subtraction of the one-loop Catani operator and the subsequent renormalization of the Wilson coefficients. However, a different Catani operator is employed here, which describes the infrared divergences of a process involving a real gluon [157]

$$
A_i^{(VR)\,\mathrm{UV+fin}} = A_i^{(VR)} - \mathcal{I}_{q\bar{q}g}^{(1)}(\varepsilon)A_i^{(g)}, \tag{4.90}
$$

where

$$
\begin{aligned}
\mathcal{I}_{q\bar{q}g}^{(1)}(\varepsilon) = -\frac{1}{2}\frac{e^{\varepsilon\gamma_E}}{\Gamma(1-\varepsilon)}\Bigg[&(2C_F-C_A)\left(\frac{1}{\varepsilon^2}+\frac{3}{2\varepsilon}\right)\left(\frac{\mu^2}{s_{12}}\right)^{\varepsilon}\\
&+\frac{1}{2}\left(\frac{2C_A}{\varepsilon^2}+\left(\frac{10}{3}C_A-\frac{2}{3}T_RN_f\right)\frac{1}{\varepsilon}\right)\left(\frac{\mu^2}{s_{1W}}+\frac{\mu^2}{s_{2W}}\right)^{\varepsilon}\Bigg].
\end{aligned} \tag{4.91}
$$

In accordance with reference [157], the total form factor in the virtual-real case with a single real gluon can be written as follows

$$A_i = \left(\frac{\alpha_s^B}{2\pi}\right)^{1/2} \left(A_i^{(g)} + \frac{\alpha_s^B}{2\pi} A_i^{(VR)} + \mathcal{O}\left(\alpha_s^2\right)\right) \tag{4.92}$$

In Eq. (4.92), the prefactor can be rewritten as

$$\left(\frac{\alpha_s^B}{2\pi}\right)^{1/2} = \left[\frac{\alpha_s}{2\pi}\left(\frac{\mu^2}{\mu_0^2}\right)^{\varepsilon} (4\pi)^{-\varepsilon} e^{\gamma_E \varepsilon}\right]^{1/2} = \left(\frac{\alpha_s}{2\pi}\right)^{1/2} \left(\frac{\mu^2 e^{\gamma_E}}{4\pi\mu_0^2}\right)^{\varepsilon/2}, \tag{4.93}$$

where α_s is the renormalized strong coupling constant. It is evident that this prefactor contributes to the finite remainder resulting from its expansion in a series of ε. Following the process of renormalisation of the coupling constant, the Catani operator (4.91) is employed for the purpose of subtracting the infrared divergences. In this case, it is sufficient to retain the expansion up to and including the finite term. This results in the cancellation of the $1/\varepsilon^2$-infrared poles, leaving only $1/\varepsilon$-ultraviolet poles still remain. The remaining divergences must be removed by the process of renormalization of the Wilson coefficients. To cancel ultraviolet divergences, we introduce the renormalization function

$$\widetilde{Z} = 1 + \frac{\alpha_s}{2\pi} \frac{\widetilde{z}^{(1,1)}}{\varepsilon} + \mathcal{O}\left(\alpha_s^2\right) \tag{4.94}$$

and write

$$\begin{aligned} A_i &= \left(\frac{\alpha_s}{2\pi}\right)^{1/2} \left(\frac{4\pi\mu^2 e^{\gamma_E}}{\mu_0^2}\right)^{\varepsilon/2} \left(A_i^{(g)} + \frac{\alpha_s}{2\pi} A_{i,\text{fin}}^{(VR)} + \mathcal{O}\left(\alpha_s^2\right)\right) = \\ &= \left(\frac{\alpha_s}{2\pi}\right)^{1/2} \left(\frac{4\pi\mu^2 e^{\gamma_E}}{\mu_0^2}\right)^{\varepsilon/2} \widetilde{Z} \left(A_i^{(g)} + \frac{\alpha_s}{2\pi} A_{i,\text{UV+fin}}^{(VR)} + \mathcal{O}\left(\alpha_s^2\right)\right]. \end{aligned} \tag{4.95}$$

Upon applying this to $A_i^{(VR)\,\text{UV + fin}}$, it can be seen that finite remainders are obtained for the form factors. It is therefore possible to adjust the number $\widetilde{z}^{(1,1)}$ in such a way that the UV-divergent part vanishes. As can be seen from the computations, this number is

$$\widetilde{z}^{(1,1)} = -\frac{C_F}{2} \tag{4.96}$$

for the form factors corresponding to the helicity amplitudes with different helicities of the incoming quarks (for C_1 and C_2). Wilson coefficients contained in the values C_3 and C_4 are also non-renormalizable in the one-loop case with a real gluon. Consequently, as in the case in the purely virtual scenario, we may introduce the 4×4 renormalization matrix

$$\widetilde{Z}_{ij} = \delta_{ij} + \frac{\alpha_s}{2\pi} \frac{\widetilde{z}_{ij}^{(1,1)}}{\varepsilon} + \mathcal{O}\left(\alpha_s^2\right), \tag{4.97}$$

where rows and columns correspond to the Wilson coefficients hidden in numbers C_1, C_2, C_3 and C_4, respectively, and write down

$$\widetilde{z}_{ij}^{(1,1)} = -\frac{C_F}{2} \begin{pmatrix} 1 & 0 & 0 & 0 \\ 0 & 1 & 0 & 0 \\ 0 & 0 & 0 & 0 \\ 0 & 0 & 0 & 0 \end{pmatrix}. \tag{4.98}$$

It is not possible to present the form factors for the virtual-real case explicitly in this thesis due to their excessive size. Nevertheless, they can be accessed in the supplementary files.

4.4.5 NNLO soft and collinear limits for a single gluon

The factorized structure of the both soft and collinear limits of the QCD amplitudes at tree level can be generalized to higher loops. The structure of formula (4.69) is also preserved in the virtual-real case

$$\mathcal{M}^{(VR)a} \xrightarrow{p_5 \to 0} g_s \varepsilon_5^{*\mu}(p_5) J_\mu^a(p_5) \mathcal{M}^{(loop)}, \tag{4.99}$$

where $\mathcal{M}_4^{(loop)}$ denotes the corresponding purely virtual amplitude. The singular dependence on p_5 is embodied in the unrenormalized soft-gluon current $J_\mu^a(p_5)$, which can be expanded in loop contributions as follows [161]

$$J_\mu^a(p_5) = J_\mu^{(0)a}(p_5) + g_s^2 \mu^{2\varepsilon} J_\mu^{(1)a}(p_5) + \mathcal{O}\left(g_s^4\right). \tag{4.100}$$

The tree-level soft-gluon current $J_\mu^{(0)a}(p_5)$ is already given in Eq. (4.70) and $J_\mu^{(1)a}(p_5)$ is its one-loop analogue. The total soft-gluon current (4.100) contains the entire singular dependence of the amplitude in the soft limit. By expanding the right-handed side of Eq. (4.99) in a series of the strong coupling constant, we can write this relation in a more explicit form for our case as

$$\mathcal{M}^{(VR)a} \xrightarrow{p_5 \to 0} g_s \varepsilon_5^{*\mu}(p_5) \Big(J_\mu^{(0)a}(p_5) \mathcal{M}^{(1)} + g_s^2 \mu^{2\varepsilon} J_\mu^{(1)a}(p_5) \mathcal{M}^{(0)} \Big). \tag{4.101}$$

In this study, the one-loop soft limit was verified and the soft-gluon current was calculated using the unrenormalized virtual-real amplitude. The resulting calculations yielded the following expression

$$J_\mu^{(1)a}(p_5) = -\frac{N_c\, t^a}{8\pi^2} \frac{1}{\varepsilon^2} \frac{\Gamma^3(1-\varepsilon)\Gamma^2(1+\varepsilon)}{\Gamma(1-2\varepsilon)} \left(\frac{p_{1\mu}}{s_{15}} - \frac{p_{2\mu}}{s_{25}} \right) \left(\frac{-8\pi s_{12}}{s_{15} s_{25}} \right)^{\varepsilon}. \tag{4.102}$$

This expression is fully consistent with that presented in reference [161], in which the one-loop soft-gluon current is derived as

$$\begin{aligned} J_\mu^{(1)a}(p_5) = &-\frac{1}{16\pi^2} \frac{1}{\varepsilon^2} \frac{\Gamma^3(1-\varepsilon)\Gamma^2(1+\varepsilon)}{\Gamma(1-2\varepsilon)} \times \\ &\times i f^{abc} \sum_{i \neq j} T_{ib} T_{jc} \left(\frac{p_{i\mu}}{(p_i \cdot p_5)} - \frac{p_{j\mu}}{(p_j \cdot p_5)} \right) \\ &\times \left(\frac{4\pi (p_i \cdot p_j) e^{-i\lambda_{ij}\pi}}{2(p_i \cdot p_5)(p_j \cdot p_5) e^{-i\lambda_{ip_5}\pi} e^{-i\lambda_{jp_5}\pi}} \right)^{\varepsilon}, \end{aligned} \tag{4.103}$$

where parameter $\lambda_{AB} = 1$ if both particles A and B are incoming or outgoing and $\lambda_{AB} = -1$ otherwise.

Relation (4.73) for the collinear limit can be extended to encompass higher orders of perturbation theory in a similar manner

$$\mathcal{M}^{(VR)a}_{\lambda_1\lambda_2;LL;\lambda_5}(p_1,p_2,p_5) \xrightarrow{p_5\|p_1} Sp^{(0)a}_{q\to qg}(p_1,p_5,\widetilde{P}_{15})\mathcal{M}^{(1)}_{\lambda_1\lambda_2;LL;\lambda_5}(p_2,\widetilde{P}_{15}) + Sp^{(1)a}(p_1,p_5,\widetilde{P}_{15})\mathcal{M}^{(0)}_{\lambda_1\lambda_2;LL;\lambda_5}(p_2,\widetilde{P}_{15}), \tag{4.104}$$

where the leading order splitting matrix $Sp^{(0)a}_{q\to qg}(p_1,p_5,\widetilde{P}_{15})$ is given in Eq. (4.74) and the one-loop splitting matrix $Sp^{(1)a}_{q\to qg}(p_1,p_5,\widetilde{P}_{15})$ is rather long, but its divergent part is entirely captured by a single hypergeometric function [168]

$$\begin{aligned} Sp^{(1)a}_{q\to qg}(p_1,p_5,\widetilde{P}_{15}) = Sp^{(0)a}_{q\to qg}(p_1,p_5,\widetilde{P}_{15})\; g_s^2\; \frac{\Gamma(1+\varepsilon)\Gamma^2(1-\varepsilon)}{(4\pi)^{2-\varepsilon}\Gamma(1-2\varepsilon)} \times \\ \times \left[-\frac{N_c}{\varepsilon^2} - \Big(\big(2C_F - N_c\big) f(\varepsilon;z_5) + N_c f(\varepsilon;z_1)\Big)\frac{1}{\varepsilon}\right] \\ + \{\text{finite terms}\}, \end{aligned} \tag{4.105}$$

where the longitudinal-momentum fractions z_1 and z_5 are defined through the longitudinal components x_i (see Eq. (4.71)) as

$$z_i = \frac{x_i}{x_1 + x_5} \tag{4.106}$$

and

$$f\big(\varepsilon;1/z\big) = \frac{1}{\varepsilon}\Big({}_2F_1\big(1,-\varepsilon,1-\varepsilon;1-z\big) - 1\Big). \tag{4.107}$$

The expansion of this function in powers of ε is as follows

$$f\big(\varepsilon;1/z\big) = \log(z) - \varepsilon\left(\mathrm{Li}_2(1-z) + \sum_{n=1}^{+\infty}\varepsilon^n \mathrm{Li}_{n+2}(1-z)\right). \tag{4.108}$$

The details of the soft and collinear limits presented in this section are applicable to three-point and four-point amplitudes, and hold for both the case where the gluon is emitted by the quark with momentum p_1 and the case where the gluon is emitted by the antiquark with momentum p_2.

4.5 Double real corrections

The final contribution to the NNLO amplitude comes from the diagrams with double real emission. A parallel calculation of the double real amplitude has been carried out by my collaborators. This allowed us to cross-check the accuracy of my own work by comparing the analytical outcomes. This kind of corrections occur in two different channels. Fig. 8(a) illustrates the Feynman diagrams for the channel $q(p_1)+\bar{q}'(p_2) \to W(p_W)+H(p_H)+g(p_5)+g(p_6)$, in which a gluon pair is emitted, while Fig. 8(b) depicts the diagrams that describe the channel $q(p_1)+\bar{q}'(p_2) \to W(p_W)+H(p_H)+Q(p_5)+\bar{Q}(p_6)$, in which a quark-antiquark pair is emitted via a gluon.

The calculation of the amplitude for the double real corrections is relatively straightforward, as it does not necessitate the evaluation of complex loop integrals. Nevertheless, certain aspects of the process, particularly those associated with infrared divergences, deserve closer attention. In particular, the two key IR-sensitive regions – namely, the soft

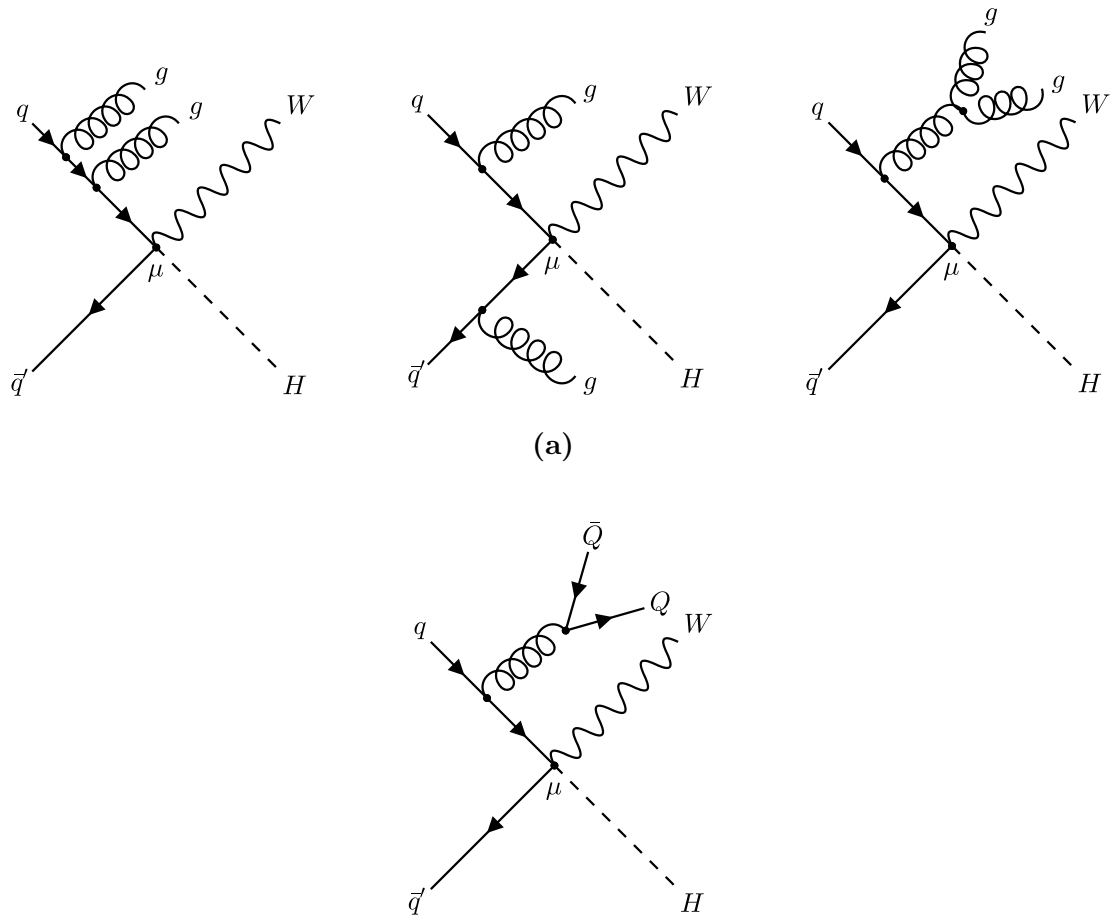

Figure 8: Representative Feynman diagrams for the double real corrections: (a) Double real gluon emission, (b) Quark-antiquark pair emission.

limit and the collinear limit – are of particular relevance. In the soft limit, divergences arise when the energy of emitted particles tends to zero, while the collinear limit refers to situations where particles become nearly parallel.

In the case of double real corrections, the situation is more intricate compared to the single emission case, since now two additional real particles are involved in the final state. This introduces a new level of complexity in both the kinematics and the behavior of the amplitude in infrared-sensitive regions. There are several distinct configurations to consider: single soft limit (one gluon becomes soft), double soft limit (two gluons become soft simultaneously), single collinear limit (one gluon is nearly parallel to an incoming parton), double collinear limit (both gluons are nearly parallel to an incoming parton(s)), and mixed soft-collinear limit.

4.5.1 Soft limits

The soft limit is typically considered for gluons (or photons in QED) rather than quarks, due to the fundamental differences in their properties. Gluons are massless particles, which means that their energy can reach zero, resulting in infrared divergences in the soft limit. This renders the soft limit especially pertinent to gluons whose emission probability rises in tandem with a decline in their energy. In contrast, quarks are massive and therefore cannot

reach arbitrarily low energy without violating the dynamics of the process. Furthermore, quarks are subject to confinement which precludes their existence as free particles. This further constrains the applicability of the soft limit to them. While collinear limits are relevant for quarks when they become nearly parallel to other particles, the soft limit remains specific to massless particles such as gluons due to their ability to generate infrared divergences in the low-energy regime.

The case of a single soft limit is almost identical to the relation (4.69) that has already been considered. The distinction lies in the fact that in the event of one of the two particles becoming soft, the amplitude is reduced not to the leading order amplitude, but rather to the tree-level amplitude with one real gluon

$$\mathcal{M}^{(gg)ab} \xrightarrow{p_5 \to 0} g_s \varepsilon_5^{\mu *}(p_5) J_\mu^{(0)a}(p_5) \mathcal{M}^{(g)b}, \tag{4.109}$$

where the tree-level soft-gluon current $J_\mu^{(0)a}(q)$ is defined in Eq. (4.70). The relation (4.109) also has relevance in regard to the gluon with momentum p_6. In this case, the only necessary modification is the exchange of momenta, whereby p_5 is replaced by p_6. To take into account the color structure, we introduce the dependence of the matrix element on the color indices $c_1, ..., c_m$ of the QCD partons as

$$\mathcal{M}_{c_1,...,c_m}(p_1, ..., p_m) = \langle c_1, ..., c_m | \mathcal{M}(p_1, ..., p_m) \rangle, \tag{4.110}$$

where $|c_1, ..., c_m\rangle$ is an abstract basis vector in the color space and $|\mathcal{M}(p_1, ..., p_m)\rangle$ is a vector in this space.

To describe the color correlations produced by soft-gluon emission, we introduce a color charge $\hat{T}_i$ with the emission of a gluon from each parton i. If the emitted gluon has color index a, the color-charge operator is

$$\hat{T}_i = \langle a | T_i^a \tag{4.111}$$

and its action onto the color space is defined by the following equation

$$\langle a, c_1, ...c_i, ..., c_m | \hat{T}_i | b_1, ...b_i, ..., b_m \rangle = \delta_{c_1 b_1} ... T^a_{c_i b_i} ... \delta_{c_m b_m}. \tag{4.112}$$

In this instance, the matrix T^a, which arises in the definition of the soft-gluon current $J_\mu^{(0)a}(q)$, in the case of gluon emission by the second, non-soft gluon, has the form $T^a_{cb} = if^{cab}$.

The case of the double soft limit is described by applying the soft limit to relation (4.109), when the gluon in the amplitude $\mathcal{M}^{(g)b}$ also becomes soft. In this case, the amplitude can also be approximated by the soft limit $p_6 \to 0$

$$\mathcal{M}^{(g)b} \xrightarrow{p_6 \to 0} g_s \varepsilon_6^{\nu *}(p_6) J_\nu^{(0)b}(p_6) \mathcal{M}^{(0)}. \tag{4.113}$$

Therefore, the double soft limit can be described as

$$\mathcal{M}^{(gg)ab} \xrightarrow{p_5, p_6 \to 0} g_s^2 \varepsilon_5^{\mu *}(p_5) J_\mu^{(0)a}(p_5) \varepsilon_6^{\nu *}(p_6) J_\nu^{(0)b}(p_6) \mathcal{M}^{(0)}, \tag{4.114}$$

where the summation over parton indices in $J_\mu^{(0)a}(p_5)$ also encompasses the gluon with momentum p_6. The specific form of the soft-gluon current varies depending on the helicity of the emitted gluons. However, in general, it has a fairly simple structure similar to that shown in equation (4.70).

4.5.2 Collinear limits

We now extend the collinear limit analysis, previously considered for the emission of a single real gluon, to the case of double real emission. In particular, we will examine the double collinear limit, in which both of the emitted gluons become collinear with external partons or with each other [166].

We begin by considering the scenario in which only one of the two emitted gluons becomes collinear with an external parton, while the other gluon remains at a general kinematic configuration. In this case, the collinear behavior of the amplitude can be analyzed in a manner analogous to the single gluon emission case studied above, utilizing the same factorization properties of the amplitude in the collinear limit.

In the event that a quark with momentum p_1 emits the gluon with momentum p_5, the factorization formula for the amplitude in the collinear limit is analogous to relation (4.73)

$$\mathcal{M}^{(gg)ab}_{\lambda_1\lambda_2;LL;\lambda_5\lambda_6}(p_1,p_2,p_5,p_6) \xrightarrow{p_5\|p_1} Sp^{(0)a}_{q\to qg}(p_1,p_5,\widetilde{P}_{15})\mathcal{M}^{(g)b}_{\lambda_1\lambda_2;LL;\lambda_6}(p_2,p_6,\widetilde{P}_{15}), \tag{4.115}$$

where the splitting matrix $Sp^{(0)a}_{q\to qg}(p_1,p_5,\widetilde{P}_{15})$ is defined in Eq. (4.74), while the momentum $\widetilde{P}_{15}$ is defined in Eq. (4.72).

In the double collinear limit, where both gluons become collinear either with an external parton or with each other, the situation becomes more intricate due to the presence of overlapping singularities. There are several possible configurations to consider, depending on the specific collinear behavior of the two gluons.

In the event that each gluon is collinear with a distinct parton, we may modify the relation (4.115) by assuming that the gluon with momentum p_6 is collinear to the antiquark with momentum p_2

$$\begin{aligned}\mathcal{M}^{(gg)ab}_{\lambda_1\lambda_2;LL;\lambda_5\lambda_6}(p_1,p_2,p_5,p_6) &\xrightarrow{p_5\|p_1,\, p_6\|p_2} \\ &Sp^{(0)a}_{q_1\to q_1g_1}(p_1,p_5,\widetilde{P}_{15})Sp^{(0)b}_{\bar{q}_2\to\bar{q}_2g_2}(p_2,p_6,\widetilde{P}_{26})\mathcal{M}^{(0)}_{\lambda_1\lambda_2;LL}(\widetilde{P}_{15},\widetilde{P}_{26}),\end{aligned} \tag{4.116}$$

where the splitting matrix $Sp^{(0)b}_{\bar{q}\to\bar{q}g}$ has the same structure as $Sp^{(0)b}_{q\to qg}$.

Another interesting case is when the two emitted partons become collinear to each other rather than to any external parton. In this scenario, the gluons form a collinear pair, and the amplitude factorizes as

$$\mathcal{M}^{(gg)ab}_{\lambda_1\lambda_2;LL;\lambda_5\lambda_6}(p_1,p_2,p_5,p_6) \xrightarrow{p_5\|p_6} Sp^{(0)a}_{g\to p_ap_b}(p_5,p_6,\widetilde{P}_{56})\mathcal{M}^{(g)b}_{\lambda_1\lambda_2;LL;\lambda_6}(p_1,p_2,\widetilde{P}_{56}), \tag{4.117}$$

where $Sp^{(0)a}_{g\to p_ap_b}(p_5,p_6,\widetilde{P}_{56})$ depends on types of partons p_a and p_b [166]. In the case of the emission of two collinear gluons, the following applies

$$\begin{aligned}Sp^{(0)a}_{g\to gg}(p_i,p_j,\widetilde{P}_{ij}) &= \frac{2g_s}{s_{ij}}\,T^a\times \\ &\times\Big[\big(p_i\cdot\varepsilon^*(\widetilde{P}_{ij})\big)\big(\varepsilon_i^*\cdot\varepsilon_j^*\big)-\big(p_i\cdot\varepsilon_j^*\big)\big(\varepsilon_i^*\cdot\varepsilon^*(\widetilde{P}_{ij})\big)+\big(p_j\cdot\varepsilon_i^*\big)\big(\varepsilon_j^*\cdot\varepsilon^*(\widetilde{P}_{ij})\big)\Big].\end{aligned} \tag{4.118}$$

In the case of the emission of a collinear quark-antiquark pair, the splitting matrix becomes

$$Sp^{(0)a}_{g\to q\bar{q}}(p_i,p_j,\widetilde{P}_{ij}) = \frac{2g_s}{s_{ij}}\, T^a\overline{U}(p_i)\not{\varepsilon}^*(\widetilde{P})U(p_j). \tag{4.119}$$

The most exceptional case occurs when both gluons are collinear with the same external parton. In this instance, the amplitude factorizes as follows

$$\mathcal{M}^{(gg)ab}_{\lambda_1\lambda_2;LL;\lambda_5\lambda_6}(p_1,p_2,p_5,p_6) \xrightarrow{p_1\|p_5\|p_6} Sp^{(0)ab}_{q\to qg_1g_2}(p_1,p_5,p_6)\mathcal{M}^{(0)}_{\lambda_1\lambda_2;LL}(p_1,p_2). \tag{4.120}$$

In Eq. (4.120), $Sp^{(0)ab}_{q\to qg_1g_2}(p_1,p_5,p_6)$ represents the double collinear splitting function, which describes the simultaneous emission of two collinear gluons from a single quark. This splitting function can be derived by combining the splitting functions for individual gluon emissions and taking into account the appropriate symmetrization [167]

$$\begin{aligned} Sp^{(0)}_{q\to qg_1g_2}(p_i,p_j,p_k) &= \frac{P_{qg}(x_k)}{s_{ijk}}\frac{P_{gg}\left(\frac{x_j}{1-x_k}\right)}{s_{ij}} + \frac{P_{qg}(1-x_i)}{s_{ijk}}\frac{P_{qg}\left(\frac{x_j}{1-x_i}\right)}{s_{jk}} \\ &+ \frac{1}{s^2_{ijk}}\left[\frac{2(1-\varepsilon)}{(1-x_i)^2}\frac{W_{jk}}{s^2_{jk}} + \frac{4(1-\varepsilon)x_k}{(1-x_i)^2}\frac{x_ks_{ij}-x_js_{ik}+x_is_{jk}}{s_{jk}}\right. \\ &+ \frac{(1-\varepsilon)^2}{1-x_k}\frac{x_ks_{ij}-x_js_{ik}+x_is_{jk}}{s_{ij}} + b_0(x_i,x_k) \\ &\left.+ b(x_i,x_j,x_k)\frac{s_{ijk}(x_ks_{ij}-x_js_{ik}+x_is_{jk})}{s_{ij}s_{jk}}\right]. \end{aligned} \tag{4.121}$$

In Eq. (4.121), x_i are longitudinal components, and the invariants $s_{ij} = (p_i+p_j)^2$, $s_{ijk} = (p_i+p_j+p_k)^2$. Additionally introduced functions are

$$\begin{aligned} W_{ij} &= (x_is_{jk}-x_js_{ik})^2 - \frac{2}{1-\varepsilon}\frac{x_ix_jx_k}{1-x_k}s_{ij}s_{ijk}, \\ b_0(x,y) &= (1-\varepsilon)\left[\frac{2y(y-2)}{(1-x)^2} + \frac{4y}{1-x} + (1-\varepsilon)\left(1-\frac{1-y}{1-x}\right)\right], \\ b(x_i,x_j,x_k) &= -\frac{x_jP_{qg}(x_j)}{x_k(1-x_i)} - \frac{2x_kP_{qg}(x_k)}{x_j(1-x_i)} + \frac{4}{1-x_i} - 3(1-\varepsilon) \end{aligned} \tag{4.122}$$

and the Altarelli-Parisi splitting functions[11] are

$$\begin{aligned} P_{qg}(x) &= \frac{2(1-x)}{x} + (1-\varepsilon)x, \\ P_{gg}(x) &= \frac{2(1-x)}{x} + \frac{2x}{1-x} + 2x(1-x). \end{aligned} \tag{4.123}$$

[11]It should be noted that the splitting function $P(x)$ and the splitting matrix $Sp(x)$, which are discussed in this thesis, are distinct entities. The splitting amplitude in the collinear limit is a more specific object. In contrast to the splitting function $P(x)$, which characterizes the splitting probability and is employed for the evolution of parton distributions, $Sp(x)$ is precisely the splitting amplitude at the level of matrix elements.

4.5.3 Mixed soft-collinear limit

In the mixed soft-collinear limit, we encounter a scenario where one of the emitted gluons becomes soft, while the second gluon becomes collinear to an external parton. This configuration combines the characteristics of both the soft and collinear limits, making it a more intricate case to analyze. However, by building on the results discussed earlier in the thesis for both the soft and collinear limits individually, we can describe how the amplitude behaves when these two limits are taken simultaneously.

When a gluon becomes soft, the amplitude factorizes in a manner consistent with the soft limit previously discussed. The soft gluon interacts universally with all external particles, and its contribution can be expressed using a soft factor. Concurrently, the second gluon, which becomes collinear with a specific external parton, displays a factorization behavior regulated by the collinear limit. Consequently, the amplitude in the mixed soft-collinear limit factorizes into the product of a soft factor and a collinear splitting matrix. In particular, for a process where the quark with momentum p_1 emits two gluons, one of them (with momentum p_5) is soft and the other one (with momentum p_6) is collinear with the quark, we have

$$\begin{aligned}\mathcal{M}^{(gg)ab}_{\lambda_1\lambda_2;LL;\lambda_5\lambda_6}(p_1,p_2,p_5,p_6) &\xrightarrow{p_6||p_1,\, p_5\to 0} \\ & g_s\varepsilon_5^{\mu*}(p_5)J^{(0)a}_{\mu}(p_5)Sp^{(0)b}_{q\to qg}(p_1,p_6,\widetilde{P}_{16})\mathcal{M}^{(0)}_{\lambda_1\lambda_2;LL}(p_1,p_2).\end{aligned} \tag{4.124}$$

The interplay between the soft and collinear limits does not introduce new types of divergences; rather, it combines the singularities from each limit. The soft gluon contributes an infrared divergence, whereas the collinear gluon gives rise to a collinear divergence. These divergences can be treated as independent factors, allowing the mixed soft-collinear limit to be addressed using established techniques developed for soft and collinear emissions.

4.6 Python implementation

In order to validate the theoretical predictions presented in this thesis, a Python program was developed for the purpose of performing numerical computations and cross-checking analytical results. The program is specifically designed to evaluate physical processes by generating phase space configurations and squared helicity amplitudes for six distinct cases that are analyzed in this work. These cases are as follows: leading order, one loop, two loops, single real gluon at tree level, virtual-real, and double real.

The program accepts a single input parameter, the center-of-mass energy $\sqrt{s_{12}}$, measured in GeV, which the user provides via the keyboard. The program generates the phase space configuration, which represents the four-momenta of all particles involved in the quantum process, for three scenarios (without additional real particles, with one real gluon, and with two real particles). Using these momenta, the program computes key kinematic quantities, such as the invariants s_{ij} and spinor products $[p_ip_j]$ and $\langle p_ip_j\rangle$.

Based on these calculations, the program assesses the form factors and calculates helicity amplitudes. Subsequently, the squared amplitudes are averaged over the spins of the initial states and summed over the colors of the final states, thereby yielding the desired quantities. Despite the program's comprehensive scope, its execution time ranges from a mere few seconds to under a minute, contingent on the number of iterations performed.

This tool provides a robust numerical framework that seamlessly integrates theoretical computations with efficient algorithms, thereby ensuring accurate and rapid results. Should the necessity arise, the program can be readily expanded by modifying the source code to accommodate additional particles (including those with a mass), alter the chiral configuration, and so forth.

The Python program is comprised of six discrete modules (files with the *.py* extension), each of which has been designed to fulfill a specific role within the overall functionality of the program. This modular structure is in accordance with the tenets of object-oriented programming, thereby ensuring clarity, maintainability, and scalability. In order to execute the program, users are required to have Python installed on their system. It is preferable that the version of Python used meets the program's requirements for compatibility with its libraries and dependencies (Python 3.11.2)[12].

The program is initiated via the *main.py* file. To initiate the program, the user must first open the file and then select the *"Run → Run Module"* option within their Python environment. This action initiates the *main* function, which orchestrates the execution of all program components by cascading through the necessary functions and modules in a structured manner.

4.6.1 Overview of the modules

1. *main.py*

This file acts as the entry point of the program. It handles user input, invokes core functions, and ensures proper flow of the computational processes. The *main* function calls upon other functions that are responsible for generating the phase spaces, which are then utilized by further functions for the computation of squared amplitudes based on the aforementioned phase spaces.

2. *phase_space.py*

This file contains the functions for the generation of the phase space. All three functions, *phase_space_generate_3*, *phase_space_generate_4*, and *phase_space_generate_5*, accept the center-of-mass energy $\sqrt{s_{12}}$ as an input and output the phase space as a matrix of particle momenta. These functions are designed to generate the phase space for the case of three, four, and five outgoing particles, respectively.

Additionally, two auxiliary functions have been included into this module in order to obviate code duplication. The phase space generation algorithm is based on the generation of random numbers. However, it considers the constraints imposed on the particle momenta, namely the conservation of momentum

$$p_1 + p_2 = p_3 + p_4 + p_H \ (+p_5 + p_6) \tag{4.125}$$

and the on-shell condition for particles, ensuring that the squares of their four-momenta are equal to the squares of their masses.

3. *amplitudes.py*

The module comprises six distinct functions. Three of the functions compute amplitudes, while the remaining three utilize their output to compute squared amplitudes,

[12] Any version of Python that is currently available for download can be accessed via the link: https://www.python.org/downloads/

average over the spins of the initial states, and sum over the colors of the final states. Each function accepts phase space as a parameter. Furthermore, the functions that address amplitudes with potential loops (i.e., with one real gluon and no real gluons) also accept the number of loops as a parameter. The final output of this module is squared amplitudes, which are then passed to the *main* module.

4. *form_factor.py*

The file contains two functions that accept the phase space as a parameter. The first function, *form_factor_loop*, is responsible for computing form factors in scenarios that do not involve the emission of real gluons. The second function, *form_factor_single_real*, is responsible for computing form factors for cases involving the emission of a single real gluon. In this module, all computed form factors are transferred to the *amplitudes* module.

5. *helicities.py*

This module contains a single function that accepts the number of outgoing particles and the phase space as input and returns kinematic objects, namely invariants s_{ij} and spinor products $[p_i p_j]$ and $\langle p_i p_j \rangle$, utilizing the approach described in Appendix C.

6. *const.py*

This file contains the constants and parameters utilized within the program. These include quantities pertaining to high-energy physics, in addition to program settings such as the maximum and minimum values of the center-of-mass energy and the degree of precision in calculations. This module allows the user to configure any parameters in such a way that they are automatically applied when the program is launched.

5 Phase-Space Integration

5.1 Partonic cross section

Once all relevant scattering amplitudes for the process under consideration have been calculated, the subsequent step is to determine the partonic cross section. In accordance with (2.4), this necessitates the integration of the spin-averaged and color-summed squared amplitude over the corresponding phase space.

In light of the fact that the calculations include corrections provided by real gluons, it is necessary to consider amplitudes with different numbers of external partons separately, as they imply distinct phase spaces. Accordingly, the amplitudes must be grouped as follows

$$\begin{aligned} \mathcal{M}_{WH} &= \mathcal{M}^{(0)} + \mathcal{M}^{(1)} + \mathcal{M}^{(2)}, \\ \mathcal{M}^{a}_{WH+g} &= \mathcal{M}^{(g)a} + \mathcal{M}^{(VR)a}, \\ \mathcal{M}^{ab}_{WH+gg} &= \mathcal{M}^{(gg)ab}, \\ \mathcal{M}_{WH+Q\bar{Q}} &= \mathcal{M}^{(Q\bar{Q})}, \end{aligned} \tag{5.1}$$

where a and b denote color indices of the real gluons. It is evident that subsequent to the summation of the color indices, the two last amplitudes in (5.1) can be regarded as a single entity.

All amplitudes have been calculated up to $\mathcal{O}\big(C_i\big)$, where C_i denotes small (divided by Λ^2) Wilson coefficients. Moreover, it is important to keep in mind that the amplitudes on the right-hand side of (5.1) correspond to distinct orders of the strong coupling constant α_s. This enables us to express the squared amplitudes for LO, NLO and NNLO in the following form

$$\begin{aligned} \big|\mathcal{M}_{LO}\big|^2 &= \big|\mathcal{M}^{(0)}\big|^2, \\ \big|\mathcal{M}_{NLO}\big|^2 &= 2\mathrm{Re}\big(\mathcal{M}^{(0)*}\mathcal{M}^{(1)}\big) + \big|\mathcal{M}^{(g)}\big|^2, \\ \big|\mathcal{M}_{NNLO}\big|^2 &= 2\mathrm{Re}\big(\mathcal{M}^{(0)*}\mathcal{M}^{(2)}\big) + 2\mathrm{Re}\big(\mathcal{M}^{(g)*}\mathcal{M}^{(VR)}\big) \\ &\quad + \big|\mathcal{M}^{(gg)}\big|^2 + \big|\mathcal{M}^{(Q\bar{Q})}\big|^2. \end{aligned} \tag{5.2}$$

The total squared amplitude is the sum of the squared helicity amplitudes. To illustrate, the leading order amplitude can be expressed as follows

$$\big|\mathcal{M}_{LO}\big|^2 = \big|\mathcal{M}^{(0)}_{LR;LL}\big|^2 + \big|\mathcal{M}^{(0)}_{RL;LL}\big|^2 + \big|\mathcal{M}^{(0)}_{LL;LL}\big|^2 + \big|\mathcal{M}^{(0)}_{RR;LL}\big|^2. \tag{5.3}$$

In order to obtain the total spin-averaged color-summed amplitude, it is necessary to average over the possible spin states which correspond to the helicity configurations. As each of the quark and antiquark can have two possible helicities (left- or right-handed), the averaging process is completed by multiplying by a factor of 1/4 which corresponds to averaging over the four possible initial helicity combinations. This ensures that all potential helicity combinations of the incoming quark and antiquark are accounted for. In contrast, for the final-state leptons, there is no need for averaging over spins, as they are fixed to be left-handed by the weak interaction.

Given that quarks carry color charge, it is necessary to consider the color degrees of freedom of the quarks in the initial state. In the context of QCD, quarks are represented as triplets within the fundamental representation of the color $SU(3)$ group. This implies

that each quark can exist in one of the three color states, which are represented by the index N_c. This yields a factor of $1/N_c^2$ which represents the averaging over the color states of the quark and antiquark.

The final state in this process is color neutral, as the weak boson W decays into colorless leptons. Nevertheless, when quarks and antiquarks annihilate into a color singlet, the color indices of the quark and antiquark are contracted. Summing over all possible color configurations thus leads to an additional factor of N_c in the numerator.

In consideration of both the spin averaging and the color factor, the total expression for the spin-averaged color-summed squared leading order amplitude is given by

$$\overline{\left|\mathcal{M}_{LO}\right|^2} = \frac{N_c}{4N_c^2}\left(\left|\mathcal{M}^{(0)}_{LR;LL}\right|^2 + \left|\mathcal{M}^{(0)}_{RL;LL}\right|^2 + \left|\mathcal{M}^{(0)}_{LL;LL}\right|^2 + \left|\mathcal{M}^{(0)}_{RR;LL}\right|^2\right) \tag{5.4}$$

The same line of reasoning can be applied to the amplitude with one real gluon. Nevertheless, an additional factor of C_F emerges as a consequence of the summation over the final-state color matrices, resulting in the equation $t^a t_a = C_F$. The amplitude with two quarks in the final state will be multiplied by the factor $N_c C_F/2$. The calculation of the color factor for two real gluons is more intricate due to the fact that the amplitude is partitioned into two components as a result of the potential for a gluon-gluon interaction. The first of these will yield the factor $4N_c C_F^2$, while the second will yield $N_c C_F$.

Once the squared amplitudes have been calculated, it is necessary to integrate them over the phase space in order to obtain the partonic cross section (2.4)

$$\hat{\sigma}_{ij\to f} = \frac{1}{2s_{12}} \int dPS_n \overline{\left|\mathcal{M}_{ij\to f}\left(p_i, p_j | \{p_f\}\right)\right|^2}. \tag{5.5}$$

The total partonic cross section is composed of three distinct components: $\hat{\sigma}_{WH}$, $\hat{\sigma}_{WH+g}$, and $\hat{\sigma}_{WH+gg/Q\bar{Q}}$. These describe the process without real gluons, with a single real gluon, and with two real gluons or quarks, respectively. Each of these quantities is calculated by integrating over the corresponding phase space, given the differing number of outgoing particles. In the case of two incoming particles with momenta p_1 and p_2 and n outgoing particles with momenta p_i, where $i = 3, ..., n+2$, the general expression is given by

$$dPS_n = \prod_{i=3}^{n+2} \frac{1}{2E_i} \frac{d^{d-1}p_i}{(2\pi)^{d-1}} (2\pi)^d \delta^{(d)} \left(p_1 + p_2 - \sum_{j=3}^{n} p_j\right), \tag{5.6}$$

where $E_i = \sqrt{m_i^2 + |\vec{p}_i|^2}$ is energy of the i-th outgoing particle.

The total partonic cross section at NNLO (including LO and NLO) is then obtained by summing the partial cross sections

$$\hat{\sigma}_{\text{NNLO}} = \hat{\sigma}_{WH} + \hat{\sigma}_{WH+g} + \hat{\sigma}_{WH+gg/Q\bar{Q}}. \tag{5.7}$$

5.2 Phase space integration

In order to obtain the total partonic cross section, it is necessary to perform the phase-space integrals. In the partonic center-of-mass system, the external momenta are parameterized in a 4-dimensional spherical coordinate system as follows:

$$
\begin{aligned}
p_1 &= \frac{\sqrt{s_{12}}}{2}\big(1,0,0,1\big)^T, \\
p_2 &= \frac{\sqrt{s_{12}}}{2}\big(1,0,0,-1\big)^T, \\
p_W &= \big(E_W, 0, |\vec{p}_W| sin\vartheta, |\vec{p}_W| cos\vartheta\big)^T, \\
p_i &= E_i\big(1, \cos\varphi_i \sin\vartheta_i, \sin\varphi_i \sin\vartheta_i, \cos\vartheta_i\big)^T,
\end{aligned}
\tag{5.8}
$$

where i denotes additionally emitted real partons. The momenta p_1 and p_2 are associated with the two colliding partons. In the center-of-mass frame, the energy is simply given by half of the partonic center-of-mass energy which is represented by the variable $\sqrt{s_{12}}$. The variable p_W denotes the weak boson momentum, and the momenta p_i belong to the real-emitted partons. Each momentum has, in general case, three independent degrees of freedom, which are the energies E_i, and two angles, ϑ_i and φ_i. The momentum of the color singlet is then fully determined by the corresponding momentum conservation law which depends on the number of the final-state particles.

The invariant mass of the final-state system has to be in the range

$$
q^2 \in \Big[\big(m_W^2 + m_H^2\big)^2, s_{12}\Big), \tag{5.9}
$$

where the lower boundary is derived from the minimal collision energy required to produce the vector boson and the Higgs boson commonly on-shell. The upper boundary is the maximum energy of the partonic collision, and, of course, the invariant mass of the final-state system is limited by this energy scale.

The phase-space expression (5.6) has an exact analytic solution only in the limit of a small value of n. In the case of a single particle in the final state, the phase space integration is a relatively straightforward process due to the simplicity of the momentum conservation delta function. This effectively reduces the problem to a straightforward kinematic condition

$$
dPS_1 = \frac{2\pi}{s_{12}} \delta\left(1 - \frac{q^2}{s_{12}}\right). \tag{5.10}
$$

As the number of final-state particles included in the calculation increases, the complexity of the phase space integration also rises significantly. In the case of two final-state particles, the phase space integral can frequently be performed analytically, particularly if the problem exhibits symmetries that simplify the kinematics, such as in the case of two-body decays or scatterings in a center-of-mass frame. The two-particle phase space is frequently reduced to a few angular and energy integrals, which ultimately yield the following result:

$$
dPS_2 = \frac{1}{8\pi} \frac{1}{\Gamma(1-\varepsilon)} \left(\frac{4\pi}{s_{12}}\right)^{\varepsilon} \lambda^{\frac{1}{2}-\varepsilon}\big(m_W^2, m_H^2; s\big) y^{-\varepsilon} (1-y)^{-\varepsilon} dy, \tag{5.11}
$$

where the definition of the function $\lambda\big(x, y; z\big)$ is given in (2.7), and the variable y denotes

$$
y = \frac{1 - \cos\vartheta}{2}. \tag{5.12}
$$

Consequently, integration over the variable y must be performed over the interval [0,1].

The exact analytical expression for the phase space is known in the case of three final-state particles and is of a particularly intricate form. However, for $n > 3$, the phase

space integration becomes increasingly complex. The number of variables grows rapidly, and the delta function introduces non-trivial correlations between the momenta of the final-state particles. The full phase space integration for processes with three or more final-state particles generally cannot be solved analytically except in very special cases, such as highly symmetric or approximated processes. In other cases, numerical methods become indispensable.

Monte Carlo (MC) integration is a widely adopted approach to phase space integration in high-energy physics. MC methods estimate the value of the integral by randomly sampling points in the multidimensional phase space. By averaging the values of the integrand at these randomly sampled points, the total integral can be approximated. As the number of sampled points increases, the accuracy of the result improves, following a statistical error that scales as $1/\sqrt{N}$, where N is the number of samples. This approach is particularly well-suited for high-dimensional integrals, making it an effective solution for multi-particle phase space calculations.

Monte Carlo methods have been extensively developed and are now a cornerstone of computational particle physics. They form the basis of numerous cutting-edge simulation tools, including *MadGraph* [168], *Sherpa* [169], and *Pythia* [170]. These tools integrate phase space with event generation, thereby enabling the simulation of realistic scattering processes, including the production of multiple final-state particles, parton showers, and hadronization effects. They also incorporate sophisticated algorithms for phase space sampling, such as importance sampling, which optimizes the sampling process by focusing on regions where the integrand is most significant, thereby improving efficiency.

In addition to Monte Carlo integration, there are other numerical methods that can be applied to phase space integrals, such as adaptive quadrature and grid-based methods. However, these tend to be less practical for high-dimensional problems, which are common in particle physics.

In many instances, numerical computations entail the partitioning of phase space integration into two distinct categories: the Born process phase space and the phase space of the real radiation. This approach is a widely utilized method in numerical integration, particularly for processes involving real radiation corrections. This technique is motivated by the necessity of separating the core scattering process from the emission of additional soft or collinear radiation, thereby simplifying the integrand structure and enhancing computational efficiency.

The Born phase space refers to the phase space associated with the core hard scattering process, which is typically the leading-order process. In this approximation, relation (5.6) remains applicable with a limited number of final-state particles, without taking into account any real emission.

The radiation phase space is defined as the additional phase space introduced by the emission of one or more particles. The inclusion of higher-order corrections results in the emission of an additional particle in the final state, leading to an expansion of the phase space. In the case of radiation particles, this phase space can be factorized from the Born process under certain approximations, such as the soft or collinear limits.

In a process where additional radiation particles are emitted, the full phase space can be factorized into the Born phase space plus an additional radiation phase space, $dPS^{(\mathrm{rad})}$, describing the emission. The four-dimensional limit of this phase space is given by

$$\begin{aligned}\lim_{d\to 4} dPS_i^{(\mathrm{rad})} &= \frac{d^3p_i}{(2\pi)^3 2E_i}\,\vartheta\big(E_{\max}-E_i\big)\\ &= dE_i\,E_i\,\frac{d\Omega_i^{(3)}}{2(2\pi)^3}\,\vartheta\big(E_{\max}-E_i\big),\end{aligned} \tag{5.13}$$

for particles emitted in the real domain, specifically for values of $i = 5, 6$ in our case. In (5.13), the Heaviside function ensures that the particle energy is less than the total center-of-mass energy.

In practice, the division of the phase space into Born and radiation components facilitates more efficient numerical integration, particularly when coupled with subtraction techniques such as the Catani-Seymour dipole subtraction scheme [171] or the FKS (Frixione, Kunszt, Signer) subtraction [172]. These methods entail the subtraction of the soft and collinear divergences from the real radiation phase space, followed by their addition back in the form of virtual corrections. The separation into Born and radiation phase spaces guarantees that the soft and collinear singularities are isolated and treated correctly, thereby rendering the numerical integration over the remaining, finite phase space more tractable.

6 Numerical Results and Discussion

In this chapter, numerical results obtained within the analysis of Ref. [187] are presented. These results are based on the direct implementation of the squared helicity amplitudes derived in the previous chapters into the numerical framework developed by our collaborators. The numerical setup and the definition of the fiducial phase space used in Ref. [187], built upon these amplitudes, are included here for completeness.

In that calculation, ultraviolet-renormalized loop amplitudes exhibit $1/\varepsilon$ singularities arising from soft and collinear virtual partons. Similarly, real-emission contributions develop infrared divergences when emitted partons become soft or collinear with others. As a result, integrating real-emission amplitudes over the full phase space in four dimensions is not straightforward. To obtain an infrared-finite result, a subtraction scheme is employed that systematically cancels these singularities by combining real and virtual corrections. In particular, the nested soft-collinear subtraction scheme [183, 184], previously applied in studies of VH production [79, 185, 186], is used.

Since the infrared structure of real-emission amplitudes is universal, extending the previous calculations [79, 185, 186] to include EFT effects requires only modifications to the hard-scattering amplitudes. Thanks to the modular structure of the numerical framework used in these and related computations, incorporating the new contributions into the existing setup is straightforward. The analysis of Ref. [187] also verifies that the subtraction terms correctly reproduce the expected behavior in unresolved limits and that the results are consistent with known Standard Model predictions for W^+H production [79, 186].

For the numerical evaluation, the `NNPDF31_nnlo_as_0118` PDF set [188] is used in Ref. [187]. The LO, NLO, and NNLO cross sections are obtained with NNLO PDFs throughout, and the strong coupling α_s is taken from the `NNPDF` routines. The renormalization scale is chosen as $\mu = \mu_R = \sqrt{(p_{W^+} + p_H)^2}/2$, and theoretical uncertainties are estimated by varying this scale up and down by a factor of two.

To keep the fiducial phase space broad, Ref. [187] adopts only minimal kinematic requirements. The charged lepton from the W decay is required to satisfy $p_{\mathrm{T},l} > 25$ GeV, with rapidity constrained by $|\eta_l| < 2.5$. In addition, an upper bound on the transverse momentum of the W boson, $p_{\mathrm{T},W}^{\mathrm{max}} < 250$ GeV, is applied to ensure the validity of the EFT description at large energies. Although this restriction does not directly limit the invariant mass $m_{WH}^2 = (p_W + p_H)^2$, the LO kinematics imply approximately $p_{\mathrm{T},W} \lesssim m_{WH}/2$. As a consequence, the fraction of events passing the cut decreases once m_{WH} exceeds roughly 540 GeV.

Some analyses of WH production introduce an additional requirement $p_{\mathrm{T},W} > 150$ GeV to emphasize the boosted-Higgs region. Ref. [187] therefore reports fiducial cross sections both with and without this extra condition.

The SMEFT setup considered in Ref. [187] contains four dimension-six operators, listed in Eq. (2.19). As discussed earlier, these operators lead to amplitudes with distinct helicity structures for the external quarks. Among them, only the operator $Q_{\varphi q}^{(3)}$ generates an amplitude that interferes with the Standard Model contribution. The remaining operators do not interfere either with the SM or with each other, and this pattern persists through NNLO in QCD. Consequently, in this framework the differential cross section can be written as a sum of six terms, each multiplied by the corresponding Wilson coefficient:

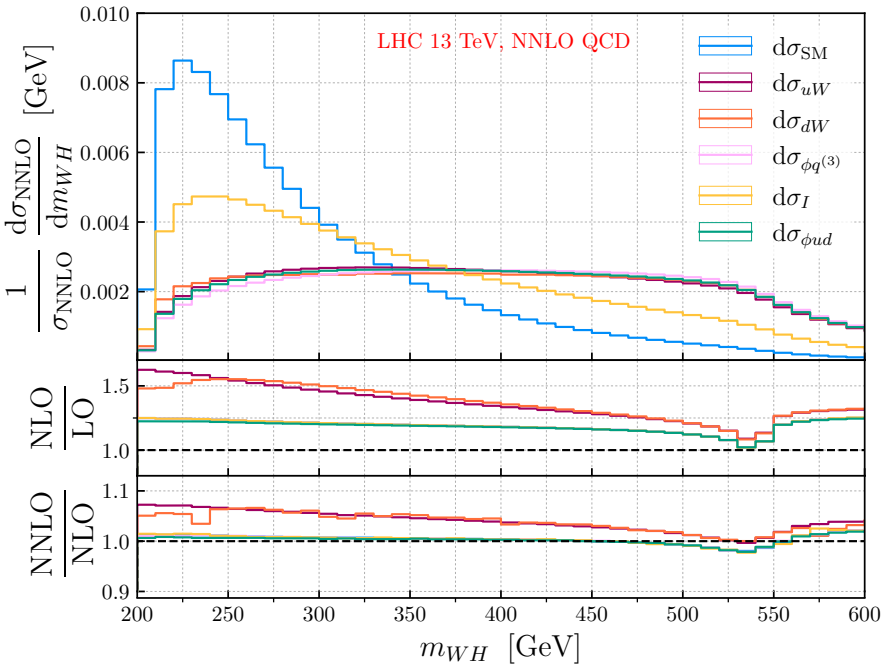

Figure 9: Normalized distribution of the invariant mass of the WH system in $pp \to W(\to l\bar{l}) + H$ at the 13 TeV LHC for the six differential contributions defined in Eq. (6.1). The upper panel shows NNLO results; the middle and lower panels present the NLO/LO and NNLO/NLO differential ratios; taken from Ref. [187].

$$d\sigma = d\sigma_{\rm SM} + C_{uW}^2\, d\sigma_{uW} + C_{dW}^2\, d\sigma_{dW} + C_{\varphi q}^{(3)}\, d\sigma_I + \left(C_{\varphi q}^{(3)}\right)^2 d\sigma_{\varphi q^{(3)}} + C_{\varphi ud}^2\, d\sigma_{\varphi ud}. \qquad (6.1)$$

The individual components are defined in a straightforward way in Ref. [187]. The quantities $d\sigma_{uW}$, $d\sigma_{dW}$, $d\sigma_{\varphi q^{(3)}}$, and $d\sigma_{\varphi ud}$ are obtained by switching on a single Wilson coefficient (set to unity) while keeping all others, including the SM coupling, switched off. The interference contribution[13] $d\sigma_I$ is determined by comparing two calculations: one with only $C_{\varphi q}^{(3)} = 1$ and one where $C_{\varphi q}^{(3)} = 1$ is kept together with the SM amplitude. Their difference isolates the linear dependence on $C_{\varphi q}^{(3)}$.

A convenient starting point is to consider the relative size of the individual contributions entering Eq. (6.1). Ref. [187] provides fiducial cross sections for all terms defined there, evaluated at LO, NLO, and NNLO in QCD. Although the explicit numerical values are not repeated here, two general observations are important for the discussion that follows.

First, under minimal fiducial cuts the SMEFT-induced cross sections are of the same order of magnitude as the Standard-Model prediction. When an additional requirement $p_{{\rm T},W} > 150$ GeV is imposed, the SMEFT terms become comparatively more important and can even exceed the SM contribution. The reason is that such a cut preferentially selects events with large invariant mass m_{WH}.

Second, the growth of the SMEFT contributions towards higher invariant masses is not only a consequence of the higher mass dimension of the operators. In the SM, the dominant amplitude proceeds through an s-channel W propagator, whose contribution

[13] Strictly speaking, $d\sigma_I$ is not a cross section, as it is not required to be positive.

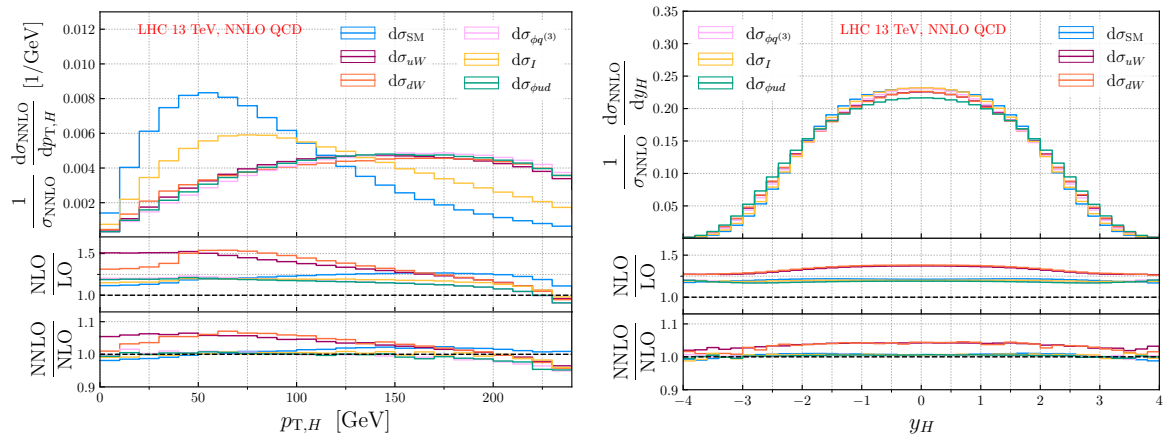

(a) **(b)**

Figure 10: Normalized distributions of the Higgs transverse momentum (a) and the Higgs rapidity (b) in $pp \to W(\to l\bar{l}) + H$ at the 13 TeV LHC, for the six differential cross sections defined in Eq. (6.1). The upper panel shows the results at NNLO in QCD. The middle and lower panels show the NLO/LO and NNLO/NLO differential factors, respectively; taken from Ref. [187].

decreases rapidly as the invariant mass of the WH system increases. By contrast, the operators considered in this analysis give rise to contact-type interactions that directly connect the initial-state quarks to the WH final state. As a result, the SMEFT terms remain comparatively unsuppressed at large m_{WH}.

These features are clearly visible in the normalized invariant-mass distribution shown in Fig. 9, where the SMEFT-induced curves fall off more slowly with m_{WH} than the SM prediction. This difference in shape is one of the key characteristics of the EFT contributions and plays an important role in the interpretation of the numerical results.

The impact of QCD corrections on the SM and SMEFT contributions is generally different, since these terms populate distinct regions of the invariant mass m_{WH}. Ref. [187] presents the quantitative results, and here we summarize only the features that are relevant for the interpretation of the distributions discussed below.

At NLO, the corrections to the SM prediction are moderate and increase the fiducial cross section by roughly 20%. For several SMEFT operators the effect is similar, while for the operators Q_{uW} and Q_{dW} the enhancement is noticeably larger. This behaviour reflects the fact that these operators primarily contribute in the lower part of the m_{WH} spectrum where NLO effects are more pronounced. The usual scale-variation procedure underestimates these NLO corrections, a known feature of Drell–Yan-like processes due to the opening of new partonic channels and the absence of explicit $\alpha_s(\mu_R)$ dependence at LO.

At NNLO, the pattern remains qualitatively similar but the corrections become considerably smaller. For most contributions the NNLO shift is at the percent level, while for Q_{uW} and Q_{dW} it is slightly larger, consistent with the higher NLO scale variation observed for these operators. Overall, the NNLO scale uncertainties provide a reliable estimate of the missing higher-order effects.

Additional insight can be obtained from the transverse-momentum and rapidity distributions of the Higgs boson shown in Fig. 10(a) and Fig. 10(b). For $p_{T,H}$ the differences between the SM and SMEFT predictions are clearly visible, while the distributions gen-

erated by different SMEFT operators are rather similar to each other. QCD corrections again display operator-dependent patterns: the enhancement is sizeable at low transverse momenta for Q_{uW} and Q_{dW}, whereas the SM prediction receives a milder and more uniform correction. The rapidity distribution is much less sensitive to the underlying production mechanism and remains essentially unchanged by SMEFT effects.

A practical aspect of SMEFT studies is the efficient evaluation of predictions for arbitrary values of the Wilson coefficients. Since the WH cross section can be written as a linear combination of six independent components, each associated with a unique coupling structure, any distribution can be reconstructed from the set of precomputed differential cross sections entering Eq. (6.1). As demonstrated in Ref. [187], the reconstructed NNLO predictions reproduce the exact results with excellent accuracy — well below the percent level for both fiducial cross sections and differential distributions, except in regions where SM and SMEFT contributions nearly coincide.

This observation enables a highly efficient strategy for precision SMEFT phenomenology. One can compute the SM and the SMEFT basis components once at NNLO accuracy and subsequently obtain predictions for any Wilson-coefficient configuration by simple linear combinations. This avoids repeated high-order calculations and allows for fast scans over multidimensional parameter spaces, which is essential for global SMEFT analyses of associated WH production.

7 Conclusion

In this thesis, we have investigated the effects of dimension-six operators in the Standard Model Effective Field Theory on associated Higgs production, $pp \to W(\to \ell\bar{\ell}) + H$, at the LHC. In particular, we have computed NNLO QCD corrections to all SMEFT-induced contributions, thereby extending the level of perturbative precision in this channel. Although NNLO calculations in associated production have become increasingly standard, the presence of CP-odd SMEFT operators introduces additional complications. These operators generate point-like $q\bar{q}'WH$ interactions mediated by tensor currents, for which two-loop amplitudes were previously unavailable. To overcome this obstacle, we carried out dedicated computations of the required tree-level, one-loop, and two-loop amplitudes to achieve full NNLO QCD accuracy.

An important consequence of helicity selection rules is that amplitudes arising from CP-odd SMEFT operators do not interfere with the Standard Model. As a result, only their squared contributions appear in the cross section, introducing an additional suppression associated with the SMEFT scale. Nevertheless, our results demonstrate that these contributions can still be phenomenologically relevant, and that their QCD corrections are sizeable, often differing substantially from those found in the Standard Model.

We have also examined the impact of the various SMEFT operators on differential observables. While certain distributions — for instance, the Higgs rapidity — exhibit limited discriminatory power, others, such as the invariant mass of the WH system and the Higgs transverse momentum, provide significantly enhanced sensitivity. QCD corrections further amplify these effects at NLO, where the behaviour varies strongly among operators; at NNLO, these differences remain but become more moderate.

The sizable SMEFT-induced cross sections, combined with characteristic distortions of the m_{WH} and $p_{\mathrm{T},H}$ spectra, offer valuable opportunities for constraining the relevant Wilson coefficients. Scale variation at NLO generally provides a reasonable estimate of missing NNLO contributions when SMEFT corrections resemble those in the Standard Model. However, this is not the case for the cross sections $\mathrm{d}\sigma_{uW}$ and $\mathrm{d}\sigma_{dW}$, which receive unusually large and structurally distinct NLO corrections. Establishing the perturbative stability of these effects required a full NNLO computation, which has been carried out in this work and provides a solid foundation for future experimental SMEFT analyses of WH production.

Beyond obtaining the analytic expressions for all amplitudes, we developed a Python-based framework enabling rapid numerical cross-checks against existing tools such as OpenLoops and MadGraph. These results have subsequently been used by our collaborators to produce numerical predictions for fiducial cross sections and kinematic distributions. A publication detailing this work is available in Ref. [187].

A Explicit Results

A.1 Pure loop corrections

This section presents the final results for our computations of helicity amplitudes with loop corrections. The explicit expressions for the helicity amplitudes at the purely virtual n-loop level are provided in Eqs. (4.29) and (4.31), while our calculations have been carried out up to two loops.

The total two-loop form factors can be expanded in perturbative chromodynamics in series of the strong coupling constant as follows:

$$A_i = A_i^{(0)} + \frac{\alpha_s}{2\pi} A_i^{(1)} + \left(\frac{\alpha_s}{2\pi}\right)^2 A_i^{(2)} + \mathcal{O}\left(\alpha_s^3\right), \tag{A.1}$$

where $i = 1, 2, 3$.

Leading order form factors

$$A_1^{(0)} = 2, \qquad A_2^{(0)} = 0, \qquad A_3^{(0)} = 1. \tag{A.2}$$

Finite remainders of the one-loop form factors

$$A_1^{(1)} = -8C_F - C_F \log\left(\frac{\mu^2}{-s_{12}}\right), \qquad A_2^{(1)} = 0, \qquad A_3^{(1)} = -4C_F. \tag{A.3}$$

Finite remainders of the two-loop form factors

$$\begin{aligned}
A_1^{(2)} = \frac{C_F}{51840}\Big[&20\big(24907C_A - 43956C_F - 3862N_f - 4536\beta_0\big) \\
&+ 15\big(403C_A + 432C_F - 58N_f + 36(4+3\pi)\beta_0\big)\pi^2 \\
&+ 9\big(-83C_A + 184C_F\big)\pi^4 \\
&+ 360\big(-593C_A + 1002C_F + 26N_f + 6(14+3\pi)\beta_0\big)\zeta(3) \\
&- 60\Big(-5245C_A + 12879C_F + 802N_f + 2(432-635\pi)\beta_0 \\
&\qquad + 3\big(-55C_A + 54C_F + 10N_f + 18(-1+4\pi)\beta_0\big)\pi^2 \\
&\qquad + 216\big(13C_A - 20C_F\big)\zeta(3)\Big)\log\left(\frac{\mu^2}{-s_{12}}\right) \\
&- 180\Big(-532C_A + 1341C_F + 88N_f + 36\beta_0\big(2-3\pi\big) \\
&\qquad + 12C_A\pi^2\Big)\log^2\left(\frac{\mu^2}{-s_{12}}\right) \\
&- 720\Big(-11C_A + 21C_F + 2N_f + 3\beta_0\big(1-2\pi\big)\Big)\log^3\left(\frac{\mu^2}{-s_{12}}\right)\Big],
\end{aligned} \tag{A.4}$$

$$A_2^{(2)} = 0, \tag{A.5}$$

$$
\begin{aligned}
A_3^{(2)} = -\frac{C_F}{103680}\Big[&5\big(134581C_A - 20655C_F - 23338N_f - 20736\beta_0\big) \\
&+ 45\big(49C_A + 48C_F + 2N_f - 20(-1+\pi)\beta_0\big)\pi^2 \\
&+ 9\big(-93C_A + 76C_F\big)\pi^4 \\
&- 360\big(467C_A - 342C_F - 26N_f + 6(-14+3\pi)\beta_0\big)\zeta(3) \\
&+ 6\Big(-16\big(9+7\pi\big)\beta_0 + 3\big(1+4\pi\big)\pi^2\beta_0 + 48C_F\zeta(3)\Big)\log\left(\frac{\mu^2}{-s_{12}}\right) \\
&- 1080\Big(-33C_A + 54C_F + 6N_f + 9\beta_0\big(1+2\pi\big) \\
&\qquad - 4C_F\pi^2\Big)\log^2\left(\frac{\mu^2}{-s_{12}}\right) \\
&- 720\Big(-11C_A + 72C_F + 2N_f + \beta_0\big(3+6\pi\big)\Big)\log^3\left(\frac{\mu^2}{-s_{12}}\right) \\
&- 8640C_F\log^4\left(\frac{\mu^2}{-s_{12}}\right)\Big].
\end{aligned}
\tag{A.6}
$$

In the context of purely loop corrections, the form factors B_i for the three-point amplitude are equal to the corresponding form factors for the four-point amplitude at all levels of the perturbative theory.

A.2 Single gluon corrections

In this section, we present the final results for our computations of helicity amplitudes involving a single real gluon correction. In the context of perturbative chromodynamics, the total virtual-real form factors at the one-loop level can be expanded in a series of the strong coupling constant as follows:

$$
A_i^{(\text{single}-\text{real})} = \left(\frac{\alpha_s}{2\pi}\right)^{1/2}\left(A_i^{(g)} + \frac{\alpha_s}{2\pi}A_i^{(VR)} + \mathcal{O}\left(\alpha_s^2\right)\right), \tag{A.7}
$$

where $i = \overline{1,23}$.

Tree-level form factors

$$
A_7^{(g)} = -\frac{2}{s_{1g}s_{2g}}, \qquad A_8^{(g)} = \frac{1}{s_{1g}}, \qquad A_9^{(g)} = -\frac{1}{s_{2g}}, \qquad A_{12}^{(g)} = -\frac{2}{s_{1g}s_{2g}}. \tag{A.8}
$$

The remaining tree-level form factors are identically zero. The form factors $B_i^{(g)}$ are equal to the corresponding form factors $A_i^{(g)}$. The virtual-real form factors $A_i^{(VR)}$ and $B_i^{(VR)}$ are too large to be included in the main text but can be found in the supplementary files.

The explicit expressions for the helicity amplitudes for virtual-real corrections, which are valid also in the case of tree-level, are presented below. The subscripts denote helicities of external particles in the following order: quark (p_1), antiquark (p_2), lepton (p_3), antilepton (p_4), and real gluon (p_5).

$$
\begin{aligned}
\mathcal{M}^{(VR)a}_{4\ LR;L;LL} = \frac{1}{\sqrt{2}} \frac{C_1 g_W t^a}{p_W^2 - m_W^2 + i\Gamma_W m_W} \times \\
\times \Bigg(& 4A^{(VR)}_{12} [p_1 p_2][p_1 p_4][p_2 p_4]\langle p_3 p_4\rangle\langle p_1 p_5\rangle\langle p_2 p_5\rangle \\
& + \left(s_{15} A^{(VR)}_{13} - A^{(VR)}_{16} \right) [p_1 p_2]\langle p_2 p_5\rangle \times \\
& \qquad \times \Big([p_1 p_2]\langle p_1 p_3\rangle[p_3 p_4]\langle p_3 p_5\rangle + [p_1 p_4][p_2 p_4]\langle p_5 p_1\rangle\langle p_3 p_4\rangle \Big) \\
& + \left(s_{15} A^{(VR)}_{14} - A^{(VR)}_{17} \right) [p_2 p_1][p_2 p_4]^2\langle p_2 p_5\rangle^2\langle p_3 p_4\rangle \\
& + \left(s_{15} A^{(VR)}_{15} - A^{(VR)}_{18} \right) s_{25}\ [p_2 p_1]\langle p_3 p_5\rangle^2[p_3 p_4] \\
& + A^{(VR)}_{19} [p_1 p_2]\langle p_3 p_5\rangle^2[p_3 p_4] \\
& + A^{(VR)}_{20} [p_1 p_2][p_1 p_4]^2\langle p_1 p_5\rangle^2\langle p_3 p_4\rangle \\
& + A^{(VR)}_{21} [p_2 p_1]\langle p_1 p_5\rangle \times \\
& \qquad \times \Big([p_1 p_2]\langle p_3 p_2\rangle\langle p_3 p_5\rangle[p_3 p_4] + [p_1 p_4][p_2 p_4]\langle p_3 p_4\rangle\langle p_2 p_5\rangle \Big) \\
& + A^{(VR)}_{22} [p_2 p_1][p_1 p_4][p_2 p_4]\langle p_1 p_5\rangle\langle p_2 p_5\rangle\langle p_3 p_4\rangle \\
& + A^{(VR)}_{23} [p_1 p_2][p_2 p_4]^2\langle p_2 p_5\rangle\langle p_3 p_4\rangle \Bigg)
\end{aligned}
\tag{A.9}
$$

$$
\begin{aligned}
\mathcal{M}^{(VR)a}_{4\,RL;L;LL} = \frac{1}{\sqrt{2}}\frac{C_2 g_W t^a}{p_W^2 - m_W^2 + i\Gamma_W m_W}\times \\
\times \Bigg(& 8A_8^{(VR)}\langle p_2 p_3\rangle[p_3 p_4]\langle p_3 p_5\rangle\langle p_1 p_5\rangle \\
& + 4A_9^{(VR)}\langle p_1 p_3\rangle\langle p_2 p_5\rangle[p_3 p_4]\langle p_3 p_5\rangle \\
& + 2A_{10}^{(VR)}\langle p_1 p_5\rangle\langle p_2 p_5\rangle\Big(s_{1W}\langle p_3 p_5\rangle[p_4 p_5] - s_{5W}\langle p_1 p_3\rangle[p_1 p_4]\Big) \\
& + 2A_{11}^{(VR)}\langle p_1 p_5\rangle\langle p_2 p_5\rangle\Big(s_{2W}\langle p_3 p_5\rangle[p_4 p_5] - s_{5W}\langle p_2 p_3\rangle[p_2 p_4]\Big) \\
& + 2A_{12}^{(VR)}[p_1 p_2]\langle p_1 p_3\rangle\langle p_2 p_3\rangle[p_4 p_3]\langle p_1 p_5\rangle\langle p_2 p_5\rangle \\
& + A_{13}^{(VR)}\langle p_1 p_5\rangle^2\langle p_2 p_5\rangle[p_1 p_2]\times \\
& \qquad \times\Big(\langle p_3 p_1\rangle\langle p_2 p_3\rangle[p_1 p_5][p_3 p_4] + [p_1 p_4][p_4 p_5]\langle p_4 p_3\rangle\langle p_1 p_2\rangle\Big) \\
& + A_{14}^{(VR)}s_{25}[p_1 p_2]\langle p_2 p_3\rangle^2[p_3 p_4]\langle p_1 p_5\rangle^2 \\
& + A_{15}^{(VR)}[p_1 p_2]\langle p_1 p_5\rangle^2\langle p_2 p_5\rangle^2\langle p_4 p_3\rangle[p_4 p_5]^2 \\
& + A_{16}^{(VR)}[p_1 p_4]\langle p_2 p_3\rangle\langle p_5 p_1\rangle\langle p_2 p_5\rangle\Big(\langle p_3 p_1\rangle[p_2 p_3] + \langle p_1 p_4\rangle[p_2 p_4]\Big) \\
& + A_{17}^{(VR)}[p_2 p_4]\langle p_2 p_3\rangle\langle p_5 p_1\rangle\langle p_2 p_5\rangle\Big(\langle p_3 p_2\rangle[p_2 p_3] + \langle p_2 p_4\rangle[p_2 p_4]\Big) \\
& + A_{18}^{(VR)}[p_5 p_4]\langle p_2 p_3\rangle\langle p_5 p_1\rangle\langle p_2 p_5\rangle\Big(\langle p_3 p_5\rangle[p_2 p_3] + \langle p_5 p_4\rangle[p_2 p_4]\Big) \\
& + A_{19}^{(VR)}\langle p_1 p_2\rangle[p_3 p_4]\langle p_3 p_5\rangle^2 \\
& + A_{20}^{(VR)}\langle p_1 p_2\rangle[p_1 p_4]^2\langle p_1 p_5\rangle^2\langle p_3 p_4\rangle \\
& + A_{21}^{(VR)}\langle p_1 p_2\rangle\langle p_1 p_5\rangle\times \\
& \qquad \times\Big([p_1 p_2]\langle p_3 p_2\rangle\langle p_3 p_5\rangle[p_3 p_4] + [p_1 p_4][p_2 p_4]\langle p_3 p_4\rangle\langle p_2 p_5\rangle\Big) \\
& + A_{22}^{(VR)}\langle p_1 p_2\rangle[p_1 p_4][p_2 p_4]\langle p_1 p_5\rangle\langle p_2 p_5\rangle\langle p_3 p_4\rangle \\
& + A_{23}^{(VR)}\langle p_1 p_2\rangle[p_2 p_4]^2\langle p_2 p_5\rangle\langle p_3 p_4\rangle\Bigg)
\end{aligned}
\tag{A.10}
$$

$$
\begin{aligned}
\mathcal{M}^{(VR)a}_{4\ LR;R;LL} = \frac{1}{\sqrt{2}} \frac{C_1 g_W t^a}{p_W^2 - m_W^2 + i\Gamma_W m_W} \times \\
\times \Bigg(& 8A_8^{(VR)} [p_2 p_3][p_3 p_4]\langle p_3 p_5\rangle[p_5 p_1] \\
& + 4A_9^{(VR)} [p_3 p_1][p_2 p_5][p_3 p_4]\langle p_3 p_5\rangle \\
& + 2A_{10}^{(VR)} [p_1 p_5][p_2 p_5]\Big(s_{5W}\langle p_1 p_3\rangle[p_1 p_4] - s_{1W}\langle p_3 p_5\rangle[p_4 p_5]\Big) \\
& + 2A_{11}^{(VR)} [p_1 p_5][p_2 p_5]\Big(s_{5W}\langle p_2 p_3\rangle[p_2 p_4] - s_{2W}\langle p_3 p_5\rangle[p_4 p_5]\Big) \\
& + 2A_{12}^{(VR)} [p_1 p_2][p_1 p_3][p_2 p_3][p_4 p_3]\langle p_1 p_5\rangle\langle p_2 p_5\rangle \\
& + A_{13}^{(VR)} \langle p_1 p_5\rangle^2\langle p_2 p_5\rangle[p_1 p_2] \times \\
& \qquad \times \Big([p_1 p_3][p_2 p_3][p_1 p_5][p_3 p_4] + [p_1 p_4][p_4 p_5]\langle p_3 p_4\rangle[p_1 p_2]\Big) \\
& + A_{14}^{(VR)} s_{25}[p_1 p_2][p_2 p_3]^2[p_3 p_4]\langle p_1 p_5\rangle^2 \\
& + A_{15}^{(VR)} [p_1 p_2]\langle p_1 p_5\rangle^2\langle p_2 p_5\rangle^2[p_3 p_4][p_4 p_5]^2 \\
& + A_{16}^{(VR)} [p_1 p_4][p_2 p_3][p_1 p_5][p_2 p_5]\Big(\langle p_3 p_1\rangle[p_2 p_3] + \langle p_1 p_4\rangle[p_2 p_4]\Big) \\
& + A_{17}^{(VR)} [p_2 p_4][p_2 p_3][p_1 p_5][p_2 p_5]\Big(\langle p_3 p_2\rangle[p_2 p_3] + \langle p_2 p_4\rangle[p_2 p_4]\Big) \\
& + A_{18}^{(VR)} [p_5 p_4][p_2 p_3][p_1 p_5][p_2 p_5]\Big(\langle p_3 p_5\rangle[p_2 p_3] + \langle p_5 p_4\rangle[p_2 p_4]\Big) \\
& + A_{19}^{(VR)} [p_2 p_1][p_3 p_4]\langle p_3 p_5\rangle^2 \\
& + A_{20}^{(VR)} [p_2 p_1][p_1 p_4]^2\langle p_1 p_5\rangle^2\langle p_3 p_4\rangle \\
& + A_{21}^{(VR)} [p_2 p_1]\langle p_1 p_5\rangle \times \\
& \qquad \times \Big([p_1 p_2]\langle p_3 p_2\rangle\langle p_3 p_5\rangle[p_3 p_4] + [p_1 p_4][p_2 p_4]\langle p_3 p_4\rangle\langle p_2 p_5\rangle\Big) \\
& + A_{22}^{(VR)} [p_2 p_1][p_1 p_4][p_2 p_4]\langle p_1 p_5\rangle\langle p_2 p_5\rangle\langle p_3 p_4\rangle \\
& + A_{23}^{(VR)} [p_2 p_1][p_2 p_4]^2\langle p_2 p_5\rangle\langle p_3 p_4\rangle \Bigg)
\end{aligned}
\tag{A.11}
$$

$$
\begin{aligned}
\mathcal{M}^{(VR)a}_{4\ RL;R;LL} = \frac{1}{\sqrt{2}} \frac{C_2 g_W t^a}{p_W^2 - m_W^2 + i\Gamma_W m_W} \times \\
\times \Bigg(& 4A^{(VR)}_{12} \langle p_2 p_1 \rangle [p_1 p_4] [p_2 p_4] \langle p_3 p_4 \rangle \langle p_1 p_5 \rangle \langle p_2 p_5 \rangle \\
& + \left(s_{15} A^{(VR)}_{13} - A^{(VR)}_{16} \right) \langle p_2 p_1 \rangle \langle p_2 p_5 \rangle \times \\
& \qquad \times \Big(\langle p_2 p_1 \rangle \langle p_1 p_3 \rangle [p_3 p_4] \langle p_3 p_5 \rangle + [p_1 p_4] [p_2 p_4] \langle p_5 p_1 \rangle [p_3 p_4] \Big) \\
& + \left(s_{15} A^{(VR)}_{14} - A^{(VR)}_{17} \right) \langle p_1 p_2 \rangle [p_2 p_4]^2 \langle p_2 p_5 \rangle^2 \langle p_3 p_4 \rangle \\
& + \left(s_{15} A^{(VR)}_{15} - A^{(VR)}_{18} \right) s_{25} \ \langle p_1 p_2 \rangle \langle p_3 p_5 \rangle^2 [p_3 p_4] \\
& + A^{(VR)}_{19} \langle p_2 p_1 \rangle \langle p_3 p_5 \rangle^2 [p_3 p_4] \\
& + A^{(VR)}_{20} \langle p_2 p_1 \rangle [p_1 p_4]^2 \langle p_1 p_5 \rangle^2 \langle p_3 p_4 \rangle \\
& + A^{(VR)}_{21} \langle p_1 p_2 \rangle \langle p_1 p_5 \rangle \times \\
& \qquad \times \Big([p_1 p_2] \langle p_3 p_2 \rangle \langle p_3 p_5 \rangle [p_3 p_4] + [p_1 p_4] [p_2 p_4] \langle p_3 p_4 \rangle \langle p_2 p_5 \rangle \Big) \\
& + A^{(VR)}_{22} \langle p_1 p_2 \rangle [p_1 p_4] [p_2 p_4] \langle p_1 p_5 \rangle \langle p_2 p_5 \rangle \langle p_3 p_4 \rangle \\
& + A^{(VR)}_{23} \langle p_2 p_1 \rangle \langle p_2 p_4 \rangle^2 \langle p_2 p_5 \rangle \langle p_3 p_4 \rangle \Bigg)
\end{aligned}
\tag{A.12}
$$

$$
\begin{aligned}
\mathcal{M}^{(VR)a}_{3\;LR;L;LL} = \frac{1}{\sqrt{2}} \frac{v C_1 g_W^2 m_W t^a}{\left(p_W^2 - m_W^2 + i\Gamma_W m_W\right)\left(s_{12} - m_W^2 + i\Gamma_W m_W\right)} \times \\
\times \Bigg(2B_{12}^{(VR)} [p_1 p_2]^2 \langle p_1 p_5\rangle \langle p_2 p_5\rangle \Big(\langle p_1 p_3\rangle [p_1 p_4] - \langle p_2 p_3\rangle [p_2 p_4] \Big) \\
+ B_{13}^{(VR)} s_{15} [p_1 p_2] \langle p_2 p_5\rangle \Big(\langle p_3 p_1\rangle [p_1 p_4] [p_2 p_1] \langle p_1 p_5\rangle - s_{12} [p_2 p_4] \langle p_3 p_5\rangle \Big) \\
+ B_{14}^{(VR)} s_{15} [p_1 p_2] \langle p_2 p_5\rangle \Big(\langle p_3 p_2\rangle [p_2 p_4] [p_2 p_1] \langle p_1 p_5\rangle - s_{12} [p_2 p_4] \langle p_3 p_5\rangle \Big) \\
+ B_{15}^{(VR)} s_{15} [p_1 p_2] \langle p_2 p_5\rangle \Big(\langle p_3 p_5\rangle [p_5 p_4] [p_2 p_1] \langle p_1 p_5\rangle - s_{5W} [p_2 p_4] \langle p_3 p_5\rangle \Big) \\
+ B_{16}^{(VR)} [p_1 p_2] \langle p_2 p_5\rangle \Big(\langle p_1 p_3\rangle [p_1 p_4] \langle p_1 p_5\rangle [p_2 p_1] + s_{12} [p_2 p_4] \langle p_3 p_5\rangle \Big) \\
+ B_{17}^{(VR)} [p_1 p_2] \langle p_2 p_5\rangle \Big(\langle p_2 p_3\rangle [p_2 p_4] \langle p_1 p_5\rangle [p_2 p_1] + s_{12} [p_2 p_4] \langle p_3 p_5\rangle \Big) \\
+ B_{18}^{(VR)} [p_1 p_2] \langle p_2 p_5\rangle \Big(\langle p_3 p_5\rangle [p_4 p_5] \langle p_1 p_5\rangle [p_2 p_1] + s_{5W} [p_2 p_4] \langle p_3 p_5\rangle \Big) \\
+ B_{19}^{(VR)} [p_1 p_2] \langle p_3 p_5\rangle \Big(\langle p_1 p_5\rangle [p_1 p_4] + \langle p_2 p_5\rangle [p_2 p_4] \Big) \\
+ B_{20}^{(VR)} [p_1 p_2]^2 [p_1 p_4] \langle p_2 p_3\rangle \langle p_1 p_5\rangle^2 \\
+ B_{21}^{(VR)} [p_1 p_2]^2 [p_2 p_4] \langle p_2 p_3\rangle \langle p_2 p_5\rangle^2 \\
+ B_{22}^{(VR)} [p_1 p_2]^2 [p_1 p_4] \langle p_2 p_3\rangle \langle p_2 p_5\rangle^2 \\
+ B_{23}^{(VR)} [p_1 p_2]^2 [p_2 p_4] \langle p_2 p_3\rangle \langle p_2 p_5\rangle^2 \Bigg)
\end{aligned}
\tag{A.13}
$$

$$
\begin{aligned}
\mathcal{M}^{(VR)a}_{3\;RL;L;LL} = \frac{1}{\sqrt{2}} \frac{v C_2 g_W^2 m_W t^a}{\left(p_W^2 - m_W^2 + i\Gamma_W m_W\right)\left(s_{12} - m_W^2 + i\Gamma_W m_W\right)} \times \\
\times \Bigg(4\Big(B_8^{(VR)} + B_9^{(VR)}\Big)\langle p_1 p_5\rangle\langle p_2 p_5\rangle\Big(\langle p_2 p_3\rangle[p_2 p_4] + \langle p_1 p_3\rangle[p_1 p_4]\Big) \\
+ 2B_{10}^{(VR)}\langle p_1 p_5\rangle\langle p_2 p_5\rangle\Big(s_{5W}\langle p_3 p_1\rangle[p_1 p_4] - s_{12}\langle p_3 p_5\rangle[p_5 p_4]\Big) \\
+ 2B_{11}^{(VR)}\langle p_1 p_5\rangle\langle p_2 p_5\rangle\Big(s_{5W}\langle p_3 p_2\rangle[p_2 p_4] - s_{12}\langle p_3 p_5\rangle[p_5 p_4]\Big) \\
+ 2B_{12}^{(VR)} s_{12}\langle p_1 p_5\rangle\langle p_2 p_5\rangle\Big(\langle p_2 p_3\rangle[p_2 p_4] - \langle p_1 p_3\rangle[p_1 p_4]\Big) \\
+ B_{13}^{(VR)} s_{15}\langle p_1 p_2\rangle\langle p_2 p_5\rangle\Big(\langle p_3 p_1\rangle[p_1 p_4][p_2 p_1]\langle p_1 p_5\rangle - s_{12}[p_2 p_4]\langle p_3 p_5\rangle\Big) \\
+ B_{14}^{(VR)} s_{15}\langle p_1 p_2\rangle\langle p_2 p_5\rangle\Big(\langle p_3 p_2\rangle[p_2 p_4][p_2 p_1]\langle p_1 p_5\rangle - s_{12}[p_2 p_4]\langle p_3 p_5\rangle\Big) \\
+ B_{15}^{(VR)} s_{15}\langle p_1 p_2\rangle\langle p_2 p_5\rangle\Big(\langle p_3 p_5\rangle[p_5 p_4][p_2 p_1]\langle p_1 p_5\rangle - s_{5W}[p_2 p_4]\langle p_3 p_5\rangle\Big) \\
+ B_{16}^{(VR)}\langle p_1 p_2\rangle\langle p_2 p_5\rangle\Big(\langle p_1 p_3\rangle[p_1 p_4]\langle p_1 p_5\rangle[p_2 p_1] + s_{12}[p_2 p_4]\langle p_3 p_5\rangle\Big) \\
+ B_{17}^{(VR)}\langle p_1 p_2\rangle\langle p_2 p_5\rangle\Big(\langle p_2 p_3\rangle[p_2 p_4]\langle p_1 p_5\rangle[p_2 p_1] + s_{12}[p_2 p_4]\langle p_3 p_5\rangle\Big) \\
+ B_{18}^{(VR)}\langle p_1 p_2\rangle\langle p_2 p_5\rangle\Big(\langle p_3 p_5\rangle[p_4 p_5]\langle p_1 p_5\rangle[p_2 p_1] + s_{5W}[p_2 p_4]\langle p_3 p_5\rangle\Big) \\
+ B_{19}^{(VR)}\langle p_1 p_2\rangle\langle p_3 p_5\rangle\Big(\langle p_1 p_5\rangle[p_1 p_4] + \langle p_2 p_5\rangle[p_2 p_4]\Big) \\
+ B_{20}^{(VR)} s_{12}[p_1 p_4]\langle p_3 p_2\rangle\langle p_1 p_5\rangle^2 \\
+ B_{21}^{(VR)} s_{12}[p_2 p_4]\langle p_3 p_2\rangle\langle p_2 p_5\rangle^2 \\
+ B_{22}^{(VR)} s_{12}[p_1 p_4]\langle p_3 p_2\rangle\langle p_2 p_5\rangle^2 \\
+ B_{23}^{(VR)} s_{12}[p_2 p_4]\langle p_3 p_2\rangle\langle p_1 p_5\rangle^2 \Bigg)
\end{aligned}
\tag{A.14}
$$

$$
\begin{aligned}
\mathcal{M}^{(VR)a}_{3\;LR;R;LL} = &-\frac{1}{\sqrt{2}}\frac{vC_1 g_W^2 m_W t^a}{\left(p_W^2 - m_W^2 + i\Gamma_W m_W\right)\left(s_{12} - m_W^2 + i\Gamma_W m_W\right)}\times \\
&\times\Bigg(8B_8^{(VR)}[p_1p_2]\langle p_1p_3\rangle[p_1p_5][p_4p_5] \\
&\quad + 8B_9^{(VR)}[p_1p_2]\langle p_2p_3\rangle[p_2p_5][p_4p_5] \\
&\quad + 2B_{10}^{(VR)}[p_1p_5][p_2p_5]\Big(s_{12}\langle p_3p_5\rangle[p_4p_5] - s_{5W}\langle p_1p_3\rangle[p_1p_4]\Big) \\
&\quad + 2B_{11}^{(VR)}[p_1p_5][p_2p_5]\Big(s_{12}\langle p_3p_5\rangle[p_4p_5] - s_{5W}\langle p_2p_3\rangle[p_2p_4]\Big) \\
&\quad + 2B_{12}^{(VR)}s_{12}[p_1p_5][p_2p_5]\Big(\langle p_2p_3\rangle[p_2p_4] - \langle p_1p_3\rangle[p_1p_4]\Big) \\
&\quad + \Big(s_{15}B_{13}^{(VR)} + B_{16}^{(VR)}\Big)[p_2p_1][p_2p_5]\times \\
&\qquad\quad \times\Big(\langle p_3p_1\rangle[p_1p_4]\langle p_1p_2\rangle[p_1p_5] + s_{12}\langle p_2p_3\rangle[p_4p_5]\Big) \\
&\quad + \Big(s_{15}B_{14}^{(VR)} + B_{17}^{(VR)}\Big)[p_2p_1][p_2p_5]\langle p_2p_3\rangle\times \\
&\qquad\quad \times\Big(\langle p_2p_1\rangle[p_2p_4][p_1p_5] + s_{12}[p_4p_5]\Big) \\
&\quad + \Big(s_{15}B_{15}^{(VR)} + B_{18}^{(VR)}\Big)[p_2p_1][p_2p_5][p_4p_5]\times \\
&\qquad\quad \times\Big(\langle p_2p_1\rangle[p_1p_5]\langle p_3p_5\rangle + s_{5W}\langle p_2p_3\rangle\Big) \\
&\quad + B_{19}^{(VR)}[p_2p_1]\langle p_3p_5\rangle\Big([p_1p_5][p_1p_4] + [p_2p_5][p_2p_4]\Big) \\
&\quad + \Big(s_{15}B_{20}^{(VR)} + s_{25}B_{22}^{(VR)}\Big)[p_1p_2]^2[p_1p_4]\langle p_2p_3\rangle \\
&\quad + \Big(s_{25}B_{21}^{(VR)} + s_{15}B_{23}^{(VR)}\Big)[p_1p_2]^2[p_2p_4]\langle p_2p_3\rangle\Bigg)
\end{aligned}
\tag{A.15}
$$

$$
\begin{aligned}
\mathcal{M}^{(VR)a}_{3\;RL;R;LL} = -\frac{1}{\sqrt{2}}\frac{vC_2 g_W^2 m_W t^a}{\big(p_W^2 - m_W^2 + i\Gamma_W m_W\big)\big(s_{12} - m_W^2 + i\Gamma_W m_W\big)}\times \\
\times\Bigg(2B_{12}^{(VR)}\langle p_1p_2\rangle^2[p_1p_5][p_2p_5]\Big(\langle p_1p_3\rangle[p_1p_4] - \langle p_2p_3\rangle[p_2p_4]\Big) \\
+\Big(s_{15}B_{13}^{(VR)} + B_{16}^{(VR)}\Big)\langle p_1p_2\rangle[p_2p_5]\times \\
\times\Big(\langle p_3p_1\rangle[p_1p_4]\langle p_1p_2\rangle[p_1p_5] + s_{12}\langle p_2p_3\rangle[p_4p_5]\Big) \\
+\Big(s_{15}B_{14}^{(VR)} + B_{17}^{(VR)}\Big)\langle p_1p_2\rangle[p_2p_5]\langle p_2p_3\rangle\times \\
\times\Big(\langle p_2p_1\rangle[p_2p_4][p_1p_5] + s_{12}[p_4p_5]\Big) \\
+\Big(s_{15}B_{15}^{(VR)} + B_{18}^{(VR)}\Big)\langle p_1p_2\rangle[p_2p_5][p_4p_5]\times \\
\times\Big(\langle p_2p_1\rangle[p_1p_5]\langle p_3p_5\rangle + s_{5W}\langle p_2p_3\rangle\Big) \\
+B_{19}^{(VR)}\langle p_1p_2\rangle\langle p_3p_5\rangle\Big([p_1p_5][p_1p_4] + [p_2p_5][p_2p_4]\Big) \\
+\Big(s_{15}B_{20}^{(VR)} + s_{25}B_{22}^{(VR)}\Big)s_{12}[p_1p_4]\langle p_2p_3\rangle \\
+\Big(s_{25}B_{21}^{(VR)} + s_{15}B_{23}^{(VR)}\Big)s_{12}[p_2p_4]\langle p_2p_3\rangle\Bigg)
\end{aligned}
\tag{A.16}
$$

$$\mathcal{M}^{(VR)a}_{4\ LL;L;LL} = \frac{1}{\sqrt{2}}\frac{C_3 g_W t^a}{p_W^2 - m_W^2 + i\Gamma_W m_W}\times$$
$$\times\Bigg(\Big(s_{12}A_1^{(VR)} + s_{12}A_2^{(VR)} + s_{125}A_3^{(VR)} + 2s_{25}A_7^{(VR)}\Big)\langle p_5 p_2\rangle\langle p_5 p_3\rangle[p_4 p_1]$$
$$+ A_4^{(VR)}\langle p_3 p_1\rangle[p_1 p_4]\langle p_2 p_5\rangle^2[p_1 p_2] + A_5^{(VR)}\langle p_3 p_2\rangle[p_2 p_4]\langle p_2 p_5\rangle^2[p_1 p_2]$$
$$+ A_6^{(VR)}\langle p_3 p_5\rangle[p_5 p_4]\langle p_2 p_5\rangle^2[p_1 p_2] + 2A_7^{(VR)}\langle p_2 p_5\rangle\langle p_1 p_5\rangle[p_2 p_1]\langle p_2 p_3\rangle[p_4 p_1]\Bigg) \tag{A.17}$$

$$\mathcal{M}^{(VR)a}_{4\ RR;L;LL} = \frac{1}{\sqrt{2}}\frac{C_4 g_W t^a}{p_W^2 - m_W^2 + i\Gamma_W m_W}\times$$
$$\times\Bigg(A_1^{(VR)}\langle p_3 p_1\rangle[p_1 p_4]\langle p_1 p_5\rangle^2[p_2 p_1] + A_2^{(VR)}\langle p_3 p_2\rangle[p_2 p_4]\langle p_1 p_5\rangle^2[p_2 p_1]$$
$$+ A_3^{(VR)}\langle p_3 p_5\rangle[p_5 p_4]\langle p_1 p_5\rangle^2[p_2 p_1] + 2A_7^{(VR)}\langle p_1 p_5\rangle\langle p_2 p_5\rangle[p_2 p_1][p_2 p_4]\langle p_3 p_1\rangle$$
$$+ \Big(s_{12}A_4^{(VR)} + s_{12}A_5^{(VR)} + s_{125}A_6^{(VR)} - 2s_{15}A_7^{(VR)}\Big)\langle p_5 p_1\rangle[p_2 p_4]\langle p_3 p_5\rangle\Bigg) \tag{A.18}$$

$$\mathcal{M}^{(VR)a}_{4\ LL;R;LL} = \frac{1}{\sqrt{2}}\frac{C_3 g_W t^a}{p_W^2 - m_W^2 + i\Gamma_W m_W}\times$$
$$\times\Bigg(A_1^{(VR)}\langle p_3 p_1\rangle[p_1 p_4][p_1 p_5]^2\langle p_1 p_2\rangle + A_2^{(VR)}\langle p_3 p_2\rangle[p_2 p_4][p_1 p_5]^2\langle p_1 p_2\rangle$$
$$+ A_3^{(VR)}\langle p_3 p_5\rangle[p_5 p_4][p_1 p_5]^2\langle p_1 p_2\rangle + 2A_7^{(VR)}[p_1 p_5][p_2 p_5]\langle p_1 p_2\rangle\langle p_2 p_3\rangle[p_4 p_1]$$
$$+ \Big(s_{12}A_4^{(VR)} + s_{12}A_5^{(VR)} + s_{125}A_6^{(VR)} - 2s_{15}A_7^{(VR)}\Big)[p_1 p_5]\langle p_2 p_3\rangle[p_4 p_5]\Bigg) \tag{A.19}$$

$$\mathcal{M}^{(VR)a}_{4\ RR;R;LL} = \frac{1}{\sqrt{2}}\frac{C_4 g_W t^a}{p_W^2 - m_W^2 + i\Gamma_W m_W}\times$$
$$\times\Bigg(\Big(s_{12}A_1^{(VR)} + s_{12}A_2^{(VR)} + s_{125}A_3^{(VR)} + 2s_{25}A_7^{(VR)}\Big)[p_2 p_5][p_5 p_4]\langle p_3 p_1\rangle$$
$$+ A_4^{(VR)}\langle p_3 p_1\rangle[p_1 p_4][p_2 p_5]^2\langle p_2 p_1\rangle + A_5^{(VR)}\langle p_3 p_2\rangle[p_2 p_4][p_2 p_5]^2\langle p_2 p_1\rangle$$
$$+ A_6^{(VR)}\langle p_3 p_5\rangle[p_5 p_4][p_2 p_5]^2\langle p_2 p_1\rangle + 2A_7^{(VR)}[p_1 p_5][p_2 p_5]\langle p_2 p_1\rangle[p_2 p_4]\langle p_3 p_1\rangle\Bigg) \tag{A.20}$$

The three-point helicity amplitudes with initial state quarks having equal helicities can be readily derived from the corresponding four-point helicity amplitudes by exchanging the pre-factor in accordance with the expressions given in (4.1) and (4.2). This is due to the fact that the amplitudes with an open index μ possess the same structural form.

The amplitudes for the double real correction are similarly unavailable in the main text, due to the considerable number of such amplitudes (there are 32 of them in total). All they can be found in the supplementary files.

B Dirac Matrices in d-dimensional Spacetime

This thesis employs a d-dimensional spacetime framework and utilizes the 't Hooft–Veltman dimensional regularization approach [145, 146] to extract ultraviolet and infrared divergences in terms of $1/\varepsilon$-poles. Furthermore, four-component notation is employed, with the understanding that $d = 4 - 2\varepsilon$, where $\varepsilon \neq 0$ is the parameter of dimensional regularization. Additionally, we represent Dirac matrices in the Weyl basis, where they are expressed as follows:

$$\gamma^\mu = \begin{pmatrix} 0 & \sigma^\mu \\ \bar{\sigma}^\mu & 0 \end{pmatrix}, \tag{B.1}$$

with $\mu = \overline{1,4}$ and

$$\sigma^\mu = (1, \vec{\sigma}) \qquad \bar{\sigma}^\mu = (1, -\vec{\sigma}), \tag{B.2}$$

where the well known Pauli matrices are

$$\sigma_1 = \begin{pmatrix} 0 & 1 \\ 1 & 0 \end{pmatrix}, \qquad \sigma_1 = \begin{pmatrix} 0 & -i \\ i & 0 \end{pmatrix}, \qquad \sigma_1 = \begin{pmatrix} 1 & 0 \\ 0 & -1 \end{pmatrix}. \tag{B.3}$$

Matrix γ_5 is given in this basis by

$$\gamma_5 = \begin{pmatrix} -1 & 0 \\ 0 & 1 \end{pmatrix} \tag{B.4}$$

and, therefore, left- and right-handed projectors can be written as

$$P_L = \frac{1-\gamma_5}{2} = \begin{pmatrix} 1 & 0 \\ 0 & 0 \end{pmatrix}, \qquad P_R = \frac{1+\gamma_5}{2} = \begin{pmatrix} 0 & 0 \\ 0 & 1 \end{pmatrix}, \tag{B.5}$$

respectively. In Eqs. (B.4) and (B.5), block matrix notation was employed, whereby $1 \equiv 1_{2\times 2}$.

B.1 Dirac matrices γ^μ

The Dirac algebra in d dimensions, with $d = 4 - 2\varepsilon$, differs from the case $d = 4$. This is due to the fact that in d dimensions, $g^{\mu\nu} g_{\mu\nu} = d \neq 4$ which gives rise to new identities between gamma matrices.

It is, however, essential to recognize that relations obtained in this Appendix can only be applied to loop momenta. External momenta will always remain four-dimensional, and thus we are working within the 't Hooft–Veltman dimensional regularization scheme. This is the reason why we did not obtain the ε-term at leading order.

The anticommutative relation employed in the definition of the gamma matrices retains its form as it does in the four-dimensional case

$$\{\gamma^\mu, \gamma^\nu\} = \gamma^\mu\gamma^\nu + \gamma^\nu\gamma^\mu = 2g^{\mu\nu}. \tag{B.6}$$

If we consider the contraction $\gamma^\mu\gamma_\mu$, we can express it as

$$\begin{aligned} \gamma^\mu\gamma_\mu = g_{\mu\nu}\gamma^\mu\gamma^\nu = \frac{1}{2}\left(g_{\mu\nu} + g_{\nu\mu}\right)\gamma^\mu\gamma^\nu = \frac{1}{2}\left(g_{\mu\nu}\gamma^\mu\gamma^\nu + g_{\nu\mu}\gamma^\mu\gamma^\nu\right) = \\ = \frac{1}{2}\left(g_{\mu\nu}\gamma^\mu\gamma^\nu + g_{\mu\nu}\gamma^\nu\gamma^\mu\right) = \frac{g_{\mu\nu}}{2}\left(\gamma^\mu\gamma^\nu + \gamma^\nu\gamma^\mu\right) = \frac{g_{\mu\nu}}{2}\cdot 2g^{\mu\nu}. \end{aligned} \tag{B.7}$$

In the first line of Eq. (B.7), the symmetry of $g^{\mu\nu}$ with respect to index permutation has been employed, whereas in the second line, the indices of the γ-matrices have been renamed, with μ and ν interchanged. Finally,

$$\gamma^\mu \gamma_\mu = d. \tag{B.8}$$

We may now consider an expression involving a γ-matrix between the two other γ-matrices with equal indices contracted

$$\gamma^\mu \gamma^\nu \gamma_\mu = \left(2g^{\mu\nu} - \gamma^\nu \gamma^\mu\right) \gamma_\mu = 2\gamma^\nu - \gamma^\nu \cdot d = (2-d)\gamma^\nu. \tag{B.9}$$

Similarly, by employing the previous identity on each occasion, one can arrive at the following conclusions

$$\gamma^\mu \gamma^\nu \gamma^\lambda \gamma_\mu = (d-4)\gamma^\nu \gamma^\lambda + 4g^{\nu\lambda}, \tag{B.10}$$

$$\gamma^\mu \gamma^\nu \gamma^\lambda \gamma^\rho \gamma_\mu = -2\gamma^\rho \gamma^\lambda \gamma^\nu + (4-d)\gamma^\nu \gamma^\lambda \gamma^\rho. \tag{B.11}$$

In the most general case, one can derive in a similar manner

$$\gamma^\mu \gamma^{\nu_1} ... \gamma^{\nu_n} \gamma_\mu = 2\sum_i^n (-1)^{i+n} \gamma^{\nu_i} \gamma^{\nu_1} ... \gamma^{\nu_{i-1}} \gamma^{\nu_{i+1}} ... \gamma^{\nu_n} + (d-4)(-1)^n \gamma^{\nu_1} ... \gamma^{\nu_n}. \tag{B.12}$$

The relations (B.8) through (B.12) are called the *Miscellaneous identities*. In four-dimensional space, these relations are identical to those observed in four dimensions.

B.2 Matrix γ_5

In the context of d-dimensional spacetime, the primary challenge arises from the presence of the γ_5 matrix. This matrix plays a pivotal role in the calculations at all levels, from the leading order onwards. Nevertheless, in the helicity amplitudes approach, dealing with γ_5 is straightforward. The issue arises when one considers diagrams with a closed fermion loop, where γ_5 appears under the trace operator. This results in the trace of a product of some combination of d-dimensional Dirac matrices and a single γ_5 which is actually a four-dimensional object. This is confirmed by its definition

$$\gamma_5 = -\frac{i}{4!} \varepsilon^{\mu\nu\lambda\rho} \gamma_\mu \gamma_\nu \gamma_\lambda \gamma_\rho, \tag{B.13}$$

where $\varepsilon^{\mu\nu\lambda\rho}$ is the totally antisymmetric Levi-Civita pseudotensor, a purely four-dimensional object. For this reason, naive working with γ_5 in an extended spacetime by $d = 4 - 2\varepsilon$ is, strictly speaking, incorrect.

But modern theoretical investigations in particle physics present [173] a challenge in handling chiral couplings in dimensional regularization, where one must address the issue of dealing with γ_5 in non-natural number of dimensions. The familiar anticommutative relation

$$\{\gamma^\mu, \gamma_5\} = 0 \tag{B.14}$$

remains as for four-dimensional spacetime and simultaneous work with traces using the conventional algebra of γ-matrices is not compatible, as is has been emphasized in [173].

The Dirac trace $\mathrm{tr}\,(\gamma^\mu\gamma^\nu\gamma^\sigma\gamma^\rho\gamma_5) = -4i\varepsilon^{\mu\nu\sigma\rho}$, the simplest non-zero trace containing γ_5 in four dimensions, must either vanish in dimensional regularization or be a reason to modify algebraic rules of γ-matrices. As a formal reason, it should be noted that there is no d-dimensional analogue for the Levi-Civita symbol in the dimensional regularization schemes we will now consider. Nevertheless, we accept the familiar properties of γ_5

$$\gamma_5^2 = 1, \qquad \gamma_5^\dagger = \gamma_5. \tag{B.15}$$

In order to utilize dimensional regularization with respect to matrix γ_5, one can explicitly distinguish four-dimensional and (-2ε)-dimensional parts of the d-dimensional spacetime. Concurrently, d-dimensional objects are also split as follows:

$$k_i^\mu = \bar{k}_i^\mu + \hat{k}_i^\mu, \qquad \gamma^\mu = \bar{\gamma}^\mu + \hat{\gamma}^\mu, \qquad g^{\mu\nu} = \bar{g}^{\mu\nu} + \hat{g}^{\mu\nu}, \tag{B.16}$$

where bar and hat symbols are used to indicate four- and (-2ε)-dimensional objects, respectively. It is important to note that the scalar product of any two objects, one of which is four-dimensional and the other is (-2ε)-dimensional, must necessarily be equal to zero:

$$\begin{aligned}
\bar{\gamma}^\mu\hat{\gamma}_\mu = 0, \qquad & \bar{\gamma}^\mu\hat{k}_{i\mu} = 0, \qquad & \hat{\gamma}^\mu\bar{k}_{i\mu} = 0, \\
\bar{g}^{\mu\nu}\hat{g}_{\mu\nu} = 0, \qquad & \bar{g}^{\mu\nu}\hat{\gamma}_\mu = 0, \qquad & \hat{g}^{\mu\nu}\bar{\gamma}_\mu = 0, \\
(\bar{k}_i^\mu \cdot \hat{k}_{j\mu}) = 0, \qquad & \bar{g}^{\mu\nu}\hat{k}_{i\mu} = 0, \qquad & \hat{g}^{\mu\nu}\bar{k}_{i\mu} = 0
\end{aligned} \tag{B.17}$$

and any product of two objects with equal dimensions obeys the usual rules.

Before proceeding to the study of dimensional regularization schemes, it is important to note the scalar product of the form $\bar{g}_{\mu\nu}k_i^\mu k_j^\nu$. It is therefore beneficial to explicitly state that

$$\begin{aligned}
\bar{g}_{\mu\nu}k_i^\mu k_j^\nu &= (g_{\mu\nu} - \hat{g}_{\mu\nu})k_i^\mu k_j^\nu = \\
&= g_{\mu\nu}k_i^\mu k_j^\nu - \hat{g}_{\mu\nu}(\bar{k}_i^\mu + \hat{k}_i^\mu)(\bar{k}_j^\nu + \hat{k}_j^\nu) = \\
&= (k_i \cdot k_j) - \hat{g}_{\mu\nu}\bar{k}_i^\mu\bar{k}_j^\nu - \hat{g}_{\mu\nu}\bar{k}_i^\mu\hat{k}_j^\nu - \hat{g}_{\mu\nu}\hat{k}_i^\mu\bar{k}_j^\nu - \hat{g}_{\mu\nu}\hat{k}_i^\mu\hat{k}_j^\nu.
\end{aligned} \tag{B.18}$$

The application of relations (B.16) and (B.17) leads to a definitive conclusion

$$\bar{g}_{\mu\nu}k_i^\mu k_j^\nu = (k_i \cdot k_j) - (\hat{k}_i \cdot \hat{k}_j). \tag{B.19}$$

The HVBM's scheme [174 – 176] and the Kreimer's scheme [177 – 179] represent the two principal variants of dimensional regularization employed in the field of modern high-energy physics. As previously stated in this section, the precise treatment of γ_5 in these schemes has a profound impact on either the Feynman rules or the handling of Dirac traces. Four-dimensional Dirac trace identities which rely on γ_5 manipulations must be, depending on the scheme, either carefully reformulated or abandoned.

B.2.1 HVBM's dimensional regularization scheme

In HVBM's scheme, developed by 't Hooft, Veltman, Breitenlohner, and Maison, we do not accept the anticommutation relation (B.14). Instead, we maintain the cyclicity of the trace. In accordance with the fact that γ_5 is a purely four-dimensional object, alternative rules are accepted

$$\{\bar{\gamma}^\mu, \gamma_5\} = 0, \qquad [\hat{\gamma}^\mu, \gamma_5] = 0. \tag{B.20}$$

This modification of Eq. (B.14) has an impact on the form of the Feynman rules in dimensional regularization, as a result of which they cease to be Hermitian. Consequently, prior to applying Eq. (B.13), one can perform a "four-dimensional" transformation

$$\begin{aligned} \gamma^\mu\gamma_5 &= \frac{1}{2}\gamma^\mu\gamma_5 + \frac{1}{2}\gamma^\mu\gamma_5 = \frac{1}{2}\gamma^\mu\gamma_5 + \frac{1}{2}\Big(\{\gamma^\mu, \gamma_5\} - \gamma_5\gamma^\mu\Big) = \\ &= \frac{1}{2}\gamma^\mu\gamma_5 - \frac{1}{2}\gamma_5\gamma^\mu = \frac{1}{2}[\gamma^\mu, \gamma_5] \end{aligned} \tag{B.21}$$

in order to be able to throw γ_5 away from the calculations in (-2ε)-dimensional space.

In order to compute the trace of a product of an even number of γ-matrices without γ_5 one can utilize the well-known recursive formula

$$\mathrm{tr}\,(\gamma^{\mu_1}...\gamma^{\mu_n}) = \sum_{i=1}^{n-1}(-1)^{i+1} g^{\mu_1\mu_{i+1}}\mathrm{tr}\,(\gamma^{\mu_2}...\gamma^{\mu_i}\gamma^{\mu_{i+2}}...\gamma^{\mu_n}) \tag{B.22}$$

with the termination criterion $\mathrm{tr}(1) = 4$. This encompasses the standard four-dimensional identities. As is customary, the trace of a product of an odd number of γ-matrices is equal to zero.

In order to ascertain the trace identities with γ_5 we utilize its definition (B.13) and compute the trace of a product of $n+4$ γ-matrices applying Eq. (B.22). As can be seen from the above, the usual trace identities remain valid. For example,

$$\mathrm{tr}\,(\gamma_5) = -\frac{i}{4!}\varepsilon^{\mu\nu\lambda\rho}\,\mathrm{tr}\,(\gamma_\mu\gamma_\nu\gamma_\lambda\gamma_\rho) = -\frac{i}{3!}\varepsilon^{\mu\nu\lambda\rho}\,(g_{\mu\nu}g_{\lambda\rho} - g_{\mu\lambda}g_{\nu\rho} + g_{\mu\rho}g_{\nu\lambda}) = 0, \tag{B.23}$$

since contraction of a symmetric tensor with an antisymmetric one is always equal to zero.

$$\mathrm{tr}\,(\gamma_5 \text{ and an odd number of } \gamma^\mu) = 0, \tag{B.24}$$

since γ_5 always provides four more γ-matrices.

B.2.2 Kreimer's dimensional regularization scheme

In contrast, the Kreimer's scheme maintains the anticommutation relation (B.14) at the expense of the cyclicity of traces. Larin's principle [180] asserts that these two schemes must yield the same ultimate outcome. The Kreimer's scheme offers a practical advantage over the HVBM's scheme in that it does not necessitate a modification of the algebraic form for any Feynman rule when considering interactions in d spacetime dimensions. Consequently, one can evaluate Dirac traces and perform numerator algebra prior to splitting the space.

In addition to the HVBM scheme, the trace of any product of an odd number of γ-matrices, with or without γ_5, is equal to zero. With regard to the trace of a product of an even number of γ-matrices, it was defined that

$$\mathrm{tr}\,(\gamma^{\mu_1}...\gamma^{\mu_{2n}}) = 4\sum_{\sigma}(-1)^{\mathrm{sgn}(\sigma)} g^{\mu_{i_1}\mu_{j_1}}...g^{\mu_{i_n}\mu_{j_n}} \tag{B.25}$$

without γ_5 and

$$\mathrm{tr}\left(\gamma^{\mu_1}...\gamma^{\mu_{2n}}\gamma_5\right) = -\frac{i}{3!}\varepsilon^{\mu_{2n+1}\mu_{2n+2}\mu_{2n+3}\mu_{2n+4}}\sum_{\sigma}(-1)^{\mathrm{sgn}(\sigma)}g^{\mu_{i_1}\mu_{j_1}}...g^{\mu_{i_{n+2}}\mu_{j_{n+2}}} \tag{B.26}$$

with γ_5. In Eqs. (B.25) and (B.26), σ is the set of permutations of the $2m$ indices that appear in the sums on the right-hand sides of these equations, and

$$1 = i_1 < ... < i_m, \qquad\qquad i_k < j_k \quad \text{for all } k = \overline{1,m}. \tag{B.27}$$

The trace identities (B.25) and (B.26) are equivalent to the corresponding relations in the HVBM's scheme, and thus lead to the same result.

B.3 Levi-Civita symbol

We will now turn our attention to the Levi-Civita symbol. As previously stated, this entity is inherently four-dimensional in nature. As is customary, the Levi-Civita symbol is defined as follows:

$$\varepsilon_{1234} = +1, \tag{B.28}$$

and the sign on the right-handed side changes by any permutation of any two adjacent indices. Consequently, all components with a minimum of two equal indices are equal to zero.

The product of two Levi-Civita symbols is represented through a four-rank determinant involving four-dimensional components of the metric tensor

$$\varepsilon^{\mu\nu\lambda\rho}\varepsilon_{\alpha\beta\gamma\sigma} = \begin{vmatrix} \bar{g}^{\mu}_{\alpha} & \bar{g}^{\mu}_{\beta} & \bar{g}^{\mu}_{\gamma} & \bar{g}^{\mu}_{\sigma} \\ \bar{g}^{\nu}_{\alpha} & \bar{g}^{\nu}_{\beta} & \bar{g}^{\nu}_{\gamma} & \bar{g}^{\nu}_{\sigma} \\ \bar{g}^{\lambda}_{\alpha} & \bar{g}^{\lambda}_{\beta} & \bar{g}^{\lambda}_{\gamma} & \bar{g}^{\lambda}_{\sigma} \\ \bar{g}^{\rho}_{\alpha} & \bar{g}^{\rho}_{\beta} & \bar{g}^{\rho}_{\gamma} & \bar{g}^{\rho}_{\sigma} \end{vmatrix}. \tag{B.29}$$

In the event that this product contains any pair of equal upper and lower indices, it can be concluded that a metric tensor with equal indices in the determinant is present. This is exemplified by the value $\bar{g}^{\mu}_{\mu} = 4$. Consequently, the following relations are applicable:

$$\varepsilon^{\mu\nu\lambda\rho}\varepsilon_{\mu\beta\gamma\sigma} = \begin{vmatrix} 4 & \bar{g}^{\mu}_{\beta} & \bar{g}^{\mu}_{\gamma} & \bar{g}^{\mu}_{\sigma} \\ \bar{g}^{\nu}_{\mu} & \bar{g}^{\nu}_{\beta} & \bar{g}^{\nu}_{\gamma} & \bar{g}^{\nu}_{\sigma} \\ \bar{g}^{\lambda}_{\mu} & \bar{g}^{\lambda}_{\beta} & \bar{g}^{\lambda}_{\gamma} & \bar{g}^{\lambda}_{\sigma} \\ \bar{g}^{\rho}_{\mu} & \bar{g}^{\rho}_{\beta} & \bar{g}^{\rho}_{\gamma} & \bar{g}^{\rho}_{\sigma} \end{vmatrix} = \begin{vmatrix} \bar{g}^{\nu}_{\beta} & \bar{g}^{\nu}_{\gamma} & \bar{g}^{\nu}_{\sigma} \\ \bar{g}^{\lambda}_{\beta} & \bar{g}^{\lambda}_{\gamma} & \bar{g}^{\lambda}_{\sigma} \\ \bar{g}^{\rho}_{\beta} & \bar{g}^{\rho}_{\gamma} & \bar{g}^{\rho}_{\sigma} \end{vmatrix} \tag{B.30}$$

for one pair of contracted indices,

$$\varepsilon^{\mu\nu\lambda\rho}\varepsilon_{\mu\nu\gamma\sigma} = \begin{vmatrix} 4 & \bar{g}^{\mu}_{\nu} & \bar{g}^{\mu}_{\gamma} & \bar{g}^{\mu}_{\sigma} \\ \bar{g}^{\nu}_{\mu} & 4 & \bar{g}^{\nu}_{\gamma} & \bar{g}^{\nu}_{\sigma} \\ \bar{g}^{\lambda}_{\mu} & \bar{g}^{\lambda}_{\nu} & \bar{g}^{\lambda}_{\gamma} & \bar{g}^{\lambda}_{\sigma} \\ \bar{g}^{\rho}_{\mu} & \bar{g}^{\rho}_{\nu} & \bar{g}^{\rho}_{\gamma} & \bar{g}^{\rho}_{\sigma} \end{vmatrix} = 2\left(\bar{g}^{\lambda}_{\gamma}\bar{g}^{\rho}_{\sigma} - \bar{g}^{\lambda}_{\sigma}\bar{g}^{\rho}_{\gamma}\right) \tag{B.31}$$

for two pairs of contracted indices,

$$\varepsilon^{\mu\nu\lambda\rho}\varepsilon_{\mu\nu\lambda\sigma} = \begin{vmatrix} 4 & \bar{g}^{\mu}_{\nu} & \bar{g}^{\mu}_{\lambda} & \bar{g}^{\mu}_{\sigma} \\ \bar{g}^{\nu}_{\mu} & 4 & \bar{g}^{\nu}_{\lambda} & \bar{g}^{\nu}_{\sigma} \\ \bar{g}^{\lambda}_{\mu} & \bar{g}^{\lambda}_{\nu} & 4 & \bar{g}^{\lambda}_{\sigma} \\ \bar{g}^{\rho}_{\mu} & \bar{g}^{\rho}_{\nu} & \bar{g}^{\rho}_{\lambda} & \bar{g}^{\rho}_{\sigma} \end{vmatrix} = 6\bar{g}^{\rho}_{\sigma} \tag{B.32}$$

for three pairs of contracted indices, and, finally,

$$\varepsilon^{\mu\nu\lambda\rho}\varepsilon_{\mu\nu\lambda\rho} = \begin{vmatrix} 4 & \bar{g}^{\mu}_{\nu} & \bar{g}^{\mu}_{\lambda} & \bar{g}^{\mu}_{\rho} \\ \bar{g}^{\nu}_{\mu} & 4 & \bar{g}^{\nu}_{\lambda} & \bar{g}^{\nu}_{\rho} \\ \bar{g}^{\lambda}_{\mu} & \bar{g}^{\lambda}_{\nu} & 4 & \bar{g}^{\lambda}_{\rho} \\ \bar{g}^{\rho}_{\mu} & \bar{g}^{\rho}_{\nu} & \bar{g}^{\rho}_{\lambda} & 4 \end{vmatrix} = 24, \tag{B.33}$$

if all four pairs of indices are contracted.

C Spinor Helicity Formalism

The spinor helicity formalism has become an invaluable tool in modern quantum field theory, particularly in high-energy physics, due to its efficiency and elegance in simplifying amplitude calculations. This formalism employs the properties of spinors to express particle helicities and kinematic variables in a manner that inherently preserves Lorentz invariance which makes it particularly suited for analyzing scattering processes. The spinor helicity method not only streamlines calculations but also reveals hidden symmetries by replacing cumbersome momentum and polarization vectors with spinor variables, thereby facilitating the derivation of compact and physically meaningful expressions. Furthermore, working with the γ_5 matrix is also significantly simplified in this framework, thereby further enhancing its applicability to chiral theories. This appendix provides an overview of the fundamental principles of the spinor helicity formalism and illustrates its value in the context of the calculations presented in this work.

C.1 Spinor identities

In order to facilitate analysis of helicity amplitudes, a four-component spinor is introduced in the following form [131]:

$$U(p) = \begin{pmatrix} u_L(p) \\ u_R(p) \end{pmatrix}, \tag{C.1}$$

where $u_L(p)$ and $u_R(p)$ are the two-component spinors which satisfy the common convention

$$u_R(p) = i\sigma_2 u_L^*(p). \tag{C.2}$$

In principle, the use of Eq. (C.2) allows for the reduction of abstractedness through the representation of two-component spinors in terms of complex numbers, specifically a and b. This can be expressed as follows:

$$\begin{aligned} u_L(p) &= \begin{pmatrix} a_p \\ b_p \end{pmatrix}, \\ u_L^\dagger(p) &= \begin{pmatrix} a_p \\ b_p \end{pmatrix}^\dagger = \begin{pmatrix} a_p^* & b_p^* \end{pmatrix}, \\ u_R(p) &= i\sigma_2 u_L^*(p) = i \begin{pmatrix} 0 & -i \\ i & 0 \end{pmatrix} \begin{pmatrix} a_p \\ b_p \end{pmatrix}^* = \begin{pmatrix} b_p^* \\ -a_p^* \end{pmatrix}, \\ u_R^\dagger(p) &= \begin{pmatrix} b_p^* \\ -a_p^* \end{pmatrix}^\dagger = \begin{pmatrix} b_p & -a_p \end{pmatrix}. \end{aligned} \tag{C.3}$$

In returning to four-component notation, the left- and right-handed spinors are expressed as:

$$U_L(p) = P_L U(p), \qquad U_R(p) = P_R U(p), \tag{C.4}$$

where left- and right-handed projectors, P_L and P_R, are defined in Eq. (B.5).

In order to avoid the unnecessary bulkiness of the calculations, a specific notation for left- and right-handed four-component spinors is introduced

$$
\begin{aligned}
|p] = U_L(p) &= N_p \begin{pmatrix} u_L(p) \\ 0 \end{pmatrix}, & |p\rangle = U_R(p) &= N_p \begin{pmatrix} 0 \\ u_R(p) \end{pmatrix}, \\
\langle p| = \overline{U}_L(p) &= N_p \begin{pmatrix} 0 & u_L^\dagger(p) \end{pmatrix}, & [p| = \overline{U}_R(p) &= N_p \begin{pmatrix} u_R^\dagger(p) & 0 \end{pmatrix},
\end{aligned}
\tag{C.5}
$$

where $N_p = \sqrt{2p_0}$ is the normalization constant computed from the condition of completeness

$$
\sum_{\lambda=L,R} U_\lambda(p) \otimes \overline{U}_\lambda(p) = \frac{N_p^2}{2p_0} \left[\begin{pmatrix} 0 & \sigma^\mu p_\mu \\ 0 & 0 \end{pmatrix} + \begin{pmatrix} 0 & 0 \\ \bar{\sigma}^\mu p_\mu & 0 \end{pmatrix} \right] = \frac{N_p^2}{2p_0} \gamma^\mu p_\mu. \tag{C.6}
$$

By taking Eq. (C.5) into account, we can derive some useful relations of spinor algebra, which will facilitate the computation of helicity amplitudes. By employing the matrix representation of the left- and right-handed projectors (B.5), it becomes evident that

$$
\begin{aligned}
P_R U_L(p) &= 0, & P_L U_L(p) &= U_L(p), \\
P_L U_R(p) &= 0, & P_R U_R(p) &= U_R(p), \\
\overline{U}_R(p) P_R &= 0, & \overline{U}_L(p) P_R &= \overline{U}_L(p), \\
\overline{U}_L(p) P_L &= 0, & \overline{U}_R(p) P_L &= \overline{U}_R(p).
\end{aligned}
\tag{C.7}
$$

It should be further noted that a scalar product of any two spinors with equal helicities will necessarily be zero. Indeed,

$$
\langle pq] = \overline{U}_L(p) U_L(q) = N_p N_q \begin{pmatrix} 0 & u_L^\dagger(p) \end{pmatrix} \begin{pmatrix} u_L(q) \\ 0 \end{pmatrix} = 0. \tag{C.8}
$$

Similarly,

$$
[pq\rangle = \overline{U}_R(p) U_R(q) = N_p N_q \begin{pmatrix} u_R^\dagger(p) & 0 \end{pmatrix} \begin{pmatrix} 0 \\ u_R(q) \end{pmatrix} = 0. \tag{C.9}
$$

Another important relation indicates that

$$
[pq] = \langle qp\rangle^*. \tag{C.10}
$$

The proof of this relation can also be demonstrated in a straightforward manner:

$$
\begin{aligned}
[pq] = \overline{U}_R(p) U_L(q) &= N_p N_q \begin{pmatrix} u_R^\dagger(p) & 0 \end{pmatrix} \begin{pmatrix} u_L(q) \\ 0 \end{pmatrix} = N_p N_q u_R^\dagger(p) u_L(q) \\
&= N_p N_q \big(u_R^*(p)\big)^T u_L(q) = \Big[N_p N_q \big(u_R^*(p)\big)^T u_L(q) \Big]^T \\
&= N_p N_q u_L^T(q) u_R^*(p) = N_p N_q \Big(u_L^\dagger(q) u_R(p) \Big)^* = \Big(\overline{U}_L(q) U_R(p) \Big)^* = \langle qp\rangle^*,
\end{aligned}
\tag{C.11}
$$

where in the second line, we performed a transposition of the entire expression, as it is an ordinary complex number.

The antisymmetry property is also of importance and can be expressed as follows:

$$
[pq] = -[qp], \qquad \langle pq\rangle = -\langle qp\rangle \tag{C.12}
$$

This can be readily demonstrated for the case of $[pq]$ through the utilization of the explicit representation of spinors in Eq. (C.3):

$$\begin{aligned}[pq] = \overline{U}_R(p)U_L(q) = N_pN_q\begin{pmatrix}-b_p & a_p & 0 & 0\end{pmatrix}\begin{pmatrix}a_q\\ b_q\\ 0\\ 0\end{pmatrix} = \\ = N_pN_q\left(-b_pa_q + a_pb_q\right) = -N_pN_q\left(-b_qa_p + a_qb_p\right) = -[qp]\end{aligned} \tag{C.13}$$

and similarly for $\langle pq\rangle$. Relations (C.12) enable the derivation of supplementary properties

$$[pp] = 0, \qquad \langle pp\rangle = 0 \tag{C.14}$$

that facilitate the substantial simplification of expressions within the helicity formalism method.

One of the most important relations of the spinor algebra is the product of two scalar spinor products. This product allows for a transition back to classical vector notation following a calculation, thereby facilitating the representation of amplitudes in a manner that is readily comprehensible

$$\begin{aligned}\langle pq\rangle[qp] = \overline{U}_L(p)U_R(q)\cdot\overline{U}_R(q)U_L(p) = \mathrm{tr}\Big(U_L(p)\otimes\overline{U}_L(p)\cdot U_R(q)\otimes\overline{U}_R(q)\Big) \\ = \mathrm{tr}\left[\begin{pmatrix}0 & \sigma^\mu p_\mu\\ 0 & 0\end{pmatrix}\begin{pmatrix}0 & 0\\ \bar\sigma^\nu q_\nu & 0\end{pmatrix}\right] = p_\mu q_\nu \mathrm{tr}\big(\sigma^\mu\bar\sigma^\nu\big) = p_\mu q_\nu\cdot 2g^{\mu\nu},\end{aligned} \tag{C.15}$$

where the condition of completeness has been applied. From Eq. (C.15) one can conclude that

$$\langle pq\rangle[qp] = 2\left(p\cdot q\right). \tag{C.16}$$

By direct substitution of0Eqs. (B.1) and (C.5), one can derive the following relations

$$\begin{aligned}\langle p|\gamma^\mu|q\rangle = 0, \qquad & \langle p|\gamma^\mu\gamma^\nu|q] = 0,\\ [p|\gamma^\mu|q] = 0, \qquad & [p|\gamma^\mu\gamma^\nu|q\rangle = 0.\end{aligned} \tag{C.17}$$

By employing some technical tricks (see [131] for further details) one can derive even more useful relations. These include the spinor representation of a slashed momentum

$$\not{p} = \gamma^\mu p_\mu = |p]\langle p| + |p\rangle[p|, \tag{C.18}$$

scalar products of two vectors

$$\begin{aligned}\langle p|\gamma^\mu|q]\langle l|\gamma_\mu|m] = 2\langle pl\rangle[mq],\\ [p|\gamma^\mu|q\rangle\langle l|\gamma_\mu|m] = 2[pm]\langle lq\rangle\end{aligned} \tag{C.19}$$

and a vector contraction with γ-matrix

$$\langle p|\gamma^\mu|q]\gamma_\mu = 2\big(|q]\langle p| + |p\rangle[q|\big). \tag{C.20}$$

It is also of great importance to consider the Schouten identities which allow for a clear understanding of the gauge invariance of amplitudes in cases of real parton emission

$$\begin{aligned}[pq][lm] + [pl][mq] + [pm][ql] = 0,\\ \langle pq\rangle\langle lm\rangle + \langle pl\rangle\langle mq\rangle + \langle pm\rangle\langle ql\rangle = 0.\end{aligned} \tag{C.21}$$

C.2 Vector boson representation

In order to comprehend the manner in which massless vector bosons may be represented within the spinor helicity formalism, it is necessary to construct a vector $\varepsilon_\mu(p)$ that satisfies the conditions of transversality, gauge choice, and normalization. These conditions may be mathematically represented as follows:

$$\varepsilon_\mu(p)p^\mu = 0, \qquad \varepsilon_\mu(p)r^\mu = 0, \qquad \varepsilon_\mu(p)\varepsilon^{*\mu}(p) = -1, \tag{C.22}$$

where r^μ is an arbitrary massless reference vector. Furthermore, the sum over two polarizations should be calculated as follows:

$$\sum_{\lambda\in(L,R)} \varepsilon_{\lambda\mu}(p)\varepsilon^*_{\lambda\nu}(p) = -g_{\mu\nu} + \frac{p_\mu r_\nu + p_\nu r_\mu}{(p\cdot r)}. \tag{C.23}$$

Given that conditions (C.22) involve two massless vectors, it is straightforward to construct a vector that will satisfy the criteria of transversality and the gauge choice. Two variants may be selected for the two polarizations:

$$\varepsilon_{\mu,1}(p) = N_1\,[r|\gamma_\mu|p\rangle, \qquad \varepsilon_{\mu,2}(p) = N_2\langle r|\gamma_\mu|p], \tag{C.24}$$

where N_1 and N_2 are normalization constants. In order to select these vectors as polarization vectors of massless bosons, it is necessary to normalize them (as indicated in the final condition of Eq. (C.22)) and verify their orthogonality, given that polarizations must be orthogonal. Moreover, it is required that vectors (C.24) satisfy the condition (C.23). By calculating the complex conjugation of one of the vectors in Eq. (C.24), it can be determined that

$$\begin{aligned}\varepsilon^*_{\mu,1}(p) &= \Big(N_1\,\overline{U}_R(r)\gamma_\mu U_R(p)\Big)^* = \Big(N_1N_rN_p\,u^\dagger_R(r)\sigma_\mu u_R(p)\Big)^*\\ &= N_rN_pN_1^*\,u^T_R(r)\big(\sigma_\mu\big)^* u^*_R(p).\end{aligned} \tag{C.25}$$

By employing the relation (C.2), one is able to express $\varepsilon^*_{\mu,1}(p)$ as follows:

$$\begin{aligned}\varepsilon^*_{\mu,1}(p) &= N_rN_pN_1^*\,u^\dagger_L(r)\sigma_2^T\big(\sigma_\mu\big)^*\sigma_2^* u_L(p) = N_rN_pN_1^*\,u^\dagger_L(r)\bar\sigma_\mu u_L(p)\\ &= N_1^*\,\overline{U}_L(r)\gamma_\mu U_L(p) = N_1^*\langle r|\gamma_\mu|p].\end{aligned} \tag{C.26}$$

This implies that $\varepsilon^*_{\mu,1}(p) = \varepsilon_{\mu,2}(p)$, if $N_1^* = N_2$. This result helps us to demonstrate that

$$\varepsilon^*_{\mu,1}(p)\varepsilon^\mu_2(p) = N_1^*N_2\,\langle r|\gamma_\mu|p]\langle r|\gamma^\mu|p] = 2N_2^2\langle rr\rangle[pp] = 0, \tag{C.27}$$

that implies the orthogonality of the vectors (C.24). In order to ascertain the normalization constant, we may utilize the condition of normalization

$$-1 = \varepsilon_{\mu,1}(p)\varepsilon_1^{*\mu}(p) = N_1N_1^*\,[r|\gamma_\mu|p\rangle\langle r|\gamma_\mu|p] = 2N_1N_1^*\langle pr\rangle[pr] \tag{C.28}$$

that allows us to choose $N_1 = 1/\sqrt{2}\,[pr]$. Upon evaluation of vectors $\varepsilon_{\mu,1}(p)$ and $\varepsilon_{\mu,2}(p)$ in any familiar kinematic case [131], it can be concluded that they correspond to the

polarizations of right- and left-handed massless bosons, respectively. As our focus is on outgoing bosons, we can thus write that

$$\varepsilon^*_{\mu,L}(p) = \frac{[r|\gamma_\mu|p\rangle}{\sqrt{2}\,[pr]}, \qquad \varepsilon^*_{\mu,R}(p) = -\frac{\langle r|\gamma_\mu|p]}{\sqrt{2}\,\langle pr\rangle}. \tag{C.29}$$

In the event that a massive vector boson with mass M_V is also taken into account, it is imperative to consider the third type of polarization, namely the longitudinal mode. The present work is not concerned with this particular case; therefore, we will simply present the expression for the third polarization [181]

$$\varepsilon^*_{\mu,0}(p) = -\frac{p^r_\mu}{M_V} + \frac{M_V}{2\,(p^r \cdot r)} r_\mu, \tag{C.30}$$

where

$$p^r_\mu = \frac{\Big[\operatorname{sgn}(p\cdot r)\,\sqrt{\Delta} + (p\cdot r)\Big]\,p_\mu - p^2 r_\mu}{2\,\operatorname{sgn}(p\cdot r)\,\sqrt{\Delta}} \tag{C.31}$$

with $\Delta = (p\cdot r)^2 - p^2 r^2$.

C.3 Representation for numerical computation

In certain cases, it is advantageous to represent spinors in explicit form. This approach enables the rewriting of helicity amplitudes in a numerical format and their combination as complex numbers. To construct the explicit form of spinors, one can express the equation for the parameters a_p and b_p from Eq. (C.6) as follows:

$$(\vec{n}\cdot\vec{\sigma})\begin{pmatrix} a \\ b \end{pmatrix} = -\begin{pmatrix} a \\ b \end{pmatrix}, \tag{C.32}$$

which is equivalent to finding the wave function of the spin 1/2 state polarized along $-\vec{n}$. The solution of this equation for

$$\vec{n} = \begin{pmatrix} \sin\vartheta\cos\varphi & \sin\vartheta\sin\varphi & \cos\vartheta \end{pmatrix} \tag{C.33}$$

can be written as [131]

$$a = -\sin\frac{\vartheta}{2} e^{-\frac{i\varphi}{2}}, \qquad b = \cos\frac{\vartheta}{2} e^{\frac{i\varphi}{2}}. \tag{C.34}$$

As a brief test one can calculate the product $\langle pp\rangle$, which should be equal to zero in accordance with Eq. (C.14). Indeed,

$$\begin{aligned} \langle pp\rangle = \overline{U}_L(p) U_R(p) &= N_p \begin{pmatrix} 0 & u^\dagger_L(p) \end{pmatrix} N_p \begin{pmatrix} 0 \\ u_R(p) \end{pmatrix} = \\ &= N_p^2 \Big(-\sin\frac{\vartheta}{2}\cos\frac{\vartheta}{2} e^{\frac{i\varphi}{2}} e^{-\frac{i\varphi}{2}} + \cos\frac{\vartheta}{2}\sin\frac{\vartheta}{2} e^{-\frac{i\varphi}{2}} e^{\frac{i\varphi}{2}} \Big) = 0. \end{aligned} \tag{C.35}$$

However, a more crucial understanding to be gleaned from this topic is that of how to combine the products of spinors to yield the scalar products of conventional vectors. In accordance with the notation delineated in Eq. (C.3), it is possible to ascertain the following:

$$
\begin{aligned}
[pq]\langle qp\rangle &= -N_p^2 N_q^2 \left(a_q b_p - a_p b_q\right)\left(a_p^* b_q^* - b_p^* a_q^*\right) = \\
&= -N_p^2 N_q^2 \left(a_q b_p a_p^* b_q^* - a_q b_p b_p^* a_q^* - a_p b_q a_p^* b_q^* + a_p b_q b_p^* a_q^*\right).
\end{aligned}
\tag{C.36}
$$

By substituting explicit expressions from Eq. (C.34) and exchanging N_p^2 and N_q^2 by $2p_0$ and $2q_0$, respectively, one can demonstrate, through the use of trigonometric algebra, that

$$
[pq]\langle qp\rangle = 2p_0 q_0 \big[1 - \cos\vartheta_p \cos\vartheta_q - \cos(\varphi_p - \varphi_q)\sin\vartheta_p \sin\vartheta_q\big]. \tag{C.37}
$$

On the other hand, if we consider two four-vectors in Minkowski space

$$
\begin{aligned}
p &= \begin{pmatrix} p_0 & p_0\sin\vartheta_p\cos\varphi_p & p_0\sin\vartheta_p\sin\varphi_p & p_0\cos\varphi_p \end{pmatrix}^T, \\
q &= \begin{pmatrix} q_0 & q_0\sin\vartheta_q\cos\varphi_q & q_0\sin\vartheta_q\sin\varphi_q & q_0\cos\varphi_q \end{pmatrix}^T,
\end{aligned}
\tag{C.38}
$$

their scalar product reads

$$
\begin{aligned}
(p\cdot q) &= p_0 q_0 - p_0\sin\vartheta_p\cos\varphi_p q_0\sin\vartheta_q\cos\varphi_q - \\
&\quad - p_0\sin\vartheta_p\sin\varphi_p q_0\sin\vartheta_q\sin\varphi_q - p_0\cos\varphi_p q_0\cos\varphi_q = \\
&= p_0 q_0\big[1 - \cos\vartheta_p\cos\vartheta_q - \cos(\varphi_p - \varphi_q)\sin\vartheta_p\sin\vartheta_q\big].
\end{aligned}
\tag{C.39}
$$

Comparing Eqs. (C.37) and (C.39) we can conclude that

$$
[pq]\langle qp\rangle = 2(p\cdot q). \tag{C.40}
$$

It is possible to rewrite any helicity amplitude explicitly as a complex number, compute a conjugated one, and then multiply these two numbers to obtain the squared amplitude. Furthermore, the squared amplitude can be expressed in terms of Mandelstam variables through the explicit notation for spinors.

The spinor products $[p_i p_j]$ and $\langle p_i p_j\rangle$ can be calculated from the external momenta with positive energies ($p_i^0 > 0$ and $p_j^0 > 0$) using the following formulae, as outlined in reference [182]

$$
\langle p_i p_j\rangle = \sqrt{|s_{ij}|}\, e^{i\varphi_{ij}}, \qquad\qquad [p_i p_j] = -\sqrt{|s_{ij}|}\, e^{-i\varphi_{ij}}, \tag{C.41}
$$

with $s_{ij} = (p_i + p_j)^2 = 2(p_i\cdot p_j)$, $e^{\pm i\varphi_{ij}} = \cos\varphi_{ij} \pm i\sin\varphi_{ij}$ and

$$
\cos\varphi_{ij} = \frac{p_i^1(p_j^0 + p_j^3) - p_j^1(p_i^0 + p_i^3)}{\sqrt{|s_{ij}|(p_i^0 + p_i^3)(p_j^0 + p_j^3)}}, \qquad \sin\varphi_{ij} = \frac{p_i^2(p_j^0 + p_j^3) - p_j^2(p_i^0 + p_i^3)}{\sqrt{|s_{ij}|(p_i^0 + p_i^3)(p_j^0 + p_j^3)}}. \tag{C.42}
$$

References

[1] J.J. Thomson, *Cathode Rays*, *The London, Edinburgh, and Dublin Philosophical Magazine and Journal of Science* **44** (1897) 293–316.

[2] E. Rutherford, *The Scattering of α and β Particles by Matter and the Structure of the Atom*, *Philosophical Magazine* **21** (1911) 669–688.

[3] S. Tomonaga, *On a Relativistically Invariant Formulation of the Quantum Theory of Wave Fields*, *Progress of Theoretical Physics* **1 no. 2** (1946) 27–42.

[4] J. Schwinger, *On Quantum Electrodynamics and the Magnetic Moment of the Electron*, *Physical Review* **73 no. 4** (1948) 416–417.

[5] R.P. Feynman, *Space-time Approach to Quantum Electrodynamics*, *Physical Review* **76** (1949) 769–789.

[6] R.P. Feynman and M. Gell-Mann, *Theory of the Fermi Interaction*, *Phys. Rev.* **109** (1958) 193–198.

[7] S.L. Glashow, *Partial-symmetries of Weak Interactions*, *Nucl. Phys.* **22** (1961) 579–588.

[8] A. Salam, *Weak and Electromagnetic Interactions*, *World Scientific Series in 20th Century Physics*, (1968) 244–254.

[9] S. Weinberg, *A Model of Leptons*, *Phys. Rev. Lett.* **19** (1967) 1264–1266.

[10] J. Goldstone, A. Salam, and S. Weinberg, *Broken Symmetries*, *Phys. Rev.* **127** (1962) 965–970.

[11] P.W. Higgs, *Broken symmetries, massless particles and gauge fields*, *Phys. Lett.* **12** (1964) 132–133.

[12] P.W. Higgs, *Broken Symmetries and the Masses of Gauge Bosons*, *Phys. Rev. Lett.* **13** (1964) 508–509.

[13] P.W. Higgs, *Spontaneous Symmetry Breakdown without Massless Bosons*, *Phys. Rev.* **145** (1966) 1156–1163.

[14] F. Englert and R. Brout, *Broken Symmetry and the Mass of Gauge Vector Mesons*, *Phys. Rev. Lett.* **13** (1964) 321–323.

[15] G.S. Guralnik, C.R. Hagen, and T.W.B. Kibble, *Global Conservation Laws and Massless Particles*, *Phys. Rev. Lett.* **13** (1964) 585–587.

[16] M. Gell-Mann, *Symmetries of Baryons and Mesons*, *Phys. Rev.* **125** (1962) 1067–1084.

[17] H. Fritzsch, M. Gell-Mann, and H. Leutwyler, *Advantages of the color octet gluon picture*, *Phys. Lett. B* **47** (1973) 365–368.

[18] D.J. Gross and F. Wilczek, *Ultraviolet Behavior of Non-Abelian Gauge Theories*, *Phys. Rev. Lett.* **30 no. 26** (1973) 1343–1346.

[19] H.D. Politzer, *Reliable Perturbative Results for Strong Interactions?*, *Phys. Rev. Lett.* **30 no. 26** (1973) 1346–1349.

[20] UA1 Collaboration, G. Arnison, *et al.*, *Experimental observation of isolated large transverse energy electrons with associated missing energy at* $s = 540\,GeV$, *Phys. Lett. B* **122** (1983) 103–116.

[21] UA2 Collaboration, M. Banner, *et al.*, *Observation of single isolated electrons of high transverse momentum in events with missing transverse energy at the CERN pp collider*, *Phys. Lett. B* **122 no. 5** (1983) 476–485.

[22] ATLAS Collaboration, *Observation of a new particle in the search for the Standard Model Higgs boson with the ATLAS detector at the LHC*, *Phys. Lett. B* **716** (2012) 1–29, [arXiv:1207.7214].

[23] CMS Collaboration, *Observation of a new boson at a mass of 125 GeV with the CMS experiment at the LHC*, *Phys. Lett. B* **716** (2012) 30–61, [arXiv:1207.7235].

[24] Planck Collaboration, *Planck 2018 results. VI. Cosmological parameters*, *Astronomy & Astrophysics* **A6** (2020) 641, [arXiv:1807.06209].

[25] G. Bertone, D. Hooper, and J. Silk, *Particle dark matter: Evidence, Candidates and Constraints*, *Phys. Rep.* **405** (2005) 279–390, [arXiv:hep-ph/0404175].

[26] A.G. Riess, *et al.*, *Observational Evidence from Supernovae for an Accelerating Universe and a Cosmological Constant*, *The Astronomical Journal*, **116 no. 3** (1998) 1009–1038, [arXiv:astro-ph/9805201].

[27] C. Kiefer, *Quantum Gravity: General Introduction and Recent Developments*, *Annalen der Physik* **15 no. 1-2** (2005) 129–148, [arXiv:gr-qc/0508120].

[28] A. Ashtekar and J. Lewandowski, *Background Independent Quantum Gravity: A Status Report*, *Classical and Quantum Gravity* **21 no. 15** (2004) R53–R152, [arXiv:gr-qc/0404018].

[29] K. Abe, *et al. (T2K Collaboration)*, *Constraint on the matter–antimatter symmetry-violating phase in neutrino oscillations*, *Nature* **580** (2020) 339–344, [arXiv:1910.03887].

[30] The Super-Kamiokande Collaboration, Y. Fukuda, *et al.*, *Evidence for Oscillation of Atmospheric Neutrinos*, *Phys. Rev. Lett.* **81** (1998) 1562–1567, [arXiv:hep-ex/9807003].

[31] Q.R. Ahmad, *et al.*, (SNO Collaboration), *Measurement of the rate of* $\nu_e + d \rightarrow p{+}p{+}e^-$ *interactions produced by 8B solar neutrinos at the Sudbury Neutrino Observatory*, *Phys. Rev. Lett.* **87** (2001), [arXiv:nucl-ex/0106015].

[32] Q.R. Ahmad, *et al.*, (SNO Collaboration), *Direct Evidence for Neutrino Flavor Transformation from Neutral-Current Interactions in the Sudbury Neutrino Observatory*, *Phys. Rev. Lett.* **89** (2002), [arXiv:nucl-ex/0204008].

[33] M. Aker, *et al.*, (KATRIN Collaboration), *First direct neutrino-mass measurement with sub-eV sensitivity*, *Nat. Phys.* **18** (2022) 160–166, [arXiv:2105.08533].

[34] S. Weinberg, *Effective Field Theories, Past and Future*, *PoS CD09* **086** (2009) 001, [arXiv:0908.1964].

[35] S. Weinberg, *On the Development of Effective Field Theory*, *Eur.Phys.J.H* **46** (2021) 1, 6, [arXiv:2101.04241].

[36] R. Penco, *An Introduction to Effective Field Theories*, (2020), [arXiv:2006.16285].

[37] A. Falkowski, *Lectures on Effective Field Theories*, (2017).

[38] I.W. Steward, *Effective Field Theory*, (2014).

[39] A.V. Manohar, *Introduction to Effective Field Theories*, *Les Houches Lect.Notes* **108** (2020), [arXiv:1804.05863].

[40] T. Appelquist and J. Carrazone, *Infrared Singularities and Massive Fields*, *Phys. Rev. D* **11** (1975) 2856.

[41] S. Weinberg, *Effective Gauge Theories*, *Phys. Lett. B* **91** (1980) 51.

[42] K.G. Wilson and J. Kogut, *The Renormalization Group and the ϵ-expansion*, *Phys. Repts.* **12C** (1974) 75.

[43] M.E. Peskin and D.V. Schroeder, *An Introduction to Quantum Field Theory*.

[44] A.B. Goncharov, M. Spradlin, C. Vergu, and A. Volovich, *Classical Polylogarithms for Amplitudes and Wilson Loops*, *Phys. Rev. Lett.* **105** 151605 (2010), [arXiv:1006.5703].

[45] S. Muller-Stach, S. Weinzierl, and R. Zayadeh, *Picard–Fuchs equations for Feynman Integrals*, *Commun. Math. Phys.* **326** (2013) 237–249, [arXiv:1212.4389].

[46] J.M. Henn, *Multiloop Integrals in Dimensional Regularization Made Simple*, *Phys. Rev. Lett.* **110** (2013) 251301, [arXiv:1304.1806].

[47] J. Broedel, C. Duhr, F. Dulat, and L. Tancredi, *Elliptic polylogarithms and iterated integrals on elliptic curves I: general formalism*, *JHEP* **05** 093 (2018), [arXiv:1712.07089].

[48] J. Broedel, C. Duhr, F. Dulat, and L. Tancredi, *Elliptic polylogarithms and iterated integrals on elliptic curves II: an application to the sunrise integral*, *Phys. Rev. D* **97** 116009 (2018), [arXiv:1712.07095].

[49] S. Weinzierl, *Feynman Integrals*, *UNITEXT for Physics* (2022), [arXiv:2201.03593].

[50] ATLAS Collaboration, G. Aad, *et al.*, *Measurements of fiducial and differential cross sections for Higgs boson production in the diphoton decay channel at $\sqrt{s}$ = 8 TeV with ATLAS*, *JHEP* **09** (2014) 112, [arXiv:1407.4222].

[51] ATLAS Collaboration, G. Aad, *et al.*, *Fiducial and differential cross sections of Higgs boson production measured in the four-lepton decay channel in pp collisions at $\sqrt{s}$ = 8 TeV with the ATLAS detector*, *Phys. Lett. B* **738** (2014) 234–253, [arXiv:1408.3226].

[52] ATLAS Collaboration, G. Aad, *et al.*, *Measurements of the Total and Differential Higgs Boson Production Cross Sections Combining the $H \to \gamma\gamma$ and $H \to ZZ^* \to 4l$ Decay Channels at $\sqrt{s}$ =8 TeV with the ATLAS detector*, *Phys. Rev. Lett.* **115** no. 9091801 (2015), [arXiv:1504.05833].

[53] ATLAS Collaboration, G. Aad, *et al.*, *Measurement of fiducial differential cross sections of gluon-fusion production of Higgs bosons decaying to $WW^* \to e\nu\mu\nu$ with the ATLAS detector at $\sqrt{s}$ = 8 TeV*, *JHEP* **08** 104 (2016), [arXiv:1604.02997].

[54] CMS Collaboration, S. Chatrchyan, *et al.*, *Measurement of differential cross sections for Higgs boson production in the diphoton decay channel in pp collisions at $\sqrt{s}$ = 8 TeV*, *Eur. Phys. J. C* **76** (2016) 13, [arXiv:1508.07819].

[55] CMS Collaboration, V. Khachatryan, *et al.*, *Measurement of differential and integrated fiducial cross sections for Higgs boson production in the four-lepton decay channel in pp collisions at $\sqrt{s}$ = 7 and 8 TeV*, *JHEP* **04** 005 (2016), [arXiv:1512.08377].

[56] CMS Collaboration, V. Khachatryan, *et al.*, *Measurement of the transverse momentum spectrum of the Higgs boson produced in pp collisions at $\sqrt{s}$ = 8 TeV using H to WW decays*, *JHEP* **03** (2017) 032, [arXiv:1606.01522].

[57] ATLAS Collaboration, M. Aaboud, *et al.*, *Measurement of inclusive and differential cross sections in the $H \to ZZ^* \to 4l$ decay channel in pp collisions at $\sqrt{s}$ = 13 TeV with the ATLAS detector*, *JHEP* **10** (2017) 132, [arXiv:1708.02810].

[58] ATLAS Collaboration, M. Aaboud, *et al.*, *Measurements of Higgs boson properties in the diphoton decay channel with 36 fb^{-1} of pp collision data at $\sqrt{s}$ = 13 TeV with the ATLAS detector*, *Phys. Rev. D* **98** (2018), 052005 [arXiv:1802.04146].

[59] CMS Collaboration, A.M. Sirunyan, *et al.*, *Measurements of properties of the Higgs boson decaying into the four-lepton final state in pp collisions at $\sqrt{s}$ = 13 TeV*, *JHEP* **11** (2017) 047, [arXiv:1706.09936].

[60] H. Baer, B. Bailey, and J.F. Owens, *$\mathcal{O}(\alpha_s)$ Monte Carlo approach to W + Higgs-boson associated production at hadron supercolliders*, *Phys. Rev. D* **47** (1993) 2730–2734.

[61] J. Ohnemus and W.J. Stirling, *Order α_s corrections to the differential cross-section for the W H intermediate mass Higgs signal*, *Phys. Rev. D* **47** (1993) 2722–2729.

[62] S. Mrenna and C.P. Yuan, *Effects of QCD Resummation on W^+h and $t\bar{b}$ Production at the Tevatron*, *Phys. Lett. B* **416** (1998) 200–207, [arXiv:hep-ph/9703224].

[63] T. Han and S. Willenbrock, *QCD correction to the $PP \to WH$ and ZH total cross-sections*, *Phys. Lett. B* **273** (1991) 167–172.

[64] M. Spira, *QCD Effects in Higgs Physics*, *Fortsch. Phys.* **46** (1998) 203–284, [arXiv:hep-ph/9705337].

[65] A. Djouadi and M. Spira, *SUSY-QCD corrections to Higgs boson production at hadron colliders*, *Phys. Rev. D* **62** (2000) 014004, [arXiv:hep-ph/9912476].

[66] M. Ciccolini, S. Dittmaier, and M. Kramer, *Electroweak radiative corrections to associated WH and ZH production at hadron colliders*, *Phys. Rev. D* **68** (2003) 073003, [arXiv:hep-ph/0306234].

[67] A. Denner, S. Dittmaier, S. Kallweit, and A. Muck, *Electroweak corrections to Higgs-strahlung off W/Z bosons at the Tevatron and the LHC with HAWK*, *JHEP* **03** (2012) 075, [arXiv:1112.5142].

[68] A. Denner, S. Dittmaier, S. Kallweit, and A. Muck, *HAWK 2.0: A Monte Carlo program for Higgs production in vector-boson fusion and Higgs strahlung at hadron colliders*, *Comput. Phys. Commun.* **195** (2015) 161, [arXiv:1412.5390].

[69] F. Granata, J.M. Lindert, C. Oleari, and S. Pozzorini, *NLO QCD+EW predictions for HV and HV + jet production including parton-shower effects*, *JHEP* **09** (2017) 012, [arXiv:1706.03522].

[70] P. Obul, S. Dulat, T.J. Hou, A. Tursun, and N. Yalkun, *Next-to-leading order QCD and electroweak corrections to Higgs-strahlung processes at the LHC*, *Chin. Phys. C* **42** (2018) 093105, [arXiv:1801.06851].

[71] O. Brein, A. Djouadi, and R. Harlander, *NNLO QCD corrections to the Higgs-strahlung processes at hadron colliders*, *Phys. Lett. B* **579** (2004) 149, [arXiv:hep-ph/0307206].

[72] O. Brein, R. Harlander, M. Wiesemann, and T. Zirke, *Top-Quark Mediated Effects in Hadronic Higgs-Strahlung*, *Eur. Phys. J. C* **72** (2012) 1868, [arXiv:1111.0761].

[73] O. Brein, R.V. Harlander, and T.J. Zirke, *vh@nnlo - Higgs Strahlung at hadron colliders*, *Comput. Phys. Commun.* **184** (2013) 998, [arXiv:1210.5347].

[74] R.V. Harlander, J. Klappert, S. Liebler, and L. Simon, *vh@nnlo-v2: New physics in Higgs Strahlung*, *JHEP* **05** (2018) 089, [arXiv:1802.04817].

[75] G. Ferrera, M. Grazzini, and F. Tramontano, *Associated WH production at hadron colliders: a fully exclusive QCD calculation at NNLO*, *Phys. Rev. Lett.* **107** (2011) 152003, [arXiv:1107.1164].

[76] G. Ferrera, M. Grazzini, and F. Tramontano, *Higher-order QCD effects for associated WH production and decay at the LHC*, *JHEP* **04** (2014) 039, [arXiv:1312.1669].

[77] G. Ferrera, M. Grazzini, and F. Tramontano, *Associated ZH production at hadron colliders: the fully differential NNLO QCD calculation*, *Phys. Lett. B* **740** (2015) 51–55, [arXiv:1407.4747].

[78] J.M. Campbell, R.K. Ellis, and C. Williams, *Associated production of a Higgs boson at NNLO*, *JHEP* **06** (2016) 179, [arXiv:1601.00658].

[79] F. Caola, G. Luisoni, K. Melnikov, and R. Röntsch, *NNLO QCD corrections to associated W H production and $H \to b\bar{b}$ decay*, *Phys. Rev. D* **97** no. 7, (2018) 074022, [arXiv:1712.06954].

[80] G. Ferrera, G. Somogyi, and F. Tramontano, *Associated production of a Higgs boson decaying into bottom quarks at the LHC in full NNLO QCD*, *Phys. Lett. B* **780** (2018) 346, [arXiv:1705.10304].

[81] R. Gauld, A. Gehrmann-De Ridder, E. Glover, A. Huss, and I. Majer, *Associated production of a Higgs boson decaying into bottom quarks and a weak vector boson decaying leptonically at NNLO in QCD*, *JHEP* **10** (2019) 002, [arXiv:1907.05836].

[82] R. Gauld, A. Gehrmann-De Ridder, E. W. N. Glover, A. Huss, and I. Majer, *Precise predictions for WH+jet production at the LHC*, *Phys. Lett. B* **817** (2021) 136335, [arXiv:2009.14209].

[83] G. Luisoni, P. Nason, C. Oleari, and F. Tramontano, *$HW^{\pm}/HZ$ + 0 and 1 jet at NLO with the POWHEG BOX interfaced to GoSam and their merging within MiNLO*, *JHEP* **10** (2013) 083, [arXiv:1306.2542].

[84] D. Goncalves, F. Krauss, S. Kuttimalai, and P. Maierhöfer, *Higgs-Strahlung: Merging the NLO Drell-Yan and Loop-Induced 0+1 jet Multiplicities*, *Phys. Rev. D* **92** (2015) 073006, [arXiv:1509.01597].

[85] B. Hespel, F. Maltoni, and E. Vryonidou, *Higgs and Z boson associated production via gluon fusion in the SM and the 2HDM*, *JHEP* **06** (2015) 065, [arXiv:1503.01656].

[86] W. Astill, W. Bizon, E. Re, and G. Zanderighi, *NNLOPS accurate associated HZ production with decay at NLO $H \to b\bar{b}$*, *JHEP* **11** (2018) 157, [arXiv:1804.08141].

[87] W. Bizon, E. Re, and G. Zanderighi, *NNLOPS description of the $H \to b\bar{b}$ decay with MiNLO*, *JHEP* **06** (2020) 006, [arXiv:1912.09982].

[88] B. A. Kniehl, *Associated Production of Higgs and Z Bosons From Gluon Fusion in Hadron Collisions*, *Phys. Rev. D* **42** (1990) 2253–2258.

[89] D.A. Dicus and C. Kao, *Higgs Boson - Z^0 Production From Gluon Fusion*, *Phys. Rev. D* **38** (1988) 1008.

[90] R.V. Harlander, S. Liebler, and T. Zirke, *Higgs Strahlung at the Large Hadron Collider in the 2-Higgs-Doublet Model*, *JHEP* **02** (2014) 023, [arXiv:1307.8122].

[91] C. Englert, M. McCullough, and M. Spannowsky, *Gluon-initiated associated production boosts Higgs physics*, *Phys. Rev. D* **89** (2014) 013013, [arXiv:1310.4828].

[92] L. Altenkamp, S. Dittmaier, R.V. Harlander, H. Rzehak, and T.J.E. Zirke, *Gluon-induced Higgs-strahlung at next-to-leading order QCD*, *JHEP* **02** (2013) 078, [arXiv:1211.5015].

[93] A. Hasselhuhn, T. Luthe, and M. Steinhauser, *On top quark mass effects to $gg \to ZH$ at NLO*, *JHEP* **01** (2017) 073, [arXiv:1611.05881].

[94] L. Chen, G. Heinrich, S.P. Jones, M. Kerner, J. Klappert, and J. Schlenk, *ZH production in gluon fusion: two-loop amplitudes with full top quark mass dependence*, *JHEP* **03** (2021) 125, [arXiv.2011.12325].

[95] R.V. Harlander, A. Kulesza, V. Theeuwes, and T. Zirke, *Soft gluon resummation for gluon-induced Higgs Strahlung*, *JHEP* **11** (2014) 082, [arXiv:1410.0217].

[96] F. Demartin, F. Maltoni, K. Mawatari, B. Page, and M. Zaro, *Higgs characterisation at NLO in QCD: CP properties of the top-quark Yukawa interaction*, *Eur. Phys. J. C* **74** (2014) 3065, [arXiv:1407.5089].

[97] K. Mimasu, V. Sanz, and C. Williams, *Higher Order QCD predictions for Associated Higgs production with anomalous couplings to gauge bosons*, *JHEP* **08** (2016) 039, [arXiv:1512.02572].

[98] C. Degrande, B. Fuks, K. Mawatari, K. Mimasu, and V. Sanz, *Electroweak Higgs boson production in the standard model effective field theory beyond leading order in QCD*, *Eur. Phys. J. C* **77** (2017) 262, [arXiv:1609.04833].

[99] F. Maltoni, E. Vryonidou, and C. Zhang, *Higgs production in association with a top-antitop pair in the Standard Model Effective Field Theory at NLO in QCD*, *JHEP* **10** (2016) 123, [arXiv:1607.05330].

[100] A. Greljo, G. Isidori, J.M. Lindert, D. Marzocca, and H. Zhand, *Electroweak Higgs production with HiggsPO at NLO QCD*, *Eur. Phys. J. C* **77** (2017) 838, [arXiv:1710.04143].

[101] S. Alioli, W. Dekens, M. Girard, and E. Mereghetti, *NLO QCD corrections to SM-EFT dilepton and electroweak Higgs boson production, matched to parton shower in POWHEG*, *JHEP* **08** (2018) 205, [arXiv:1804.07407].

[102] U. Haisch, D.J. Scott, M. Wiesemann, G. Zanderighi, and S. Zanoli, *NNLO event generation for $pp \to Zh \to l^+l^-b\bar{b}$ production in the SM effective field theory*, *J. High Energ. Phys.* **22** (2022).

[103] R.P. Feynman, *Parton–Hadron Interactions*, *Benjamin, Reading*, MA (1972).

[104] O. Brein, R.V. Harlander, M. Wiesemann, and T. Zirke, *Top-quark mediated effects in hadronic Higgs-Strahlung*, *Eur. Phys. J. C* **72** (2012) 1868, [arXiv:1111.0761].

[105] S.D. Drell and T.M. Yan, *Massive Lepton-Pair Production in Hadron-Hadron Collisions at High Energies*, *Phys. Rev. Lett.* **25** (1970) 316–320.

[106] T. Han and S. Willenbrock, *QCD correction to the $pp \to WH$ and ZH total cross sections*, *Phys. Lett. B* **273** (1991) 167–172.

[107] O. Brein, A. Djouadi, and R.V. Harlander, *NNLO QCD corrections to the Higgs-strahlung processes at hadron colliders*, *Phys. Lett. B* **579** (2004) 149–156, [arXiv:hep-ph/0307206].

[108] E. Fermi, *Versuch einer Theorie der β-Strahlen*, *I, Z. Phys.* **88** (1934) 161–177.

[109] (in Italian) E. Fermi, *Tentativo di una teoria dei raggi β*, *Il Nuovo Cimento*, **11(1)** (1934) 1–19;

(in German) E. Fermi, *Versuch einer Theorie der beta-Strahlen*, *Zeitschrift für Physik*, 88:161 (1934);

F.L. Wilson, *Fermi's Theory of Beta Decay*, *American Journal of Physics*, **36** (12) (1968) 1150–1160.

[110] Y. Nagashima, *Elementary Particle Physics, Vol. 2: Foundations of the Standard Model*.

[111] U.J. Wiese, *The Standard Model of Particle Physics*.

[112] T. Appelquist and J. Carazzone, *Infrared singularities and massive fields*, *Phys. Rev. D* **11** (1975) 2856.

[113] S. Weinberg, *Baryon- and Lepton-Nonconserving Processes*, *Phys. Rev. Lett.* **43** (1979) 1566.

[114] S. Mertens, *Direct Neutrino Mass Experiments*, *Journal of Physics. Conference Series (Online)*, **v. 718(2)** 9, [arXiv:1605.01579].

[115] K.A. Olive *et al.*, (Particle Data Group), *Review of Particle Physics*, *Chin. Phys. C* **38** (2014) 090001.

[116] N. Palanque-Delabrouille *et al.*, *Neutrino masses and cosmology with Lyman-alpha forest power spectrum*, *JCAP* **11** (2015) 011, [arXiv:1506.05976].

[117] KamLAND-Zen Collaboration, *Limit on Neutrinoless $\beta\beta$ Decay of Xe-136 from the First Phase of KamLAND-Zen and Comparison with the Positive Claim in Ge-76*, *Phys. Rev. Lett.* **110** (2013) 062502, [arXiv:1211.3863].

[118] W. Buchmuller and D. Wyler, *Effective Lagrangian Analysis of New Interactions and Flavor Conservation*, *Nucl.Phys. B* **268** (1986) 621–653.

[119] K. Hagiwara, S. Ishihara, R. Szalapski, and D. Zeppenfeld, *Low-energy effects of new interactions in the electroweak boson sector*, *Phys.Rev. D* **48** (1993) 2182–2203.

[120] L. Lehman and A. Martin, *Low-derivative operators of the Standard Model effective field theory via Hilbert series methods*, *JHEP* **02** (2016) 081, [arXiv:1510.00372].

[121] B. Grzadkowski, M. Iskrzynski, M. Misiak, and J. Rosiek, *Dimension-Six Terms in the Standard Model Lagrangian*, *JHEP* **1010** (2010) 085, [arXiv:1008.4884.]

[122] G. Giudice, C. Grojean, A. Pomarol, and R. Rattazzi, *The Strongly-Interacting Light Higgs*, *JHEP* **0706** (2007) 045, [arXiv:hep-ph/0703164].

[123] R. Contino, M. Ghezzi, C. Grojean, M. Muhlleitner, and M. Spira, *Effective Lagrangian for a light Higgs-like scalar*, *JHEP* **1307** (2013) 035, [arXiv:1303.3876].

[124] R.S. Gupta, A. Pomarol, and F. Riva, *BSM Primary Effects*, *Phys. Rev. D* **91** no. 3 (2015), 035001, [arXiv:1405.0181].

[125] L. Lehman, *Extending the Standard Model Effective Field Theory with the Complete Set of Dimension-7 Operators*, *Phys. Rev. D* **90** (2014) 12, [arXiv:1410.4193v2].

[126] G. Passarino and M. Trott, *The Standard Model Effective Field Theory and Next to Leading Order*, [arXiv 1610.08356v1].

[127] A. Dedes, *et al.*, *Feynman Rules for the Standard Model Effective Field Theory in R_ξ-gauges*, *JHEP* **1706** (2017) 143 (2017), [arXiv:1704.03888v5].

[128] N. Cabibbo, *Unitary Symmetry and Leptonic Decays*. *Phys. Rev. Lett.* **10** (12) (1963) 531–533.

[129] M. Kobayashi and T. Maskawa, *CP-violation in the renormalizable theory of weak interaction*, *Progress of Theoretical Physics* **49** (2) (1973) 652–657.

[130] R.L. Workman, *et al.* (Particle Data Group), *Review of Particle Physics (and 2023 update)*, *Progress of Theoretical and Experimental Physics* **8** (2022) 083 C01.

[131] K. Melnikov, *Modern methods for perturbative computations in QFT*.

[132] L. Dixon, *A brief introduction to modern amplitude methods*, *CERN-2014-008*, 31–67, [arXiv:1310.5353].

[133] S.J. Parke and T.R. Taylor, *An Amplitude for n-Gluon Scattering*, *Phys. Rev. Lett.* **56** (1986) 2459.

[134] R. Britto, F. Cachazo, B. Feng, *New Recursion Relations for Tree Amplitudes of Gluons*, *Nucl. Phys. B* **715** (2005) 499–522, [arXiv:hep-th/0412308].

[135] R. Britto, F. Cachazo, and B. Feng, and E. Witten, *Direct Proof of Tree-Level Recursion Relation in Yang-Mills Theory*, *Phys. Rev. Lett.* **94** (2005) 181602, [arXiv:hep-th/0501052].

[136] P. De Causmaecker, R. Gastmans, W. Troost, and T.T. Wu, *Multiple Bremsstrahlung in gauge theories at high energies. 1. General formalism for quantum electrodynamics*, *Nucl. Phys. B* **206** (1982) 53.

[137] F.A. Berends, R. Kleiss, P. De Causmaecker, R. Gastmans, W. Troost, and T.T. Wu, *Multiple Bremsstrahlung in gauge theories at high energies. 2. Single Bremsstrahlung*, *Nucl. Phys. B* **206** (1982) 61.

[138] R. Kleiss and W.J. Stirling, *Spinor techniques for calculating $pp \to W^\pm/Z^0$ + jets*, *Nucl. Phys. B* **262** (1985) 235.

[139] Z. Xu, D.H. Zhang and L. Chang, *Helicity amplitudes for multiple Bremsstrahlung in massless nonabelian gauge theories*, *Nucl. Phys. B* **291** (1987) 392.

[140] R. Gastmans and T.T. Wu, *The Ubiquitous Photon: Helicity Method for QED and QCD*, *Clarendon Press* (1990).

[141] G. Sterman and S. Weinberg, *Infrared divergences in quantum field theory*, *Phys. Rev. D* **13** (1976) 114.

[142] W. Bern, L. Dixon, and D.A. Kosower, *One-loop amplitudes for e^+e^- to four partons*, *Nucl. Phys. B* **425** (1994) 217, [arXiv:hep-ph/9708239].

[143] Z. Bern, G. Chalmers, L. Dixon, and D. Kosower, *One-loop N-gluon amplitudes with maximal helicity violation via collinear limits*, *Phys. Rev. Lett.* **72** (1994) 2134, [arXiv:hep-ph/9312333].

[144] J.C. Romao, *Advanced Quantum Field Theory*.

[145] C. Bollini and J.J. Giambiagi, *Dimensional Renormalization: The Number of Dimensions as a Regularizing Parameter*, *Nuovo Cim. B* **12** (1972) 20–26.

[146] G. t'Hooft and M. Veltman, *Regularization and renormalization of gauge fields*, *Nucl. Phys. B* **44** 1, (1972) 189–213.

[147] R.P. Feynman, *Space-time approach to quantum electrodynamics*, *Phys. Rev* **76** no. 6 (1949) 769–789.

[148] C. Studerus, *Reduze – Feynman integral reduction in C++*, *Comput. Phys. Commun.* **181** no. 7 (2010) 1293–1300, [arXiv:0912.2546].

[149] J.C. Collins, *Renormalization: An Introduction to Renormalization, The Renormalization Group, and the Operator-Product Expansion*.

[150] V.A. Smirnov, *Evaluating Feynman Integrals*, *Springer Tracts in Modern Physics* (2004).

[151] G. Passarino and M. Veltman, *One Loop Corrections for e^+e^- Annihilation into $\mu^+\mu^-$ in the Weinberg Model*, *Nucl. Phys. B* **160(1)** (1979) 151–207.

[152] G. Passarino and M.J.G. Veltman, *The technology of loop calculations. International Journal of Theoretical Physics* **19(4)** (1980) 165–193.

[153] C. Long, *A prescription for projectors to compute helicity amplitudes in D dimensions*, *Eur. Phys. J. C* **81** 417 (2021), [arXiv:1904.00705].

[154] T. Gehrmann and E. Remiddi, *Differential equations for two-loop four-point functions*, *Nucl. Phys. B* **580** (2000) 485–518, [arXiv:hep-ph/9912329].

[155] T. Gehrmann, E.W.N. Glover, T. Huber, N. Ikizlerli, and C. Studerus, *Calculation of the quark and gluon form factors to three loops in QCD*, *JHEP* **06** (2010) 094, [arXiv:1004.3653v4].

[156] N.J.A. Sloane (ed.), *Sequence A001620 (Decimal expansion of Euler's constant (or the Euler-Mascheroni constant), gamma)*, *The On-Line Encyclopedia of Integer Sequences, OEIS Foundation*.

[157] S. Catani, *The Singular behavior of QCD amplitudes at two-loop order*, *Phys. Lett. B* **470** (1998) 161–171, arXiv:hep-ph/9802439

[158] T. Becher and M. Neubert, *Infrared Singularities of Scattering Amplitudes in Perturbative QCD*, *Phys. Rev. Lett.* **102** (2009) 162001, [arXiv:0901.0722].

[159] T. Becher, G. Bell, C. Lorentzen, and S. Marti, *Transverse-momentum spectra of electroweak bosons near threshold at NNLO*, *JHEP* **02** (2014) 004, [arXiv:1309.3245].

[160] A. Bassetto, M. Ciafaloni, and G. Marchesini, *Jet structure and infrared sensitive quantities in perturbative QCD*, *Phys. Rep.* **100** (1983) 201.

[161] S. Catani and M. Grazzini, *The soft-gluon current at one-loop order*, *Nucl. Phys. B* **591** (2000) 435–454, [arXiv:hep-ph/0007142].

[162] S. Catani, D. de Florian, and G. Rodrigo, *Space-like (vs. time-like) collinear limits in QCD: is factorization violated?*, *JHEP* **07** (2012) 026, [arXiv:1112.4405].

[163] S. Catani, D. de Florian and G. Rodrigo, *The triple collinear limit of one-loop QCD amplitudes*, *Phys. Lett. B* **586** (2004) 323, [arXiv:hep-ph/0312067].

[164] L.W. Garland, T. Gehrmann, E.W.N. Glover, A. Koukoutsakis, and E. Remiddi, *Two-Loop QCD Helicity Amplitudes for $e^+e^- \to$ 3 Jets"*, *Nucl. Phys. B* **642:227** (2002), 227–262, text[arXiv:hep-ph/0206067].

[165] G. Duplancic and B. Nizic, *Dimensionally regulated one-loop box scalar integrals with massless internal lines*, *Eur. Phys. J. C* **20** (2001) 357–370, [arXiv:hep-ph/0006249].

[166] G.F.R. Sborlini, D. de Florian, and G. Rogrigo, *Double collinear splitting amplitudes at next-to-leading order. JHEP* **01** (2014) 018, [arXiv:1310.6841v2].

[167] O. Braun-White, N. Glover, *Decomposition of Triple Collinear Splitting Functions*, *J. High Energ. Phys.* (2022) 59, [arXiv:2204.10755v2].

[168] J. Alwall, *et al., The automated computation of tree-level and next-to-leading order differential cross sections, and their matching to parton shower simulations*, *JHEP* **07** (2014) 079, [arXiv:1405.0301].

[169] E. Bothmann, *et al., Event Generation with Sherpa 2.2*, *SciPost Phys.* **7** 034 (2019), [arXiv:1905.09127].

[170] C. Bierlich, *et al., A comprehensive guide to the physics and usage of PYTHIA 8.3*, *SciPost Phys. Codebases* **8** (2022), [arXiv:2203.11601].

[171] S. Catani and M.H. Seymour, *A General Algorithm for Calculating Jet Cross Sections in NLO QCD*, *Nucl. Phys. B* **485** (1997) 291–419, [arXiv:hep-ph/9605323].

[172] R. Frederix, S. Frixione, F. Maltoni, and T. Stelzer, *Automation of next-to-leading order computations in QCD: the FKS subtraction*, *JHEP* **0910** 003 (2009), [arXiv:0908.4272].

[173] M. Heller, A.v. Manteuffel, R.M. Schabinger, and H. Spiesberger, *Mixed EW-QCD two-loop amplitudes for $q\bar{q} \to l^+l^-$ and γ_5 scheme independence of multi-loop corrections*, *JHEP* **05** (2021) 213, [arXiv:2012.05918v1].

[174] P. Breitenlohner and D. Maison, *Dimensional Renormalization and the Action Principle*, *Commun. Math. Phys.* **52** (1977) 11.

[175] P. Breitenlohner and D. Maison, *Dimensionally Renormalized Green's Functions for Theories with Massless Particles. 1.*, *Commun. Math. Phys.* **52** (1977) 39.

[176] P. Breitenlohner and D. Maison, *Dimensionally Renormalized Green's Functions for Theories with Massless Particles. 2.*, *Commun. Math. Phys.* **52** (1977) 55.

[177] D. Kreimer, *The γ_5 Problem and Anomalies: A Clifford Algebra Approach*, *Phys. Lett. B* **237** (1990) 59–62.

[178] J. G. Körner, D. Kreimer, and K. Schilcher, *A practicable γ_5 scheme in dimensional regularization*, *Z. Phys. C* **54** (1992) 503–512.

[179] D. Kreimer, *Dimensionale Regularisierung im Standard Modell, PhD thesis, Johannes Gutenberg University, Faculty of Physics*, 1992.

[180] S. Larin, *The renormalization of the axial anomaly in dimensional regularization*, *Phys. Lett. B* **303** (1993) 113–118, [arXiv:hep-ph/9302240].

[181] J.L. Diaz-Cruz, B.O. Larios, and O. Meza-Aldama, *An Introduction to the Massive Helicity Formalism with applications to the Electroweak SM*, *J. Phys. Conf. Ser.* **761** (2016) 1, 012012, [arXiv:1608.04129v1].

[182] D. Maitre and P. Mastrolia, *S@M, a Mathematica Implementation of the Spinor-Helicity Formalism*, *Comput.Phys.Commun.* **179** (2008) 501-574, [arXiv: 0710.5559].

[183] F. Caola, K. Melnikov, and R. Röntsch, *Nested soft-collinear subtractions in NNLO QCD computations*, *Eur. Phys. J. C* **77**, 248 (2017), [arXiv:1702.01352].

[184] F. Caola, K. Melnikov, and R. Röntsch, *Analytic results for color-singlet production at NNLO QCD with the nested soft-collinear subtraction scheme*, *Eur. Phys. J. C* **79**, 386 (2019), [arXiv:1902.02081].

[185] W. Bizon, F. Caola, K. Melnikov, and R. Röntsch, *Anomalous couplings in associated VH production with Higgs boson decay to massive b quarks at NNLO in QCD*, *Phys. Rev. D* **105**, 014023 (2022), [arXiv:2106.06328].

[186] A. Behring, W. Bizon, F. Caola, K. Melnikov, and R. Röntsch, *Bottom quark mass effects in associated WH production with the $H \to b\bar{b}$ decay through NNLO QCD*, *Phys. Rev. D* **101**, 114012 (2020), [arXiv:2003.08321].

[187] M. Bonetti, R.V. Harlander, D. Korneev, M.-M. Long, K. Melnikov, R. Röntsch, and D.M. Tagliabue, *WH production at the LHC within SMEFT at next-to-next-to-leading order QCD*, *Phys. Rev. D* **112**, 034033 (2025), [arXiv:2502.12846].

[188] The NNPDF Collaboration: Richard D. Ball, *et al.*, *Parton distributions from high-precision collider data*, *Eur. Phys. J.C* **77** (2017) 10, 663, [arXiv:1706.00428].